A Predictive Metabolic Model for Polyhydroxyalkanoate Production by a Mixed Microbial Consortium Cultured Under Aerobic Dynamic Feeding Conditions and fed Dairy Manure Fermenter Liquor

A Thesis

Presented in Partial Fulfillment of the Requirements for the

Degree of Master of Science

with a

Major in Civil Engineering

in the

College of Graduate Studies

University of Idaho

by

Alexandre B. Crozes

Major Professor: Erik R. Coats, P.E., Ph.D.

Committee Members: Patricia J.S. Colberg, Ph.D., P.E., Armando McDonald, Ph.D.

Department Administrator: Patricia J.S. Colberg, Ph.D., P.E.

December 2019

Authorization to Submit Thesis

This thesis of Alexandre Bryce Crozes, submitted for the degree of Master of Science with a Major in Civil and Environmental Engineering and titled "A Predictive Metabolic Model for Polyhydroxyalkanoate Production by a Mixed Microbial Consortium cultured under Aerobic Dynamic Feeding Conditions and fed Dairy Manure Fermenter Liquor," has been reviewed in final form. Permission, as indicated by the signatures and dates below, is now granted to submit final copies to the College of Graduate Studies for approval.

Major Professor: _____ Date:_____
Erik R. Coats, P.E., Ph.D.

Committee Members: _____ Date:_____
Patricia J. S. Colberg, Ph.D., P.E.

_____ Date:_____
Armando McDonald, Ph.D.

Department Administrator: _____ Date:_____
Patricia J. S. Colberg, Ph.D., P.E.

Abstract

Global plastic use and disposal has become increasingly detrimental to the marine environment. The plastic problem is broad in scope with a complex solution; however, replacement of petro-plastics with bioplastics addresses the root of the issue, plastic accumulation. Polyhydroxyalkanoates (PHA) are biodegradable thermoplastics that are naturally produced by a variety of microorganisms and possess mechanical properties favorable for replacing fossil fuel derived plastics in single-use applications. Current PHA production processes utilize synthetic feed and pure cultures, a costly method that leaves economic viability to be desired. By employing an engineered PHA production process known as aerobic dynamic feeding (ADF), PHA can be synthesized by mixed microbial consortia (MMC) fed otherwise unused organic-rich waste streams. The inherent sustainability, coupled with reduced cost of substrate procurement and sterilization practices, place ADF configurations at the forefront of potentially feasible bioplastic solutions. Nevertheless, operational parameters that maximize volumetric productivity for a limited waste stream have yet to be defined. Research presented herein focused on the optimization of a three-stage ADF PHA production process by assessing the impacts of operational parameters, solids retention time (SRT) and organic loading rate (OLR). Additionally, a metabolic model was developed in order to describe ADF metabolism using complex substrate mixtures, ultimately providing insight for continued optimization efforts. Factorial-based evaluation of PHA production assessments led to the determination of a 2-day SRT and 20 Cmmol/L-d OLR as near-optimal culture enrichment operational criteria. Under said operation, the MMC converted nearly 100% of carbon to PHA resulting in an average maximum intracellular PHA accumulation of 38% (w/w). Furthermore, the metabolic model developed quantified the dynamic ADF microbial processes and led to accurate prediction of PHA composition for variable substrate mixtures.

Acknowledgements

I would like to express my upmost gratitude for my major professor, Dr. Erik R. Coats, P. E., for pushing me to be the best I can be, while providing the guidance and wisdom for me to succeed. The shear amount of time and support he gave me can only be provided by an advisor who truly cares about his students.

I would like to thank my committee members, Dr. Armando McDonald and Dr. Patricia J. S. Colberg, for providing their valuable expertise and time in reviewing this work. Additionally, I would like to thank Dr. Armando McDonald, Nick Guho, and Jason Mellin for analytical equipment and technical assistance, as well as helping with data interpretation and modeling efforts.

I would like to thank Cynthia Brinkman for her assistance and instruction of lab procedures, providing much needed humor, and for checking my attitude when it was warranted. I would like to extend my gratitude to my fellow peers: Sam Gibson, Kirsten Dolph, Lindsey Smoot, Nicole Tompkins, Maribel Alfaro, Nicolas Brouillard, Casey Bryant, Jonathon Shaber, and Willow Crites for their assistance with maintaining and sampling of the bioplastic systems. In addition, John Erstad for being the best roommate and friend someone could ask for in my last semester.

Dedication

This work is dedicated to my parents, Rilla and Gil Crozes, for their undying love, support, and guidance throughout my life and academic career.

Table of Contents

List of Tables

List of Figures

List of Equations

List of Abbreviations

ADF	Aerobic Dynamic Feeding
ASM3	Activated Sludge Model no. 3
ATP	Adenosine Triphosphate
CoASH	Coenzyme-A
COD	Chemical Oxygen Demand
CSTR	Continuous Stirred Tank Reactor
DFL	Dairy Fermenter Liquor
DO	Dissolved Oxygen
E.SRT.OLR	Enrichment Reactor Identifying Notation
EBPR	Enhanced Biological Phosphorus Removal
FAD	Flavin Adenine Dinucleotide
F-F	Feast-Famine
GAOs	Glycogen Accumulating Organisms
H	Hydrogen
HA	Hydroxyalkanoic Acids
HRT	Hydraulic Retention Time
MFA	Metabolic Flux Analysis
MLSS	Mixed Liquor Suspended Solids
MLVSS	Mixed Liquor Volatile Suspended Solids
MMC	Mixed Microbial Consortium
N	Nitrogen
NAD	Nicotinamide Adenine Dinucleotide
OHO	Ordinary Heterotrophic Organisms
OLR	Organic Loading Rate
P	Phosphorus
P.SRT.OLR	Production Reactor Identifying Notation
PAHs	Polycyclic Aromatic Hydrocarbons
PAOs	Phosphorus Accumulating Organisms
PCBs	Polychlorinated Biphenyls
PHA	Polyhydroxyalkanoates

PHB	Poly-3-hydroxybutryate
PHBV	Hydroxybutyrate-co-3-hydroxyvalerate
PHV	Poly-3-hydroxyvalerate
PMF	Proton Motive Force
RQ	Research Question
SRT	Solids Retention Time
TCA	Tricarboxylic Acid
TS	Total Solids
TSS	Total Suspended Solids
TSSr	Total Suspended Solids Recovered Post-centrifugation
VFA	Volatile Fatty Acid
VSS	Volatile Suspended Solids

Nomenclature

C_{NH3}	Concentration of Ammonia (mmol/L)
C_{PHB}	Concentration of PHB (Cmmol/L)
C_{PHV}	Concentration of PHV (Cmmol/L)
C_S	Concentration of VFAs (Cmmol/L)
$C_{VFA,i}$	Concentration of ith VFA
C_X	Concentration of Biomass (Cmmol/L)
DOF	Degree of Freedom
e	Vector of Residuals
E_R	Relative Error
E_{SS}	Steady State Error
$f_{PHB/X}$	Biomass Fraction of PHB
$f_{PHV/X}$	Biomass Fraction of PHV
k	PHA Degradation Rate Constant
K_1	ATP Requirement for Biomass Growth on Acetyl-CoA
K_2	ATP Requirement for Biomass Growth on Propionyl-CoA
K_{NH3}	Ammonia Half Saturation Coefficient
K_S	Substrate Half Saturation Coefficient
m_{ATP}	Biomass Specific ATP Consumption Rate
$m_{s,famine}$	Maintenance Term for ATP Consumption on PHA
$m_{s,feast}$	Maintenance Term for ATP Consumption on Substrate
n_{even}	Weighted Average of Even Carbons Uptaken
n_{odd}	Weighted Average of Even Carbons Uptaken
q_{PHA}	Specific Substrate Uptake Rate ($Cmmol_{PHA}/Cmmol_X$-hr)
q_S	Specific Substrate Uptake Rate ($Cmmol_{VFA}/Cmmol_X$-hr)
r_i	Reaction Rate for i^{th} Reaction
R_S	Lumped Substrate Uptake Equation
X	Biomass
y	Ratio of Odd Carbon VFA to Total VFA Flux
y_f	Ratio of PHV Degradation to Total PHA Degradation Flux

$Y_{PHA/S}$	Yield of PHA on VFAs
y_{PHV}	Ratio of PHV Flux to Total PHA Production Flux
$Y_{XAC/PHA}$	Yield of Biomass on Acetyl-CoA from PHA
$Y_{XAC/S}$	Yield of Biomass on Acetyl-CoA from VFAs
$Y_{XPr/PHA}$	Yield of Biomass on Propionyl-CoA from PHA
$Y_{XPr/S}$	Yield of Biomass on Propionyl-CoA from VFAs
μ_{famine}	Biomass Specific Growth Rate in Famine Phase
μ_{feast}	Biomass Specific Growth Rate in Feast Phase
μ_{max}	Maximum Biomass Specific Growth Rate
δ	Effeciency of Oxidative Phosphorylation (mol ATP/ mol NADH)

1. Introduction

Global plastic use has nearly doubled since 2000; the main driver of consumption and waste is single use plastics with design lifespans of less than a year, accounting for an estimated 40% of plastic produced [9]. In 2015, an estimated 34.5 million tons (MT) of plastic was generated in the United States alone, 75.4% of which ended up in landfills [10]. In general, landfilling presents many environmental concerns such as occupying of land, potential pollution of groundwater, and deferred management of waste to future generations [11]. However, landfilling is not the largest environmental concern associated with plastics; indeed, landfilling plastic is benign relative to plastic broadly distributed in the marine environment. In coastal areas of the world, a large percentage of plastic is indirectly disposed into the ocean. A 2010 study estimated 5.3-14 MT of land-based plastic waste entered the ocean from 192 coastal countries [12]. Additionally, this estimate does not embody the total oceanic plastic pollution, as it only accounts for the mass of plastics buoyant in seawater, such as polyethylene and polypropylene. Plastic entering the ocean is of serious environmental concern because of its harmful effects on aquatic biota. Plastic is harmful to aquatic life due to ingestion and entanglement [13]. Beyond mechanical organ blockage from ingestion, organic pollutants and toxic chemicals such as polychlorinated biphenyls (PCBs) and polycyclic aromatic hydrocarbons (PAHs) adsorbed by plastic debris creates a myriad of health and fertility problems for aquatic life post-consumption [11, 14]. This becomes a compounding issue in the aquatic food web and ecosystem, and ultimately can directly affect human health.

Modern attempts of containing plastic waste are founded on recycling and incineration practices. Incineration does not require significant land but releases potentially harmful compounds and greenhouse gases directly to the environment [11]. Recycling is a potentially sustainable alternative to plastic disposal, but its prevalence is relatively insignificant. For example, in the United States, 1 trillion plastic bags are produced annually, but only an estimated 5% are recycled [15]. Moreover, pollutants within the plastic reduce the reusability and yield of recycled plastic, making the expensive process inefficient [11]; in effect plastic recycling is downcycling [16]. With little to no incentive to increase recycling practices, the problem of plastic entering the environment remains.

An enticing solution to the plastics problem is to replace the use of petroleum-based plastics with biodegradable plastics derived from renewable waste streams. Bioplastics, or biopolymers, are polymers derived from natural resources that are typically biodegradable and nontoxic [17]. In particular, polyhydroxyalkanoates (PHA) are biopolymers that rival petroleum-based plastics with characteristics similar to those of polypropylene and polystyrene, all while being biodegradable and derived from renewable sources [18]. PHA can be naturally produced from a variety of feedstocks, including waste organic matter, with material properties suitable to replace many single use plastics. The comparable functionality of PHA to petrochemical plastics, coupled with the opportunity for re-purposing waste, makes it a favorable candidate for production of bio-based polymer plastics [19].

PHA is naturally produced by a variety of microorganisms reliant on carbon and energy storage reserves. Despite its obvious attractiveness, the primary reason PHA is not utilized ubiquitously are the costs associated with PHA production being much higher than that of fossil-fuel counterparts. In the late 90s, commercial PHA production focused on harvesting PHA produced directly in the chloroplasts of leaves from corn. A study on the effectiveness of this method showed that it required 2.39 kilograms (kg) of fossil fuel per kg of PHA, leading to Monsanto terminating their PHA production systems [20]. Following plant-based efforts, PHA production began revolving around using pure bacterial cultures with single substrates, requiring expensive machinery and sterilization practices. Metabolix, a former industrial producer of biopolymer products, priced polyhydroxyalkanoate-based pellets at $5 per kg, roughly three times the price of polypropylene, before terminating PHA operations [21]. Ultimately, the cost of maintaining a pure culture and refining substrate from crops proved to be too financially encumbering; moreover, these prior methods also demanded more fossil fuel that petro-plastics [22].

Despite historic failures to realize commercial PHA production, there remains hope. A promising approach for PHA production to reduce operational costs involves using a mixed microbial consortium (MMC) and waste-based substrate. Leveraging ecological selection principles to obtain enriched microbial cultures with maximum PHA production capacity could reduce production costs dramatically [11]. Additionally, using organic-rich waste as a source of carbon alleviates the cost of substrate production, and also creates opportunity for achieving resource recovery. In particular, dairy manure, with an estimated 227 billion kg of

manure produced in the US annually [15], lends itself as an abundant nutrient stream for PHA production, while indirectly closing the loop on the dairy waste cycle. PHA production using MMC and waste substrate generally involves a three-stage process [23]; a dairy manure fed variant is illustrated in Figure 1.1.

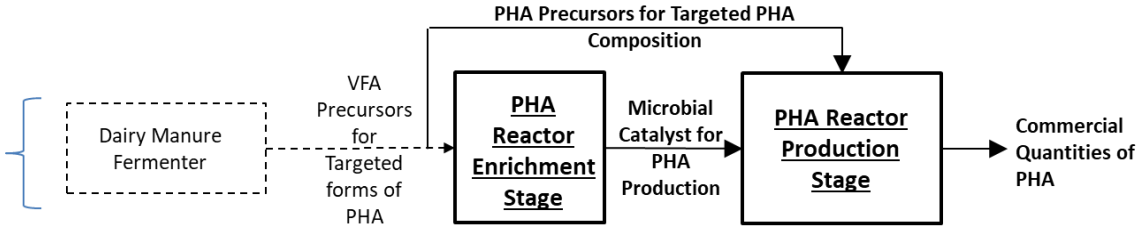

Figure 1.1: Three-Stage PHA Production Process Using Dairy Manure Feed

The first stage of the process is the fermentation stage, where organic material present in the dairy manure is converted to acetic acid and other carboxylates (collectively referred to as volatile fatty acids, VFAs, in this work) via acidogenic fermentation. Fermenter effluent is then centrifuged to minimize unwanted solids, as the VFA-rich centrate or dairy fermenter liquor (DFL) becomes the carbon source for the remaining stages. The second stage is the enrichment stage, where a MMC is maximally enriched with bacteria capable of PHA production by cycling between periods of excess carbon (feast) and extended periods of carbon shortage (famine). During the 'feast' period, the MMC principally stores carbon as PHA rather than using it directly for growth purposes. This metabolic response, originally presented by Majone et al. [24], is commonly referred to as a Feast-Famine (F-F) metabolism, and is induced under aerobic dynamic feeding (ADF) conditions; the MMC can convert in excess of 70% of carbon to storage products in the form of PHA [25-27]. The ADF configuration shifts the MMC by selecting for microorganisms capable of storing excess carbon, allowing their survival in the stressful famine phase. A portion of the enriched MMC, typically the daily waste, is then used in a side stream reactor to accomplish PHA production; this is referred to as the third, or production, stage. Intracellular PHA concentrations in the production stage exceed that of the enrichment stage by operating at a higher total organic loading rate (OLR) until PHA saturation has been achieved [23]. DFL is supplied either continuously or in pulses to sustain a 'feast' response; the feeding strategy seeks to avoid high concentrations of VFAs (currently estimated at >60 Cmmol/L) that can inhibit the storage metabolism [27]. A pulse-feeding strategy requires pulses of substrate before bulk solution

VFAs are depleted. This feeding strategy can prove quite difficult, thus online dissolved oxygen (DO) monitoring is commonly employed, indicating a pulse to be added when DO levels rise abruptly [28].

A primary issue with PHA production by MMC cultured on complex waste streams is that PHA content and overall volumetric productivity falls short when compared to pure cultures using single substrates [29]. To overcome this challenge, an optimally configured and operated ADF-driven PHA production process must achieve the following core objectives: i) conserve PHA precursors (e.g., VFA-rich fermenter liquor) for PHA production in the 3rd stage of the process; in other words, the process must minimize use of PHA precursors in the 2nd stage of the process, ii) enrich for a MMC capable of converting nearly 100% of the PHA precursors to PHA during the 'feast' metabolic response and iii) generate a MMC capable of very high PHA intracellular content in the 3rd stage. These three overarching process objectives are ultimately and necessarily intertwined in maximizing process success; morover, with a fixed substrate, i.e. fermented dairy manure, a MMC's PHA production capability becomes dependent on reactor operating conditions [28]. Since the introduction of the ADF PHA production process using complex substrates, several studies have evaluated the effect of numerous operational parameters, including organic loading rate (OLR), carbon to nitrogen ratio, enrichment reactor solids retention time (SRT), pH, oxygen concentration, and temperature on culture selection [29-36]. In the context of PHA production using fermented dairy manure and realizing the objectives articulated above, OLR and SRT are two of the most important operational parameters; however, the interrelation of the two parameters to achieve maximal process success has not been extensively studied. The combination of SRT and OLR influence all three objectives articulated above: carbon conservation, PHA yield, and intracellular PHA concentration. From biological wastewater treatment fundamentals, it is well established that SRT generally shares a positive relationship with solids content, with bioreactor solids content increasing with SRT; however, as the SRT increases, the bioreactor inorganic solids content increases, thus countering the goal to achieve higher biomass PHA content. As determined by Beun et al. [37, 38], for a fixed OLR, PHA yield is negatively impacted by SRTs below a certain threshold (suggested to be 2 days) but is otherwise independent of SRT up to 19.8 days. In commercial PHA production aimed at maximizing extraction quantities, there exists an SRT that is optimal in regards to total intracellular PHA

and PHA yield. Similarly, there exists an OLR that optimally conserves substrate for maximum PHA production in the 3rd stage. Assuming a healthy ADF process that enriches for a MMC capable of maximum PHA yield, the amount of polymer that can be synthesized is simply a function of the quantity of substrate applied; specifically, maximum PHA production results from the highest enrichment OLR that can be applied without hindering the F-F metabolism and ADF process' selective pressure on the MMC [23]. However, for a fixed quantity of substrate available for both stages of the PHA process, the optimal OLR is not solely limited by culture selection. The waste feedstock, and ultimately the fermentation stage, must be capable of accommodating substrate needs for both the enrichment stage and the production stage. Similar to the effects of increasing SRT, operating the ER at higher OLRs increases the quantity of the MMC; consequently, increased amounts of DFL are required in the production stages to reach maximum intracellular PHA concentrations and net PHA quantity. Hence, the optimal OLR is dependent on the waste source and is potentially lower than the theoretical OLR that achieves maximum PHA production. Moreover, there is likely a link between SRT and OLR to maximize process success. Further understanding the effects of SRT and OLR on overall PHA productivity – independently and in combination – is critical to increasing the viability of waste substrate and MMC becoming commercially favored.

Beyond process operational criteria, closing the gap in performance between pure cultures and MMC requires knowledge and enhanced application of the 'feast' PHA metabolism. ADF selected microorganisms grow and store PHA simultaneously in the feast phase, and then continue to grow using PHA stores throughout the famine phase. A metabolic model would be a useful tool to help understand and troubleshoot this dynamic process, wherein the stoichiometric yields and maintenance coefficients are interdependent [38]. The first model describing ADF-driven PHB production, and the associated feast-famine metabolism, under dynamic substrate supply was introduced by van Aalst-van Leeuwen et al. in 1997 [39]. The model was developed from a pure culture of *Paracoccus pantotrophus* fed acetic acid. From the original model, many extensions have been made [19, 37, 38, 40-44], with the first model describing the metabolism of PHA-producing MMC fed a complex mixture of substrate derived from sugar cane molasses introduced by Pardelha et al. [18]. Extension of said model for describing the metabolism of an MMC enriched on dairy waste feedstock could prove of

high-value in commercialization of a dairy-fed PHA production process. Understanding the internal microbial processes via a metabolic model allows for overall performance predictiveness, understanding of process upset, and the ability to determine polymer characteristics *a priori*.

Building upon the identified process needs articulated herein, research conducted in this thesis strived to increase real-world application of biopolymer production by first optimizing a dairy-fed PHA production process, focused on evaluating SRT and OLR effects, and then by expanding the ADF metabolic model to evaluating SRT and OLR effects on the feast-famine metabolism. With underlying microbial processes better understood and optimal operations exploited, bioplastics would be better positioned to find a home in the competitive plastic market.

1.1. Research Questions, Hypothesis, and Objectives

This thesis was driven by the following research questions (RQs), hypotheses, and objectives:

RQ 1: What is the optimal enrichment reactor SRT-OLR that addresses the three core process objectives: optimal distribution of PHA precursors, maximizing PHA yield on VFAs, and maximizing intracellular PHA concentration?

Hypothesis 1: There exists an SRT-OLR combination that will result in maximum PHA production.

Objective 1: Conduct a factorial-based experimental design with SRT and OLR as independent operational parameters. Statistically evaluate effects of SRT and OLR on enrichment reactor PHA production from SBR and fed-batch assessments.

RQ 2: How well can a feast-famine PHA metabolic model consistently describe PHA production in MMC fed DFL and operated under ADF conditions?

Hypothesis 2: A PHA feast-famine metabolic model will provide predictive measurement of PHA production and will mechanistically describe metabolic processes in the feast phase.

Objective 2: Develop a metabolic model to describe feast-famine PHA synthesis. Evaluate and assess measurements of PHA production from SBR and fed-batch assessments by means of the metabolic model.

RQ 3: How effectively will a PHA feast-famine metabolic model assist in establishing empirical direction towards the optimization of PHA production on fermented dairy manure? How well does the metabolic model predict the same optimal SRT-OLR combination as determined empirically?

Hypothesis 3: A calibrated/validated feast-famine PHA metabolic model will provide insight on optimizing the operational environment of an SBR for PHA production, unforeseen by lab experimentation.

Objective 3: Evaluate possible carbon flux scenarios using the metabolic model to maximize theoretical PHA production and access its extension to laboratory operation of an SBR.

2. Literature Review

2.1. Polyhydroxyalkanoates

Frenchman Maurice Lemoigne isolated and characterized the first bacterially-produced polyester in 1923, which he named “lipide-β-hydroxybutyrique” [45]. Lemoigne had effectively discovered polyhydroxyalkanoates (PHA), an intracellular carbon and energy storage product produced by a plethora of microorganisms. PHA is synthesized by bacteria under conditions of metabolic stress, typically induced either by limitation of an electron acceptor or critical macronutrient, or when substrate is supplied dynamically [29]. Once accumulated in a microbial cell, PHA can be extracted to become a biodegradable substitute to petroleum-derived plastic. The commercial viability of PHA in single-use plastic applications, coupled with its unique ability to be derived from carbon in existing waste streams, makes it a bioplastic worthy of further scrutiny.

2.1.1. PHA Composition

Bacteria store polyhydroxyalkanoates (PHA) within the cytoplasm as amorphous granules ranging in size from 0.2 to 0.5 μm [46]. PHA are natural polymers made up of hydroxyalkanoic acids (HA), structured as a spiral chain of repeating monomers (i.e. HA). While roughly 125-150 different HA have been observed [47, 48], short-chained volatile fatty acids (VFAs) primarily generate four monomers: 3-hydroxybutyrate (3HB), 3-hydroxyvalerate (3HV), 3-hydroxy-2-methylbutyrate (3H2MB), and 3-hydroxy-2-methylvalerate (3H2MV) [29]. Due to 3HV and 3H2MB being isomers, they are collectively referred to as 3HV [40]. Importantly, 3H2MV is not accumulated by most MMC and conventional analytical methods are not able to separate it efficiently. Therefore, biological systems effectively only produce 3HB and 3HV monomers and their homopolymer derivatives: poly-3-hydroxybutryate (PHB) and poly-3-hydroxyvalerate (PHV). In many cases, when both 3HB and 3HV are available, the microbe will randomly polymerize the monomers to form the co-polymer hydroxybutyrate-co-3-hydroxyvalerate (PHBV) [49] . The monomeric structure of PHB, PHV, and PHBV is shown in Figure 2.5.

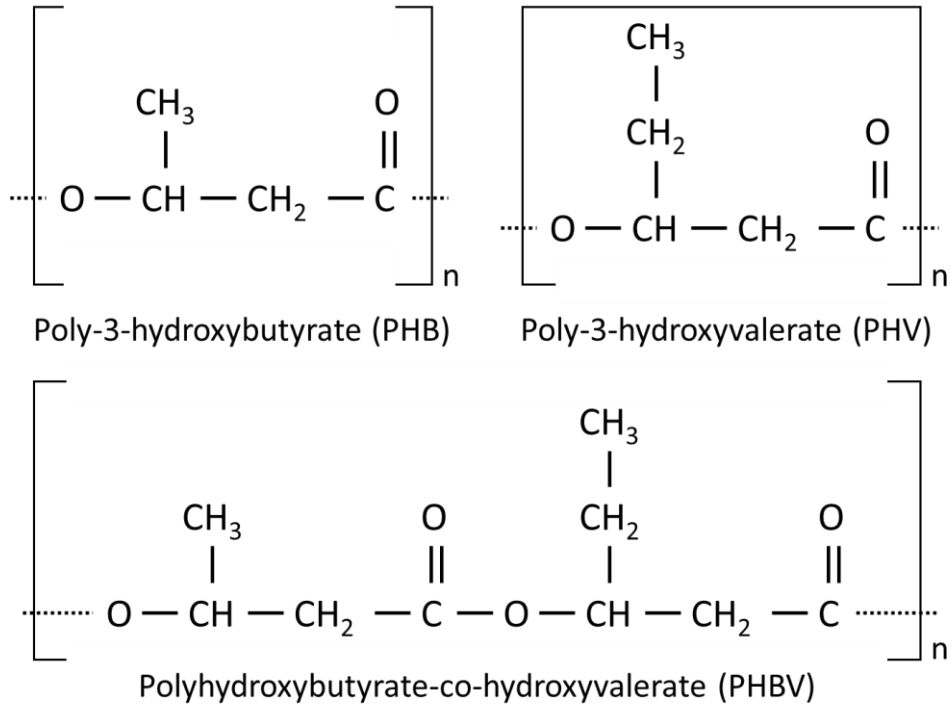

Figure 2.1: Common Polyhydroxyalkanoate Monomers [50]

Reproduced with permission.

2.1.2. PHA Material Properties

Physical properties of PHA are highly dependent on relative monomeric composition (i.e. HV fraction). Homopolymer PHB is predominantly crystalline, making it a very stiff and brittle material [51]. Additionally, PHB exhibits poor temperature stability, with pronounced molecular weight loss and decomposition at its melt temperature [1]. The aforementioned characteristics of PHB severely limit its application; however, copolymers with 3HV can exhibit attractive mechanical properties. PHBV copolymers with HV contents between 5-20% have been commercially produced, principally due to their superior melt stability and mechanical characteristics [52]. Increasing 3HV content improves mechanical properties, namely, by decreasing stiffness and brittleness, increasing its flexibility, tensile strength, and toughness [51]. However, higher 3HV content requires longer processing time due to slower crystallization rates [52].

In MMC systems, PHA composition is of great importance, as the thermal and mechanical properties thereof must outcompete synthetic plastics. For this case, PHA composition is dependent on the fermenter effluent composition [51]. Bacteria can produce PHA from a

variety of substrates, however, VFAs are the most direct precursors to PHA synthesis. VFAs are short chain (2-6 carbon) carboxylic acids that are a product of acidogenic fermentation. In general, the uptake and conversion of even-numbered carbon VFAs (i.e. acetate and butyrate) yields 3HB monomers, while odd-numbered carbon VFAs (i.e. propionate and valerate) yield 3HV monomers. Moreover, it is suggested for mixtures of VFAs, the resultant copolymer HB:HV ratio will be reflective of the ratio of even:odd carbon molecules [40]. Indeed, to produce PHA with desirable physiochemical properties, the feedstock VFA distribution should be 'controlled' accordingly.

2.1.3 PHA Biodegradability

A competitive advantage PHA has over synthetic plastics is biodegradability. Since PHA is a biologically produced storage product, the inverse, or enzymatic degradation of PHA for energy and growth can also be facilitated by a vast amount of bacteria [53]. In microbially active environments, PHA can fully degrade in as little as 30 days; moreover, no harmful intermediates or by-products are introduced by the degradation process [54]. Alternatively, as seen in packaging applications, PHA kept in a relatively cool and dry environment degrades at a negligible rate. A visual depicting the rate of PHA degradation in an aerobic sewage sludge environment is shown in Figure 2.2. In contrast, petro-plastic (e.g. polypropylene, polyethylene, and polyethylene terephthalate) monomers can be naturally synthesized, however, these polymers exhibit negligible biodegradation, owed to practically no microorganism possessing the necessary enzymes to dismantle their chemical structure [48].

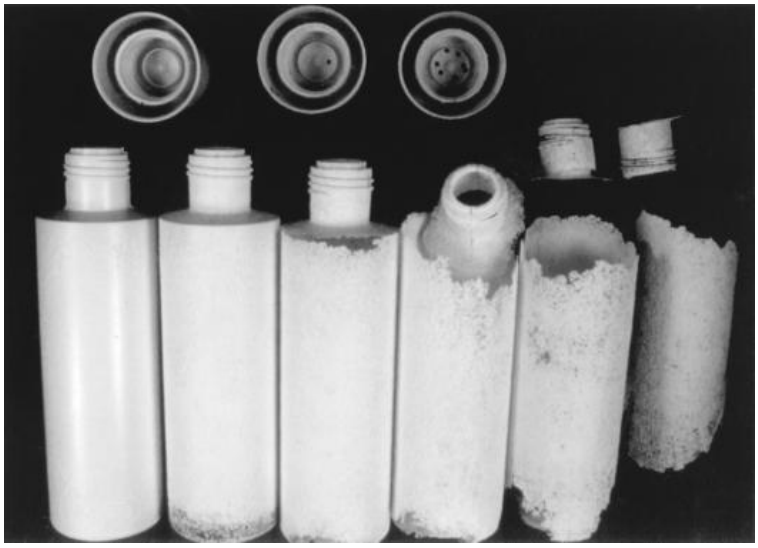

Figure 2.2: PHA Degradation in Aerobic Sewage Sludge (20°C). Duration 0, 2, 4, 6, 8, and 10 Weeks (left to right) [53].

Reproduced with permission.

2.2. PHA Synthesis, General

Certain microbes synthesize PHA in stressful environmental conditions as a means of survival, analogous to humans storing adipose tissue. The 'stress' responsible for PHA accumulation is primarily attributed to an absence of essential growth nutrients or to an exposure to a superabundance of carbon substrate. PHA synthesis can be achieved in pure-cultures and MMC, alike; however, the 'protocol' of imposed environmental pressure differs with culture complexity. In the literature, three engineered techniques for inducing microbial stress and subsequent PHA accumulation have been developed: anaerobic feeding (absence of an external terminal electron acceptor), controlled-growth feeding (nutrient deprivation), and aerobic dynamic feeding (intermittent carbon oversupply). Each is discussed in further detail below.

2.2.1. Anaerobic PHA Synthesis

In the context of engineered environments, PHA storage by MMC was originally observed in an enhanced biological phosphorus removal (EBPR) system [55]. In an EBPR system, activated sludge (biomass) is recirculated through anaerobic, anoxic, and aerobic zones, principally to remove nitrogen (N) and phosphorus (P) [56]. The MMC is first introduced in the anaerobic stage where the highest concentration of readily biodegradable carbon (VFAs) exist. With an absence of oxygen, nitrate, or nitrite as a terminal electron acceptor, ordinary

cellular function and growth is inhibited; thus, microbes capable of storing VFAs as PHA are provided a competitive advantage for survival. In the subsequent aerobic stage, stored PHA is used for growth and secondary storage reserves [29].

EBPR stability and reliability is reliant on proper enrichment of a group of microorganisms called phosphorus accumulating organisms (PAOs). These bacteria are able to uptake and store soluble P as polyphosphate, resulting in bulk solution P removal following solids separation [56]. Relevant to this thesis, PAOs leverage polyphosphate and glycogen stores to synthesize PHA. Conversely, glycogen accumulating organisms (GAOs), a PHA-synthesizing bacterium commonly enriched in EBPR systems, use solely glycogen as a secondary energy reserve and do not contribute to P removal. Increased GAO populations can outcompete PAOs for carbon, resulting in deteriorated EBPR; however, GAOs can obtain higher PHA yields [56].

PHA accumulation in EBPR systems is ultimately limited by low concentrations of VFAs inherent in raw wastewater. However, an increase in PHA storage, relative to that realized in the EBPR process, can be achieved when a portion of biomass is transferred to a separate accumulation reactor and exposed to an extended period of anaerobic or aerobic VFA feeding [57]. Anaerobic operation of said accumulation reactor is limited by initial concentrations of secondary storage products (polyphosphate and/or glycogen), as the microbes cannot perform respiration to fulfill further energy requirements for continued VFA uptake. Conversely, aerobic operation induces PHA storage through carbon oversupply; metabolically, however, the PHA synthesis response might be different than the MMC realizes in the EBPR process scheme. Of the two, aerobic operation has been shown to be superior, albeit with PHA accumulation levels warranting researchers to focus on other accumulation technologies [29, 58]. A proposed process for optimized implementation of a PHA-accumulation stage at existing treatment facilities is shown in Figure 2.3; however, research on the viability of this method is ongoing [59-61].

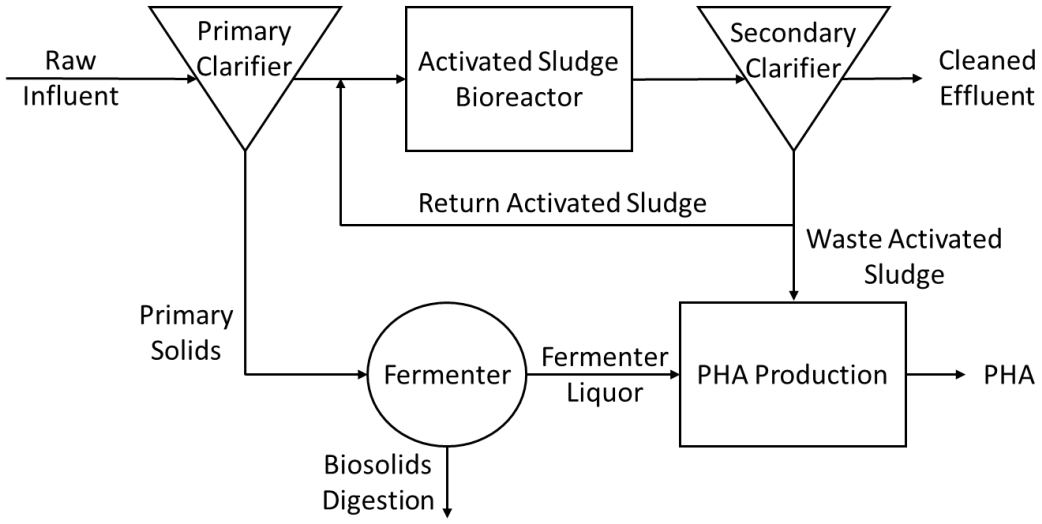

Figure 2.3: Proposed Wastewater Facility PHA Production Process [50].

Originally adapted from [62].

Reproduced with permission.

2.2.2. Controlled-Growth Feeding PHA Synthesis

Following the discovery of PHA-synthesizing bacteria in MMC, researchers directed their attention towards identifying and exploiting PHA-accumulating species and genera. This strategy was founded on the idea that pure cultures of known PHA-accumulators could be more tightly controlled to produce higher quantities of PHA than achievable by MMC [63, 64]. To date, over 300 unique PHA-synthesizing microorganisms have been identified [65]; additionally, the PHA production potential of promising pure-cultures has been extensively assessed at the industrial and laboratory level [66].

Pure-culture PHA production under a controlled-growth strategy is almost universally performed using a two-stage process [63]. In the first stage, a pure-culture known to exhibit high PHA accumulation is grown aerobically and fed high purity substrate, commonly glucose or sucrose [29]. The culture is allowed to grow without nutrient limitation until achieving critical mass, thereafter, the second or nutrient limitation stage is imposed. In the nutrient limitation stage, the microbes are deprived of nitrogen or phosphorus; thus, a lack of essential nutrients inhibits growth and forces the microbes to convert carbon into PHA. Under this operational strategy, cultures have been shown to reach intracellular PHA concentrations of 90% on a weight basis [53].

The polymer yield obtained from employing a controlled-growth feeding strategy is nothing short of exceptional; however, high costs associated with maintaining a pure culture (energy for sterilization) and procuring impurity-free substrate eliminate it from contention with cheaper petro-plastics [29, 63]. Moreover; the process' sterilization practices do not allow the use of organic-rich waste streams as substrate.

2.2.3. Aerobic Dynamic Feeding PHA Synthesis

Following lackluster pure-culture viability, investigations of potential alternative PHA production processes aimed at reducing polymer production costs narrowed on MMC systems; reason being, MMC systems can use a variety of low cost complex substrates and do not require sterilization [29]. In 1996, Majone et al. [24] discovered that biological systems exposed to alternating states of VFA excess and VFA absence, under fully aerobic conditions, select for a culture dominated by floc-forming PHA-accumulating organisms, rather than filamentous bulking organisms; however, some filamentous bacteria enriched in ADF systems (e.g. Meganema) have PHA-synthesizing capability [67, 68]. This metabolic response, coined 'feast-famine', is associated with the characteristic cyclical feeding of an engineered ADF environment [23, 50]. Contrary to anaerobic and controlled growth feeding (described above) where PHA storage is driven by inhibiting growth, ADF PHA accumulation is induced by providing excess external substrate (VFAs) [38].

Under ADF conditions, the F-F response results in the majority of carbon (VFAs) being stored as intracellular PHA rather than being used for growth, despite excess availability of requisite nutrients [1]. To take this phenomenon into account, it is hypothesized that the bacteria have a reduced metabolic capacity (rRNA or enzyme deficiency) after the famine phase, subsequently, leading to inhibited growth in the feast phase. Therefore, when excess carbon is introduced, the microbes cannot grow at their maximum rate and compensate by storing PHA. This metabolic behavior, referred to as an 'overflow metabolism' causing 'energy spilling', has been observed by microorganisms exposed to a wide array of environmental factors [69-71]. In the famine phase, stored PHA acts as a buffer for substrate, allowing the microbes to grow and sustain populations without an external carbon source for a prolonged period of time. Furthermore, the metabolic capability of storing PHA provides a competitive advantage over non-storing

microorganisms, leading to an enriched culture under ADF conditions. A typical F-F response is depicted in Figure 2.4.

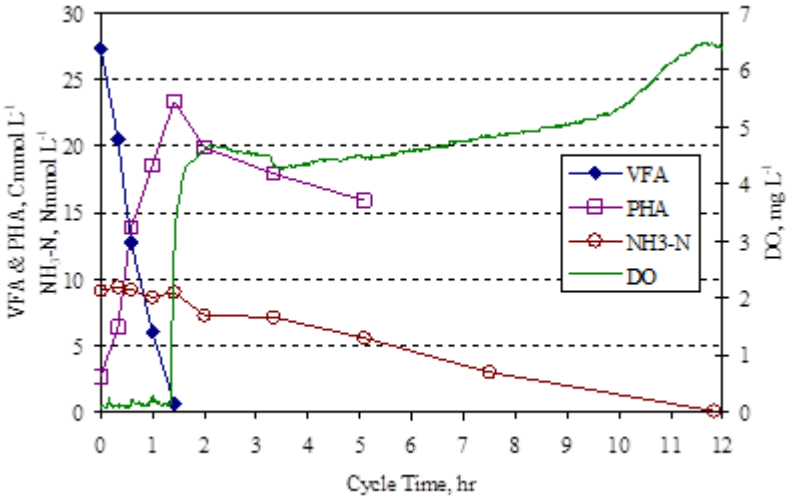

Figure 2.4: Typical Feast-Famine Response [1]

Reproduced with permission.

In theory, ADF configurations can be fed any organic-rich waste stream; however, VFAs are required in the feedstock as they are the direct pre-cursors to PHA and can be readily consumed and converted [28]. Contrary to pure cultures, other forms of carbon (e.g., carbohydrates, alcohols) do not accumulate as PHA in MMC. By providing primarily VFAs, populations of non-storing 'flanking' microorganisms, broadly referred to as Ordinary Heterotrophs (OHOs), are restricted from consuming substrate and minimized in a Darwinian way from the system. In order to maintain the dynamic conditions that promote PHA accumulator enrichment, ADF conditions are almost exclusively obtained with SBRs. A typical SBR cycle occurs in the following stages: substrate addition, reaction (e.g., feast, famine), wasting, settling, and decant.

2.3. PHA Synthesis by a MMC

To date, commercial PHA production employs a controlled-growth strategy (described above) using pure-cultures fed synthetic substrate – most commonly pure sugars refined from corn [21]. These systems reliably achieve high intracellular PHA yields (> 80%); nevertheless, costs arising from substrate procurement and maintaining axenic conditions result in PHA costs being 3-9x that of polypropylene and polyethylene by weight [21, 27]. Initially

supported by the results of Serafim et al. [27], who observed PHA accumulation in upwards of 65% using a MMC under ADF conditions, the production of PHA from MMC systems has become a promising avenue for decreasing commercial PHA production costs [27, 72]. For MMC systems using existing waste streams, the costs associated with substrate refinement and sterilization are relatively negligible; however, research has elucidated several limitations of using MMC fed complex substrates, primarily reduced intracellular yield and low PHA-producing biomass concentration.

Reported peak intracellular PHA accumulation for MMC systems operated under ADF conditions are highly variable ranging from 8% [72] to 89% [73]; comparatively, commercial production facilities using pure cultures and substrates consistently achieve greater than 80% accumulation [21]. Low PHA content and other inefficiencies associated with carbon being utilized for growth rather than storage and/or increased OHO populations effectively skyrocket production costs by requiring increased extraction duration and chemical usage. To give a frame of reference, it has been shown that an increase in intracellular PHA content from 50% to 88% can lower recovery costs from 4.8 to 0.92 $/kg [74]. Operation of a MMC system should be markedly tailored to achieve high intracellular PHA content as it is essential for commercial economic feasibility.

Relevant to PHA content, the productivity of PHA production systems is dependent on the concentration of active biomass. In commercial production operations, performed in batches, cell concentrations at the point of harvest are typically greater than 100 gTSS/L [74]. Conversely, municipal activated sludge systems, representative of the biomass accumulation potential for MMC systems, operate between 3 and 10 gTSS/L [75]. While it is suggested MMC systems operate at similar biomass concentrations to pure-culture systems for economic viability, it is not possible when using substrates with impurities. Feeding of VFA-rich waste feedstock in theoretical quantities to beget pure-culture biomass concentrations would drastically reduce PHA content by adding inert material and slowly biodegradable carbon; moreover, the required footprint and associated operational consequences (e.g. foaming) further deny feasibility. Fortunately, this large disparity in achievable biomass concentrations can potentially be relieved by MMC systems operating continuously, and thus offsetting productivity differential.

2.4. Metabolic Pathways of PHA Synthesis

Achieving optimal PHA synthesis demands a fundamental understanding of PHA-producing prokaryotes' metabolism. A cell's metabolism is the total of chemical and physical interconversions in a cell [76]. With the extraordinary number of enzymes in each cell, it is useful to map the cell's metabolism via a metabolic pathway. To this end, the specific pathways enzymes in a MMC fed complex waste feedstock use remains uncertain, thus research efforts have focused on describing metabolic pathways based on pure-cultures fed synthetic substrates. Without properly elucidated pathways for MMC, it can be assumed that process descriptions of MMC can be approximated by those described using pure cultures, in this case *R. eutropha* [4]. PHA synthesis can occur via four unique pathways [3]; however, an extensively studied three-step pathway presented in Figure 2.5 represents PHA synthesis from common VFAs in *R. eutropha*. For the metabolism of low molecular weight compounds, the major metabolic pathways are glycolysis, the pentose phosphate pathway, the citric acid cycle (e.g. TCA cycle), oxidative phosphorylation, fatty acid degradation and synthesis, gluconeogenesis and glycogen breakdown and synthesis [76]. For simplicity, metabolic pathways involved with PHA synthesis are separated into four processes: VFA activation and conversion, PHA synthesis, intracellular degradation of PHA, and the catabolic oxidation of metabolic intermediates.

2.4.1. VFA Uptake and Activation

The method of VFA transport across the microbial cell is not fully understood; however, due to the size and lipid solubility of VFAs in un-dissociated form, it is presumed to occur primarily through passive diffusion [77]. As intracellular pH is higher than the pKa for organic acids (4.7 to 4.9), acid-base equilibrium disassociates a portion of the permeated acid, resulting in the production of excess intracellular protons [78]. To maintain proton motive force (PMF), the cell is required to expel the excess protons at the expense of Adenosine Triphosphate (ATP) [79]. The ATP cost associated with VFA uptake is difficult to estimate as it is a function of the pH gradient across the cell membrane and external VFA characteristics; generally, it is assumed that one mole of ATP is required for the uptake of one mole of VFA [80].

Following transport, intracellular VFAs are activated through esterification with available Coenzyme-A (CoASH), resulting in a corresponding alkyl-CoA [7]. Activation to an alky-CoA allows the molecule to access a suite of metabolic pathways depending on VFA size, as shown in Figure 2.5 and Figure 2.6. Larger VFAs (4 carbon or greater) can enter the β-oxidation pathway to be broken down into shorter alkyl-CoAs. This cyclic process cleaves two carbons every cycle to form acetyl-CoA; for odd carbon VFA, the last cycle will form one acetyl-CoA and one propionyl-CoA. While VFA uptake is passive, activation requires CoASH and an additional mole of ATP per mole of VFA [40]. Similarly, β-oxidation consumes CoASH, but generates reducing equivalents in the form of nicotinamide adenine dinucleotide (NAD) plus hydrogen (H), NADH, and flavin adenine dinucleotide (FAD) plus two H, $FADH_2$.

In literature, it is common for models and metabolic diagrams to represent all reducing agents ($NADH + H^+$, $NADPH + H^+$, $FADH_2$) as NADH. This approach is valid when performing simple metabolic analysis as all the carriers have a power of 2 reducing equivalents (hydrogen atoms) [81].

2.4.2. Tricarboxylic Acid Cycle and Oxidative Phosphorylation

The tricarboxylic acid (TCA) cycle is a metabolic pathway used by most aerobic heterotrophs to meet energy production needs (i.e., ATP). The TCA cycle is responsible for oxidizing acetyl-CoA to CO_2, and as a result, phosphorylates ADP to synthesize ATP and transfers reducing equivalents to NAD^+, $NADP^+$, and FAD [7]. In short, the energy inherent in the acetyl-CoA molecule is captured by stripping electrons from the molecule and oxidizing it to carbon dioxide. The full cycle, depicted in Figure 2.6, results in two moles of CO_2, three moles of $NADH/H^+$, and one mole of $FADH_2$. As shown, propionyl-CoA can also be oxidized in the TCA cycle by entering the succinyl-CoA pathway [82, 83]. The transformation of propionyl-CoA to succinyl-CoA is a three-step process that consumes ATP [83]; furthermore, it lends itself as one of the five possible ways propionyl-CoA is decarboxylated to acetyl-CoA, as evidenced in cultures fed propionic and valeric acid [26]. Without inhibition, the TCA cycle will continuously produce reducing equivalents to facilitate respiration, or oxidative phosphorylation, in the next step.

Oxidative phosphorylation is a mitochondrial process in which ATP is produced via the transfer of electrons from NADH or $FADH_2$ to O_2, accounting for the large majority of aerobic microorganisms' energy production [84]. Briefly, electrons produced from the TCA cycle are transferred by protein complexes embedded in the mitochondrial inner membrane to the terminal electron acceptor, oxygen, to form H_2O [84]; meanwhile, hydrogen ions are being pumped outside the membrane. This uneven distribution of protons generates a transmembrane electrical potential resulting in PMF [84]. Finally, the enzyme, ATP synthase, creates ATP by collecting energy dissipated from hydrogen being passively transported back into the membrane, and thus restoring equilibrium [85].

The amount of ATP generated from oxidative phosphorylation is dependent on the degree of PMF (how many hydrogen ions are pumped out of the membrane) and how efficient the ATP synthase enzyme is in energy collection. Moreover, this energy yield has been shown to vary significantly by carbon source used for culture enrichment [40]. In modeling aerobic systems, this energy yield is termed the P/O ratio, denoted as δ, and has units of mole ATP per mole NADH or $2e^-$. While the theoretical maximum P/O is around 3 [40], values obtained in biological systems are in generally in the range of 1.5-2.5 mole ATP/mole NADH [37, 85, 86].

2.4.3. Growth and Maintenance

Microorganisms primarily generate ATP for growth and maintenance. Growth, commonly referred to as anabolism, is the formation of new biomass. For activated sludge systems, the assumed elemental composition of active biomass is $C_5H_7NO_2$ [75]; however, for MMC subjected to ADF conditions a biomass composition of $CH_{1.8}N_{0.2}O_{0.5}$ is commonly assumed [37, 42, 87]. Anabolism requires energy, principally from a carbon and electron source yielding ATP, and a nitrogen source. In the context of this work, growth is facilitated by VFAs providing carbon and electrons and ammonia as the nitrogen source.

Maintenance is defined as the energy demand for all essential processes not related to growth [86]. In modeling, maintenance is used as a catch-all term for ATP utilized absent of growth and substrate uptake. Hence, if the P/O ratio and maintenance term are theoretically known, an ATP balance summing to zero could be performed on a PHA-synthesizing metabolism [88, 89].

2.4.4. PHA Synthesis

The term PHA encapsulates a variety of monomers, with the distribution thereof being dependent on the VFAs available to the microorganisms. Figure 2.5 and Figure 2.6 illustrate the potential metabolic pathways of PHA production from common VFAs [1]. First, PHA production begins with VFA uptake and activation, as described above, requiring CoASH and ATP. The resulting alkyl-CoA precursors are then condensed by β-ketothiolase to form a 3-ketoacyl-CoA compound, liberating one CoASH in the process [90]. Once condensed, the 3-ketacyl-CoA molecules are reduced by acetoacetyl-CoA reductase, requiring NADPH, to generate the corresponding 3-hydroxyacyl-CoA [6]. Lastly, PHA synthase incorporates the 3-hydroxyacyl-CoA into the polymer, thereby liberating the remaining CoASH [91].

Acetic acid, typically the most abundant VFA, is activated directly to acetyl-CoA; β-ketothiolase then condenses two units of acetyl-CoA to form the 3HB precursor acetoacetyl-CoA [92]. Cultures grown on acetic acid will only produce P(3HB), with polymer content sharing a positive relationship with acetate concentration of the medium [93]. Propionic acid is activated directly to propionyl-CoA, giving rise to three possible precursors [29]. Two molecules of propionyl-CoA can condense to poly-3-hydroxy-2-methylvalerate, the direct precursor to P(3H2MV) [29]; additionally, propionyl-CoA can be decarboxylated to acetyl-CoA, for which the junction of both molecules, acetyl and propionyl-CoA, can generate P(3HV) or P(3H2MB) [26, 29, 93]. Butyric acid can either be directly condensed to the 3HB precursor acetoacetyl-CoA or form two acetyl-CoA molecules via β-oxidation. Similarly, valeric acid can generate the direct precursor for 3HV or can form one acetyl-CoA and one propionyl-CoA following β-oxidation [94]. While cultures fed butyric acid solely beget PHB, valeric acid can generate combinations of 3HV and 3HB yielding PHBV [94]. Organic acids larger than valeric acid are capable of yielding PHA via β-oxidation; however, caproic acid and other fermentation products exist in low concentrations, and thus have negligible impact on polymer composition.

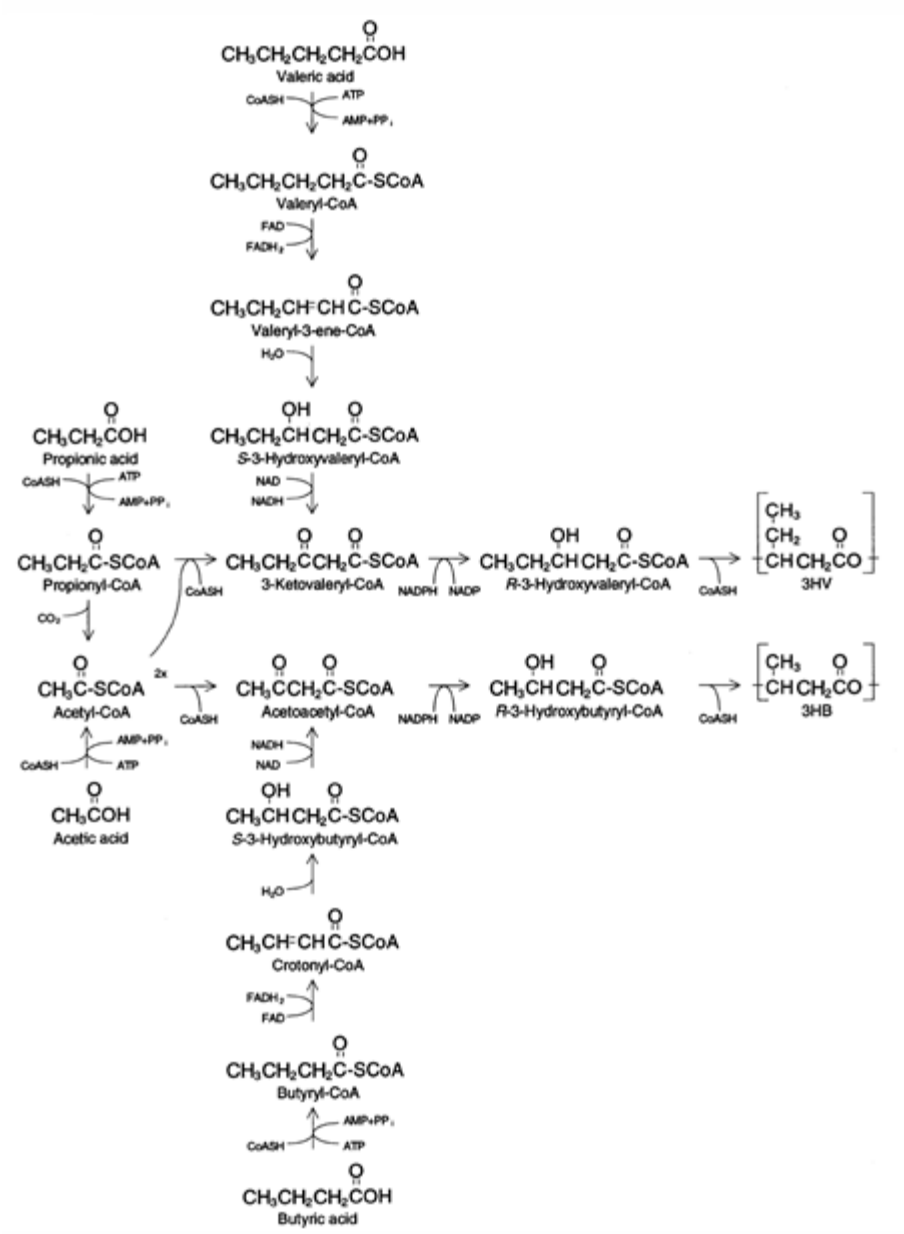

Figure 2.5: PHA Synthesis from common VFAs.

Adapted from [8].

Reproduced with permission.

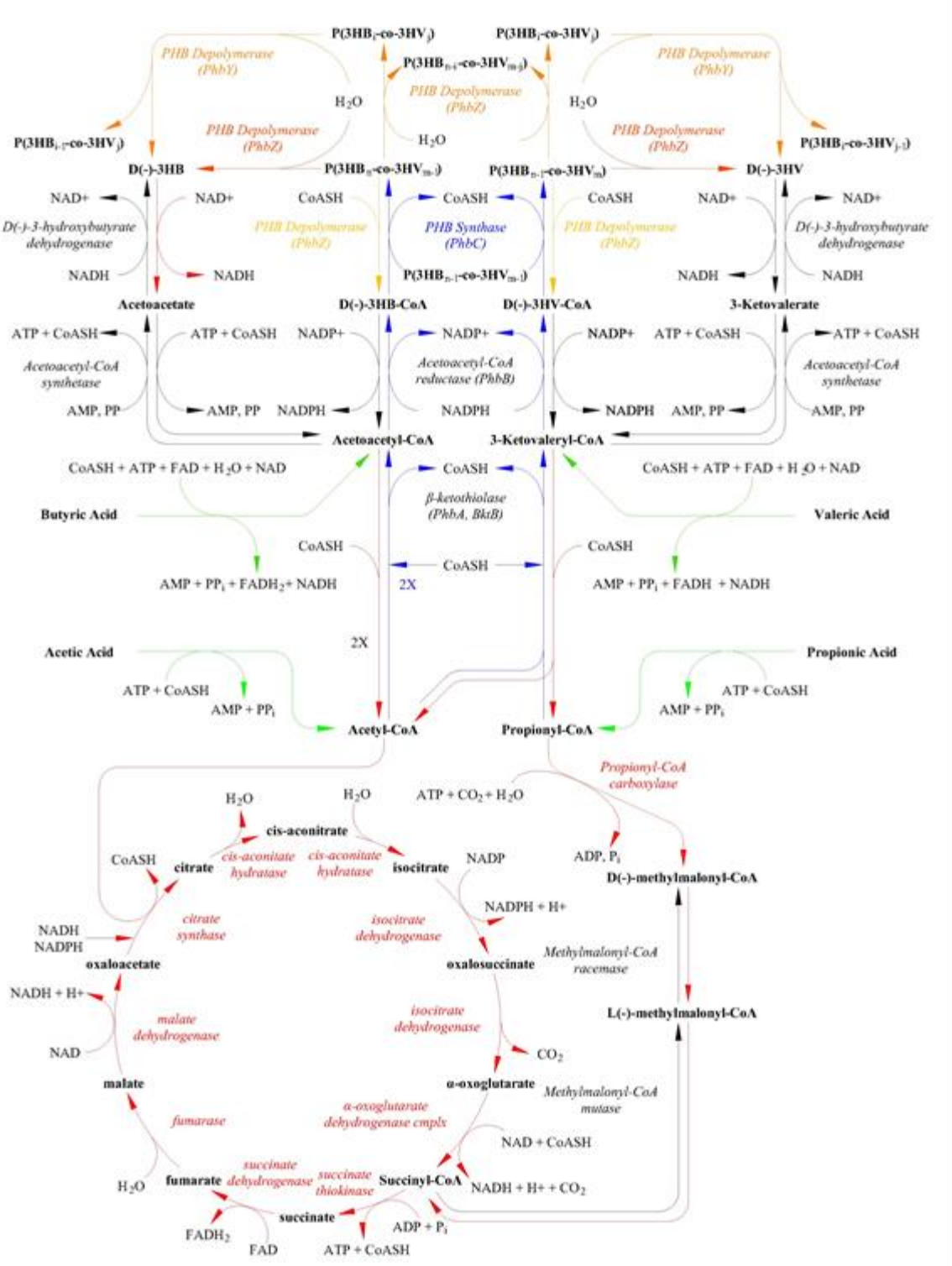

Figure 2.6: PHA Metabolisms and Regulation in Ralstonia Eutropha.

Created by [1], synthesized from [2],[3], [4], [5], [6], [7], [8].

Reproduced with permission.

2.4.5. Intracellular Degradation of PHA

The function of intracellular PHA stores in bacteria is to provide nutrients for energy and carbon metabolism in phases of starvation [95]. While extracellular PHA depolymerization is well researched, intracellular degradation has received little attention due to the difficult nature of analyzing isolated PHA granules in vitro [95]. That being said, three intracellular degradation pathways, as shown in Figure 2.6 (red-orange, orange, gold), have been elucidated.

For the context of this research, the original pathway based on the work of Senior and Dawes [2], shown in red-orange (Figure 2.6), sufficiently describes the conversion of stored PHA to metabolites that can be repurposed as energy. First, stored polymer is hydrolyzed by PHA depolymerase, PhaZ, thereby releasing 3HB. The released 3HB is then oxidized to acetoacetate by D(-)-3-hydroxybutyrate dehydrogenase, transferring reducing equivalents from NAD+ to NADH; furthermore, the acetoacetate is thiolyzed with CoASH by Acetoacetyl-CoA synthase, requiring ATP. Following the reverse condensation of acetoacetyl-CoA to acetyl-CoA, production of acetyl-CoA provides the cell a means of energy generation through catabolism, or simply put, the TCA cycle. The depolymerization of 3HV to propionyl-CoA follows the same general process. Further details regarding intracellular polymer degradation and other described metabolic processes are discussed in the following metabolic model chapter.

2.5. Three-Stage ADF Operations

Since the seminal work of Majone et al. [24], our knowledge of PHA-producing culture selection and metabolism has expanded immensely from numerous lab-scale ADF investigations. The majority of ADF studies have utilized synthetic substrates, ammonium, and other trace nutrients [23, 26-28, 37, 38, 87, 96, 97]. Understanding that substrate is one of the primary costs in PHA production [65], the use of synthetic medium at full-scale becomes rather unfeasible. As a remedy, complex waste streams in lieu of synthetic medium and pure cultures are used in a three-stage PHA production process [23]. This process has been shown to elicit high PHA storage yields and intracellular PHA content from waste substrates [62, 98]. A schematic of a three-stage PHA production process utilizing dairy waste is shown in Figure 2.7; the solids separation step is tailored to dairy manure, although ADF configurations

are comparable regardless of substrate, and solids separation would be required when solids-rich organic matter is used.

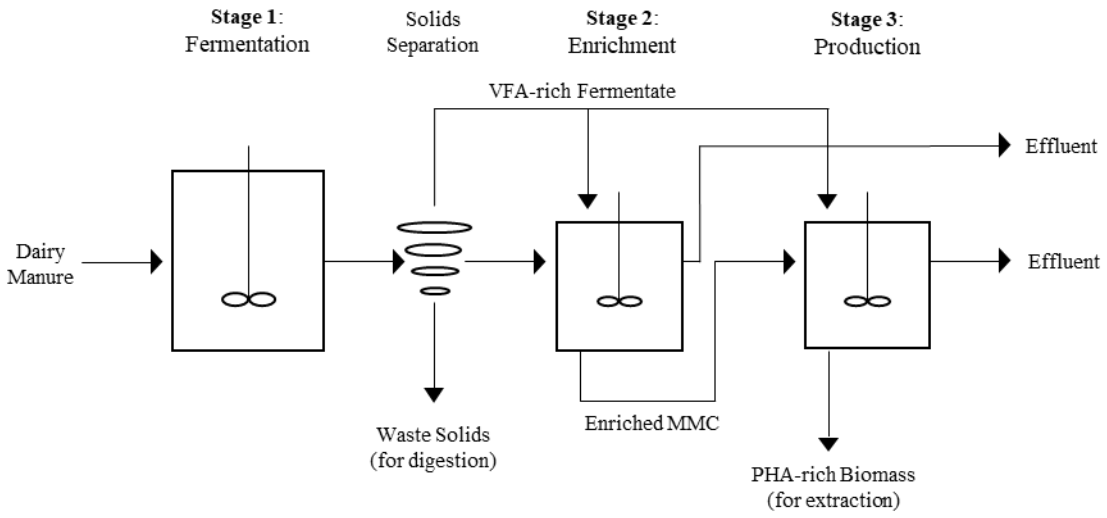

Figure 2.7: Dairy Manure Fed Three-Stage PHA Production Process Schematic

In the first stage, acidogenic fermentation converts the biodegradable waste (e.g., dairy manure) into carboxylic acids (VFAs), the preferred carbon source for feast-famine driven PHA storage [99]. This stage can be viewed as independent from the other two, yet can decide the maximum MMC enrichment and PHA storage capacity, as it provides the readily biodegradable carbon used downstream. Low VFA yield can become the three-stage process' limiting factor; additionally, the distribution of VFAs can have a pronounced effect on polymer characteristics in the later stages. Optimization of the fermentation stage has been extensively studied, including the evaluation of relevant substrate [100, 101], and involves maintaining a low SRT (< 5 days), thereby limiting the growth of methanogenic bacteria (and ultimately the consumption of VFAs) [102].

The second stage of the process is culture enrichment. Here the MMC is subjected to ADF conditions, consequently inducing F-F metabolism and enriching for and producing MMC with high storage behavior. Typically, culture enrichment, and the selective pressure thereof, is accomplished in an SBR subjected to periodic feeding (feast and famine conditions) [23, 27, 30, 37, 73, 97, 98, 103]; however, similar enrichment capabilities have been shown in two-stage continuous stirred tank reactor (CSTR) configurations [35, 104, 105]. The latter

configuration uses separate CSTRs for the feast and famine phase, with selective pressure controlled by HRT.

The third and final stage is the production stage. Excess sludge (enriched biomass), usually the decanted volume produced from the enrichment stage, is leveraged in a batch accumulation reactor. The batch reactor, or production reactor, is operated at a significantly higher organic load in order to saturate the biomass PHA storage capacity and achieve an extended ‘feast’ [23]. Once PHA saturation is achieved, the PHA-rich biomass is recovered for either an extraction phase [106], or directly as an end product for composite material manufacturing [62]. So long as substrate and a terminal electron acceptor (e.g., oxygen or nitrate [68]) are provided in excess, the biomass will accumulate higher intracellular PHA concentrations compared to the enrichment stage. However, substrate feeding must be closely monitored, as high VFA concentrations can have an inhibitory effect on PHA storage [27]. For this reason, substrate has been most-commonly supplied in pulses, begetting near zero substrate concentrations between pulses [28], yet the same goal can be achieved using continuous feeding [50, 89].

A three-stage ADF configuration is, for all intents and purposes, the primary process employed for PHA production using MMC and complex waste substrates, as each stage serves a unique and necessary purpose. Advantageously, the integrated process inherently allows the independent optimization of each stage; however, with the production inocula being sourced from the enrichment stage, the degree of culture enrichment can have powerful implications on downstream PHA accumulation performance [89]. While the basic process mechanisms for culture enrichment are well studied, operational criteria for maximizing PHA production are far from being conclusively defined. This lack of understanding is only further magnified when applying MMC systems using differing complex feed sources. Further research focused on the development of optimized ADF operational criteria could prove significant in improving commercial PHA production and its economic viability.

Specific to an SBR, the major operational parameters for an enrichment culture under ADF conditions are: solids residence time (SRT), cycle length (CL), organic loading rate (OLR), and terminal electron acceptor levels. However, research efforts should focus primarily on SRT and OLR, as they have the largest effect on selective pressure and PHA accumulation,

while being operationally simple to adjust. Minor operational parameters that are more complex to control with limited influence on process performance include: temperature, pH, and carbon to nitrogen ratio (C/N).

2.5.1. Solids Retention Time (SRT) and Cycle Length (CL)

SRT represents the average time a microbe remains in a system, typically defined by the amount of biomass in a system divided by the amount of biomass exiting the system per day. Hence, a larger SRT results in increased biomass within a system (as less biomass is removed from the system), creating a more robust and consistent MMC, as microbes unable to sustain themselves are washed out of the system. However, increased SRT can also lead to the accumulation of dead biomass and ash/minerals. From conventional microbial theory, a shorter SRT equates to higher growth rates. Applying the same logic to ADF-driven PHA-accumulating MMC, this would imply less substrate is stored as PHA as it is used primarily for growth [28]. This notion was confirmed experimentally by Beun et al. [37] and Carta et al. [107], who observed an SRT > 2 days resulted in PHA storage independent of growth rate (and SRT), while SRTs below this threshold shared a pronounced inverse relationship with PHA yield and productivity. Conversely, while longer SRTs appear advantageous, operationally there becomes a point where increasing SRT begets diminished returns. At too large of SRTs the metabolic activity of the biomass can decrease, resulting in a less active microbial population [102]. Moreover, as the SRT increases, the relative fraction of inert suspended solids (e.g. minerals) increases, and thus this disparity can result in a lower potential PHA fraction on a TSS basis. As a case in point, SRT investigations by Chua et al. [108] showed a 10% decrease in intracellular PHA content when operating at a 10 day versus a 3 day SRT. Nevertheless, despite suggested evidence that the SRT should exceed 2 days, in much of the ADF literature an SRT of 1 day is a common design value on the basis a higher percentage of active biomass results in higher intracellular PHA yields [97, 99, 109]. Ultimately, the lack of consensus on an optimal SRT remains.

Operationally associated with SRT is the cycle length (CL), which is the duration of one complete feast and famine cycle. The effect of the CL:SRT ratio on PHA accumulation has only been sparsely studied, and values have varied substantially across ADF investigations, from 0.04 to 0.5 [23, 27, 37, 73, 97, 99, 103, 110, 111]. However, the CL:SRT ratio

(day/day) has been established as a key operational criteria related to increasing intracellular PHA content in the feast phase [112]. The parameter gained significant attention when the maximum reported intracellular PHA content of 89% was achieved using a CL:SRT of 0.5, the ‘upper limit’ of CL:SRT values [73]. Further investigation of CL:SRT in comparable systems yielded similar results, with higher intracellular PHA content (> 70 wt%) being observed in larger CL:SRT operations [112]. With increased CL and constant SRT, the amount of substrate fed per cycle and the length of the famine phase increase; as a result, more substrate per individual microbe is consumed and a higher degree of selective pressure is imposed, hence, increased PHA storage capacity. Currently, the effects of CL:SRT on ADF metabolism are strictly empirical derivations, and implications for full-scale PHA production requires further study.

2.5.2. Organic Loading Rate (OLR)

The organic loading rate (OLR) is the concentration of organic matter (e.g., VFAs) applied to the MMC, reported on a per day or per cycle basis. In a ‘utopian’ ADF system, the amount of polymer produced is simply a function of substrate supplied [28]. Indeed, a linear relationship between OLR and the quantity of PHA produced was observed by Serafim et al. [27], Dionisi et al. [96], and Beun et al. [37] within ranges of 0.9-2.7, 1-8, and 0.18-1.44 g/L, respectively. Increasing OLR raises the amount of active biomass within a system, as more carbon is available to support a larger population. Within the aforementioned ranges, although variable, the results suggest an increase in biomass proportional to OLR with no change in storage kinetics.

In F-F metabolism, operating at a high OLR can have adverse effects on PHA accumulation. Generally, as OLR increases the famine phase duration decreases; as a result, the MMC can become less reliant on storing PHA due to reduced environmental stress. This shortcoming of operating at a high OLR was observed by Dionisi et al. [97], where PHA storage decreased significantly at OLRs higher than 17.6 g/L-h.

2.5.3. Feast-Famine Ratio (F-F Ratio)

Herein the F-F ratio is defined as the proportion of the feast phase duration relative to the famine phase duration, within a single cycle (hr/hr); however, a lack of a unanimous definition of feast and famine amongst researchers adds variability in reported ratios. The

transition between feast and famine phases has been defined in literature as: a sharp rise in dissolved oxygen (DO) concentration, complete VFA uptake from bulk solution, or as complete degradation of stored PHA. Nonetheless, a small F-F ratio (< 0.25) is required for a successful 'feast' PHA response. At low F-F ratios, the growth rate for non-PHA storing microorganisms required to sustain themselves becomes too large, effectively washing them out and creating a highly enriched PHA-storing population [89].

Control of the F-F Ratio is quite difficult, if not impossible, as it is a function of SRT, CL, and OLR, all of which are interdependent operational criteria. Therefore, the F-F ratio can be viewed as quantification of a metabolic response rather than an operational parameter. Independent of OLR, the F-F ratio can be reduced by increasing the CL to SRT ratio and resultant famine phase length. For a constant CL to SRT ratio, Albuquerque et al. [103] found increasing the OLR can nominally increase the F-F ratio, although at high organic loading the nutrient limitation caused biomass concentrations to increase disproportionally to OLR. Conversely, Dionisi et al. [97] found that higher OLRs resulted in shorter famine phase durations and larger F-F ratios; furthermore, increases in F-F ratio yielded lower PHA accumulation, principally due to reduced selective pressure in culture enrichment.

In ADF systems it is well understood that the F-F ratio is an indicator of the metabolic stress realized by MMC; moreover, minimization of the F-F ratio intensifies the selective pressure for PHA-accumulating microbes [103]. For limiting a growth response, a maximum F-F ratio of 0.25 was experimentally determined by Dionisi et al. [97]; alternatively, the findings of Jiang et al. [112] suggest a more conservative maximum of 0.20. The reason an upper limit is reported, rather than an optimal F-F ratio, is because F-F ratios below said maximum do not necessarily follow the 'lower is better' assertion. For instance, Jiang et al. [112] observed a decrease in PHA accumulation from 90 to 82 (wt%) when the F-F ratio was decreased from 0.10 to 0.05.

2.5.4. Supply of a Terminal Electron Acceptor

With ADF systems being wholly aerobic in the enrichment and production stage, oxygen is the primary terminal electron acceptor, however, at low dissolved oxygen (DO) concentrations facultative heterotrophs may also use nitrate and/or nitrite, particularly during the 'feast' period [68]. In an effort to ensure DO levels are not rate-limiting on VFA uptake

and storage, ADF systems are typically supplied aeration in excess [1, 73]. In this case, aeration kinetics can be reported as the volume of air provided per reactor volume or as a range of DO concentrations [1, 113]; however, in situations where the aim is to reduce operational costs of aeration, more accurate estimation is required.

Aeration or oxygen transfer rate (OTR) is typically quantified by a process' volumetric mass transfer coefficient, k_La, and oxygen concentration measurements (DO). This method has its limitations, as it is heavily reliant on proper DO probe calibration and correct measurement of k_La. Reactor k_La is determined based on evaluation of water quality, reactor geometry, mixing characteristics, and the oxygen delivery system (e.g. diffuser type) [114]. Studies on the effects of k_La on PHA storage are limited. Third et al. [87] showed that, for synthetic medium, reduced k_La (aeration) resulted in higher PHA yield on substrate. This suggests that minimizing oxygen supply rates effectively promotes PHA storage rather than growth, as the availability of reducing power is decreased. Conversely, research on real waste substrate indicated no statistical difference between k_La and carbon uptake and storage kinetics [115, 116].

2.5.5. Minor Operational Parameters

Temperature, pH, and nutrients, particularly the ratio of carbon to nitrogen (C/N), represent secondary operational parameters that are more complex to control. Often times controlling these parameters also adds unnecessary complexity and operation costs to a system [110]. An evaluation by Fang et al. [117] on the influence of operational parameters ranked the influence of each parameter studied: pH > substrate concentration (COD) > influent N concentration = influent P concentration; while a similar study by Mohan et al. [118], ranked the following parameters: microenvironment > pH > glucose > phosphorus > nitrogen > acetate = propionate = butyrate > iron > other VFAs.

PHA production is suggested to be sensitive to initial culture pH [119]. It is hypothesized, at low pH conditions (< 4.75), VFAs remain in an undissociated form in order to maintain biomass intracellular pH at equilibrium [108]. Research by Chua et al. [108] suggests this phenomenon can occur at a higher pH, between 6 to 7, and results in negligible PHA accumulation; the authors go on to recommend a pH ≥ 8. Similarly, Dionisi et al. [99] reported that maximal biomass activity and PHA storage occurred in a pH range of 7.5 to 8.5,

with a significant decrease in productivity below 7. A large amount of studies suggest peak PHA production occurs at a pH range of 8.0 to 9.0 [27, 99, 108, 111, 120]; however, reported optimal pH ranges for ADF PHA production utilizing MMC are contradictory. A pH range of 6.0 to 7.5, preferably 7.0, is suggested as optimal due to PHA enzymes being more active at a neutral pH [118, 119]. This variance in pH across studies can be attributed to differences in MMC characteristics and enrichment conditions; more importantly, it suggests less importance be put on pH control at full-scale. Legacy ADF PHA production research on dairy manure have not sought to exert pH control [1, 50, 89, 116], principally because dairy manure contains such an excess of alkalinity that any attempts to control alkalinity would demand excess chemicals and would be completely unrealistic. Ultimately, dairy manure-based operations consistently operate at a pH range of 8.0-8.6.

Nutrient concentrations, specifically nitrogen (N) and phosphorus (P), have been shown to influence PHA production, although principally in non-ADF systems. It is suggested that under conditions of nutrient excess, substrate is preferentially used for growth [72]; moreover, N- or P- limitation has been shown to increase PHA production [30]. Conventional theory suggests N-limitation restricts the potential for growth by decreasing protein synthesis and associated enzymatic activity [121]; similarly, increased PHA accumulation observed with P-limitation is thought to be a result of restricting the TCA cycle [122]. While studies implementing N-limitation generally affirm higher overall PHA accumulation, culture enrichment and PHA storing kinetics are suggested to improve in non-limiting N concentrations [30, 99]. Nutrient concentrations are important to consider in ADF processes; however, most waste substrates are very nutrient-rich, therefore limitation of N or P is not feasible.

2.5.6. Overview of Major Operational Criteria

A comparison of key operating parameters for culture selection under ADF conditions for a variety of feed types is shown in Table 2.1. The selection of studies is not comprehensive, but representatively shows the variability, or lack thereof, between operational criteria for both synthetic and complex waste mixture fed PHA production systems. Reported OLR values for enrichment reactors fed fermented dairy waste are between 5.2 – 33.4 Cmmol/L-d [50, 89, 116]. Regarding OLR units, the ratio of gCOD to Cmmol for fermented dairy liquor (DFL) is

roughly 0.035 (n > 1500); therefore, an OLR range of 10 to 30 Cmmol/L-d (this study) is approximately 0.35 to 1.06 gCOD/L-d. Comparatively, the OLR range ultimately applied in this research is low, yet the bulk solution substrate concentration realized by the biomass at the beginning of each cycle is consistent with the studies shown in Table 2.1. Furthermore, and more critically, the upper limit of OLR for the dairy-fed ADF process reflects the maximum feasible based on fermenter footprint and VFA yield potential.

Table 2.1: Reactor Operations for Various Substrates

Ref.	**HRT d**	**SRT d**	**CL h**	**OLR Cmmol L^{-1} d^{-1} *gCOD L^{-1} d^{-1}**	**F/F Ratio**	**Substrate Source**
[123]	2	2	24	*4.5	~0.017	Paper Mill Effluent
[103]	1	10	12	60, 90, 120	~0.22	Fermented Sugar Molasses
[110]	1	6	12	*1-2	N/A	Fermented Whey Permeate
[97]	1	1	2	*8.5-20 *20-31.25	< 0.33 1	Synthetic
[73]	1	1	12	27	~0.036	Synthetic
[27]	1	10	12	12	~0.012	Synthetic

2.5.7. Optimal Operation

Amongst the interrelated operating parameters that ensure proper enrichment of PHA-accumulating organisms, the maximum substrate concentration during the feast phase (related to OLR) and SRT emerge as the two critical parameters [72]. For a CL of 24 h (this work), the maximum substrate concentration becomes the OLR. Determining the optimized combination of these two parameters is an elusive goal, as previous investigations define an optimal value(s) of one parameter, independent of the other (i.e., one parameter is fixed). Sifting through the various schools of thought on optimal operation, three statements that are generally in agreement are:

i. The optimal enrichment OLR is the highest OLR that can be achieved while selective pressure vital to F-F metabolism is maintained [23].
ii. The CL to SRT ratio should be maximized in order to establish a culture enriched for microorganisms with a high PHA storage capacity [112].
iii. The optimal SRT is where peak biomass activity occurs and substrate utilization for growth is minimized.

A conceptual diagram illustrating the optimal operation range as a function of SRT and OLR is shown in Figure 2.8

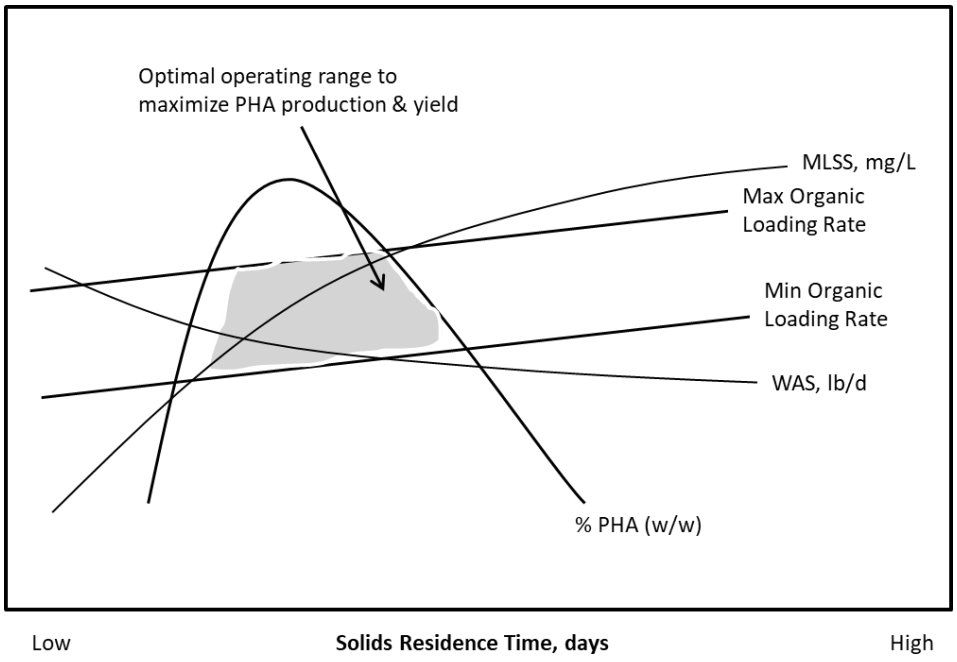

Figure 2.8: Conceptual Diagram of Optimal Enrichment Reactor Operating Conditions for Maximizing PHA Production

3. Metabolic Model

Modeling of storage products in MMC started with the Activated Sludge Model no. 3 (ASM3) [124]; however, its shortcomings in modeling dynamic metabolic processes such as simultaneous growth and PHA storage became quickly apparent. This sparked the development of a model describing ADF metabolism in pure cultures [39] and MMC [38]. Metabolic models are superior in describing dynamic processes due to the stoichiometric yield and maintenance coefficients being dependent on the same metabolic parameters [38].

With the innate capability of evaluating alternative operations mathematically, a metabolic model describing the MMC's ability to produce PHA is essential to the optimization of PHA production at the industrial level. An MMC's bioplastic production potential from a complex, diverse substrate (e.g., waste-feed stock) is also complex and diverse; a metabolic model serves to provide understanding to the underlying microbial processes. The metabolic model developed in this thesis details and quantifies internal microbial reactions occurring within an MMC under ADF conditions critical to F-F PHA synthesis. More importantly, the model provides predictive-ness of copolymer production on substrate mixtures more representative of waste-feed fermentative products, rather than single or mixed synthetic substrates. Results extracted from the metabolic model offer valuable empirical prediction and characterization of PHA synthesis for further optimization of real-world applications.

3.1. Model Focus

The metabolic model described herein is focused on the enrichment phase of the three stage ADF PHA process; see Figure 2.7. For relative simplicity, the model is confined to describing PHA synthesis from carboxylate mixtures composed of acetate, propionate, butyrate, and valerate; however, by design the model can incorporate other 4 and 5 carbon VFAs (e.g., iso-butyrate, iso-valerate). Nearly two years of fermentation data, developed from a dairy manure fed fermenter, indicates these four carboxylates represent over 95% of the total carboxylate yield (see Ch. 4). Modeling PHA synthesis from these four carboxylates extends previous models [37-40, 42, 44], while avoiding unnecessary complexity from incorporated substrates whose concentrations have little effect on copolymer production. Furthermore, the model extends the original PHA production from complex VFA mixtures framework proposed by Pardelha et al. [18, 41, 125], by incorporating famine phase processes valuable to commercial

application. It is assumed the metabolic model is robust enough to simulate diverse real-world carboxylate mixtures, with proper calibration.

3.2. Metabolic Model for Aerobic PHA Synthesis and Degradation

A schematic of the metabolic model developed in this study is illustrated in Figure 3.1 and a complete overview of the biochemical reaction stoichiometries are shown in Table 3.1. All reactions are expressed on a carbon-mole basis, which is consistent with past metabolic modeling efforts.

In the feast phase, VFAs are actively transported within the cell, requiring one mole of ATP per mole of carbon source [7]. Following transport, the carboxylates are converted to their respective acyl-CoA, requiring an additional mole of ATP per mole VFA [40]. Acetate and propionate are activated to directly to acetyl-CoA and propionyl-CoA (R_1 and R_2). While butyrate and valerate can be directly converted to HB and HV precursors, the model assumes they pass through β-oxidation and are converted to acetyl-CoA and propionyl-CoA (R_3 and R_4). This assumption is valid for modeling purposes as the net energetic, material, and reducing power balances are equivalent for both scenarios [125]. Details regarding β-oxidation are discussed in the previous chapter.

It has been reported that a fraction of propionyl-CoA can be converted to acetyl-CoA [26]; to account for this decarboxylation, the model assumes propionyl-CoA is converted to acetyl-CoA via the succinyl-CoA pathway as described by Dias et al. [40] (R_5).

Regarding PHA synthesis, acetyl-CoA and propionyl-CoA are reduced and condensed to form either 3HB, from two acetyl-CoA monomers, or 3HV, from one propionyl-CoA and one acetyl-CoA monomer. The condensation of two propionyl-CoA monomers to 3H2MV was not observed in this study; however, PH2MV was included in the model framework despite not being evaluated. For convenience, 3HB and 3HV monomers are represented by acetyl-CoA* and propionyl-CoA* (R_6 and R_7). This formality, as employed by previous investigators [40, 125-127], allows the polymerization process be omitted from the model prior to PHA formation, and thus permits the use of linear relations [127]. Subsequent PHA synthesis from these monomers requires no additional energy or reducing power (R_{13} and R_{14}). In the famine phase, PHB and PHV are degraded to acetyl-CoA and propionyl-CoA, requiring one mole of ATP per mole of building block (R_{15} and R_{16}) [44].

Acetyl-CoA is converted to CO_2 via the TCA cycle (R_{10}), as described by van Aalst-van Leeuwen et al. [39]; furthermore, it is assumed the catabolism of propionyl-CoA occurs through the TCA cycle as acetyl-CoA (R_5 is followed by R_{10}). Cellular energy in the form of ATP is generated from $NADH_2$ via oxidative phosphorylation (R_{11}). The amount of ATP generated per mole of $NADH_2$ oxidized is expressed by the P/O ratio, δ, and is synonymous with oxidative phosphorylation efficiency [128].

Biomass growth is assumed to occur from both acetyl-CoA and propionyl-CoA (R_8 and R_9). A biomass composition of $CH_{1.8}O_{0.5}N_{0.2}$ (C-mole representation) with a degree of reduction of 4.2 is used, as proposed by Beun et al. [37]. Detail on the determination of the anabolism equations is discussed below.

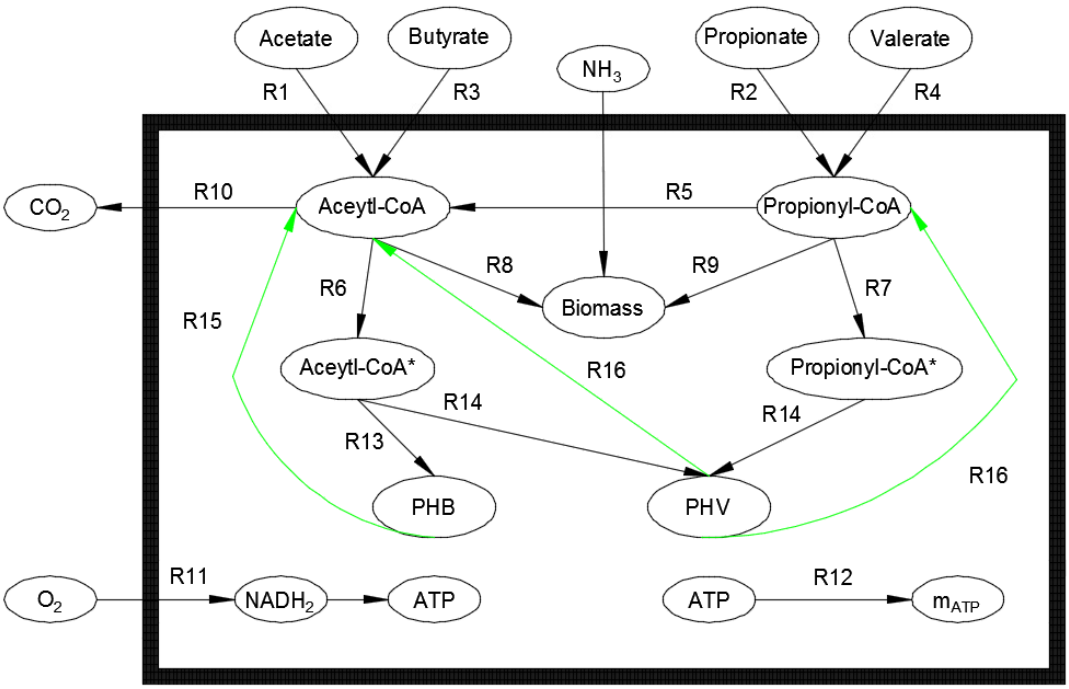

Figure 3.1: Model Metabolic Network

Adapted from [125].

Table 3.1: Metabolic Model of PHA Production from Common VFAs by MMC

Reaction	Description	Stoichiometry
R_1	Acetate Uptake	$CH_2O + ATP \rightarrow CHO_{0.5} + 0.5H_2O$
R_2	Propionate Uptake	$CH_2O_{0.67} + 0.67ATP \rightarrow CH_{1.33}O_{0.33} + 0.33H_2O$
R_3	Butyrate Uptake	$CH_2O_{0.5} + 0.5ATP \rightarrow CHO_{0.5} + 0.5NADH_2$
R_4	Valerate Uptake	$CH_2O_{0.4} + 0.4ATP \rightarrow 0.4CHO_{0.5} + 0.6CH_{1.33}O_{0.33} + 0.4NADH_2$
R_5	Propionyl-CoA decarboxylated to Acetyl-CoA	$1.5CH_{1.33}O_{0.33} + H_2O \rightarrow CHO_{0.5} + 1.5NADH_2 + 0.5CO_2$
R_6	Production of HB Precursor (Acetyl-CoA*)	$CHO_{0.5} + 0.25NADH_2 \rightarrow CH_{1.5}O_{0.5}$
R_7	Production of HV Precursor (Propionyl-CoA*)	$CH_{1.33}O_{0.33} + 0.17NADH_2 \rightarrow CH_{1.67}O_{0.33}$
R_8	Growth on Acetyl-CoA	$1.27CHO_{0.5} + 0.2NH_3 + K_1ATP + 0.4H_2O \rightarrow CH_{1.8}O_{0.5}N_{0.2} + 0.43NADH_2 + 0.27CO_2$
R_9	Growth on Propionyl-CoA	$1.06CH_{1.5}O_{0.33} + 0.2NH_3 + K_2ATP + 0.26H_2O \rightarrow CH_{1.8}O_{0.5}N_{0.2} + 0.37NADH_2 + 0.06CO_2$
R_{10}	Catabolism	$CHO_{0.5} + 1.5H_2O \rightarrow CO_2 + 2NADH_2 + 0.5ATP$
R_{11}	Oxidative Phosphorylation	$NADH_2 + 0.5O_2 \rightarrow H_2O + \delta\text{ATP}$
R_{12}	Maintenance	$ATP \rightarrow m_{ATP}$
R_{13}	PHB Production	$CH_{1.5}O_{0.5} \rightarrow \text{PHB}$
R_{14}	PHV Production	$0.4CH_{1.5}O_{0.5} + 0.6CH_{1.67}O_{0.33} \rightarrow \text{PHV}$
R_{15}	PHB Consumption	$PHB + 0.25ATP \rightarrow CHO_{0.5} + 0.25NADH_2$
R_{16}	PHV Consumption	$PHV + 0.2ATP \rightarrow 0.4CHO_{0.5} + 0.6CH_{1.33}O_{0.33} + 0.2NADH_2$

3.2.1. Growth on Acetyl-CoA and Propionyl-CoA

The reactions of biomass growth on acetyl-CoA and propionyl-CoA, R_8 and R_9, were determined from a stoichiometric and degree of reduction balance in accordance with Villadsen [81]. The degree of reduction is a measure of the available electrons per unit carbon for a given compound and can be used to calculate the amount of reducing equivalents to apply to a stoichiometric equation within a process. For said equations, ammonia was used as the nitrogen source. Anabolism for 1 C-mol of biomass from acetyl-CoA is represented in R_8 (Table 3.1). The theoretical amount of ATP required for the synthesis of biomass precursors from acetyl-CoA is 0.66 mol ATP per C-mol X [80]. Furthermore, the synthesis of 1 C-mol of biomass from biomass precursors requires an additional 1.5 mol ATP per C-mol X [129]. Applying a balance on ATP, the synthesis of 1 C-mol of biomass on acetate requires 2.16 moles of ATP, represented as K_1. The molar ratio for H_2O was determined from a balance on oxygen, with 0.267 C-mol CO_2 being produced from the synthesis of 1 C-mol X on acetate [130]. Reducing equivalents in the form of $NADH_2$ were determined from a balance on $NADH_2$.

Due to inadequate research, the amount of decarboxylation of propionate for growth purposes has not yet been quantified [126]. Alternatively, biomass synthesis on propionyl-CoA is modeled as growth on succinate, its biokinetic derivative. The synthesis of 1 C-mol of biomass on succinate yields 0.409 moles of CO_2 [130]. Utilizing the reverse succinate-propionate pathway the resulting stoichiometric values of CO_2 and $NADH_2$ for propionate as the carbon source can be determined. Although there are no published values of ATP demand for biomass synthesis on propionate, the requirement of 1.84 mol ATP per C-mol X, represented as K_2, was determined from a steady state balance on the conversion of acetyl-CoA and propionyl-CoA to succinate [126]. Anabolism for 1 C-mol of biomass on propionyl-CoA is represented in R_9 (Table 3.1). The complete derivation of R_8 and R_9 is illustrated in Appendix A.

3.4. Stoichiometric Parameters

The model consists of 16 metabolic reactions, 6 intracellular metabolites (acetyl-CoA, acetyl-CoA*, propionyl-CoA, propionyl-CoA*, ATP, and $NADH_2$), 6 input substrates (acetate, propionate, butyrate, valerate, ammonia, and oxygen), and 4 end-products (biomass, PHB,

PHV, and CO_2). The model stoichiometric matrix is not presented in this section due to its size but is illustrated in Appendix A.

3.4.1. Feast Phase Steady State Balancing of Intermediates

The feast phase is comprised of 14 metabolic reactions (R_1-R_{14}). Under steady-state conditions, the metabolic intermediates are balanced and result in a system of algebraic equations, where r_i represents the flux of reaction R_i.

Equation 3.1: Feast Phase Balance on Acetyl-CoA

$$r_1 + r_3 + 0.4r_4 + r_5 - r_6 - 1.27r_8 - r_{10} = 0$$

Equation 3.2: Feast Phase Balance on Acetyl-CoA*

$$r_6 - r_{13} - 0.4r_{14} = 0$$

Equation 3.3: Feast Phase Balance on Propionyl-CoA

$$r_2 + 0.06r_4 - 1.5 * r_5 - r_7 - 1.06 * r_9 = 0$$

Equation 3.4: Feast Phase Balance on Propionyl-CoA*

$$r_7 - 0.6r_{14} - r_{15} = 0$$

Equation 3.5: Feast Phase Balance on $NADH_2$

$$0.5r_3 + 0.4r_4 + 1.5r_5 - 0.25r_6 - 0.17r_7 + 0.43r_8 + 0.37r_9 + 2r_{10} - r_{11} = 0$$

Equation 3.6: Feast Phase Balance on ATP

$$0.5r_{10} - 0.67r_2 - 0.5r_3 - 0.4r_4 - r_1 - r_{12} + \delta r_{11} - K_1 r_8 - K_2 r_9 = 0$$

3.4.2. Feast Phase Yield and Maintenance Coefficients

The advantage of employing a metabolic model is that the theoretical yield and maintenance coefficients can be determined as a function of metabolic parameters. Modeling four unique VFAs increases model complexity and creates an undetermined system; therefore, additional constraints on metabolic parameters are required. Adopting the approach of Dias et al. [40] and Pardelha [41], VFA uptake is separated by even and odd carbon VFA using the defined ratio, y, of odd carbon flux (r_{odd}) to total carbon flux (r_s) as described in Equation 3.7.

Equation 3.7: Ratio of Odd Carbon VFA to Total VFA Flux

$$y = \frac{r_2 + r_4}{r_1 + r_2 + r_3 + r_4} = \frac{r_{odd}}{r_s}$$

Furthermore, the number of carbons of even (n_{even}) and odd (n_{odd}) substrates were defined by taking the weighted average of each VFA with their respective flux (Equation 3.8 and Equation 3.9).

Equation 3.8: Weighted Number of Even Carbons Fluxed

$$n_{even} = \frac{n_{Ac}r_1 + n_{Bu}r_3}{r_s}$$

Equation 3.9: Weighted Number of Odd Carbons Fluxed

$$n_{odd} = \frac{n_{Pr}r_2 + n_{Va}r_4}{r_s}$$

Ultimately, the defined relationships (Equations 3.1, 3.8, and 3.9) can be incorporated to form one stoichiometric equation describing substrate uptake, R_S, shown in Equation 3.10 [41].

Equation 3.10: Lumped Substrate Uptake

$$R_S: VFA + \left(\frac{2(1-y)}{n_{even}} - 2yn_{odd}\right)ATP \rightarrow \left(\frac{(n_{odd}-3)}{n_{odd}}y - y + 1\right)CHO_{0.5} + \frac{3y}{n_{odd}}CH_{1.33}O_{0.33} - \left(\frac{n_{even}-4}{2n_{even}}(y-1) + \frac{n_{odd}-5}{2n_{odd}}y\right)H_2O + \left(\frac{(n_{odd}-3)}{n_{odd}}y - \frac{n_{even}-2}{n_{even}}(1-y)\right)NADH_2$$

To further decrease the number of unknown fluxes, an additional constraint was imposed. Similar to the method used by Jiang et al. [44], the ratio of PHV formation to total PHA synthesis, y_{PHV}, was defined (Equation 3.11).

Equation 3.11: Ratio of PHV Flux to PHA Flux

$$y_{PHV} = \frac{r_{14}}{r_{13} + r_{14}} = \frac{r_{PHV}}{r_{PHA}}$$

The use of y_{PHV} allows PHA synthesis be defined by one stoichiometric relationship, as shown in Equation 3.12.

Equation 3.12: Lumped PHA Synthesis

$$R_{PHA}: \frac{3}{5}(1 - y_{PHV})CH_{1.5}O_{0.5} + \frac{3}{5}y_{PHV}CH_{1.67}O_{0.33} \rightarrow PHA$$

With the addition of the detailed modeling constraints, the system is reduced to 10 unknown flux rates which are related through 6 linear equations (Equation 3.2-3.7). Therefore, any flux rate can be defined in terms of 4 unknown flux rates. These four unknown flux rates are then defined *a priori*, via a kinetic model, to calculate the full network of fluxes [40]. The model herein defines the flux rates in terms of anabolism from acetyl-CoA and propionyl-CoA (R_8 and R_9), maintenance (R_{12}), and PHA production (R_{PHA}).

To solve the system of reactions, a method of Metabolic Flux Analysis (MFA) described by Villadsen [81] was used. Briefly, MFA allows a set of known fluxes, $\boldsymbol{v_1}$, be used to determine a set of unknown fluxes, $\boldsymbol{v_2}$, through stoichiometric balancing [40]. The MFA equation for solving $\boldsymbol{v_2}$ with $\boldsymbol{v_1}$ is shown Equation 3.13.

Equation 3.13: MFA Relationship

$$\boldsymbol{v_2} = -{T_1}^{-1} T_2 \boldsymbol{v_1}$$

For the model described herein, the vectors are defined as:

$$\boldsymbol{v_1} = \begin{bmatrix} r_8 \\ r_9 \\ r_{PHA} \\ r_{12} \end{bmatrix} \quad \boldsymbol{v_2} = \begin{bmatrix} r_S \\ r_5 \\ r_6 \\ r_7 \\ r_{10} \\ r_{11} \end{bmatrix}$$

Where T_1 and T_2 are submatrices of the model stoichiometric matrix whose columns correspond to $\boldsymbol{v_1}$and $\boldsymbol{v_2}$, and rows correspond to the conserved moieties (acetyl-CoA, acetyl-CoA*, propionyl-CoA, propionyl-CoA*, ATP, and $NADH_2$). As a result of the MFA procedure, the substrate uptake rate, $\boldsymbol{v_2}(1)$, is equivalent to:

$$-r_S = \frac{r_8}{Y_{\frac{X_{Ac}}{S}}} + \frac{r_9}{Y_{\frac{X_{Pr}}{S}}} + \frac{r_{PHA}}{Y_{\frac{PHA}{S}}} + r_{12}$$

Whether biomass is formed from either acetyl-CoA or propionyl-CoA is unmeasurable. For this model it is assumed that growth on acetyl-CoA and propionyl-CoA is proportional to the ratio y, similar to the approach of Jiang et al. [44]. Finally, the substitution of $r_X = \mu C_X$, $r_S = q_S C_X$, and $r_{PHA} = q_{PHA} C_X$ followed by division by the biomass concentration C_X, results in a Herbert-Pirt type relationship for the feast phase, shown in Equation 3.14.

Equation 3.14: Feast Herbert-Pirt Relationship

$$-q_s = (1-y)\frac{\mu_{feast}}{Y_{\frac{X_{Ac}}{S}}} + y\frac{\mu_{feast}}{Y_{\frac{X_{Pr}}{S}}} + \frac{q_{PHA,feast}}{Y_{\frac{PHA}{S}}} + m_{s,feast}$$

As shown, substrate uptake and specific substrate uptake rates are denoted with negative signs as they are consumptive processes. The above relationship couples substrate uptake to growth, PHA production, and maintenance through defined yields derived from the steady-state balance. The expressions for the yield and maintenance coefficients are compiled in Table 3.2. Importantly, the MFA methodology used produces relationships for each flux in $\boldsymbol{v_2}$ in terms of fluxes in $\boldsymbol{v_1}$. For example, $\boldsymbol{v_2}(2)$ is equivalent to the oxygen evolution of the feast phase.

Table 3.2: Feast Yield and Maintenance Coefficients on Substrate

Parameter	Description	Stoichiometry
$Y_{\frac{X_{Ac}}{S}}$	Growth from Acetyl-CoA on VFAs	$\frac{n_{even}n_{odd}(1+6\delta)+4n_{odd}(y+\delta y-1-\delta)-n_e y(5+4\delta)}{n_{even}n_{odd}(2K_1+4.2\delta+1.27)}$
$Y_{\frac{X_{Pr}}{S}}$	Growth from Propionyl-CoA on VFAs	$\frac{n_{even}n_{odd}(1+6\delta)+4n_{odd}(y+\delta y-1-\delta)-n_e y(5+4\delta)}{n_{even}n_{odd}(2K_2+4.2\delta+0.7)}$
$Y_{\frac{PHA}{S}}$	PHA storage on VFAs	$\frac{n_{even}n_{odd}(1+6\delta)+4n_{odd}(y+\delta y-1-\delta)-n_e y(5+4\delta)}{n_{even}n_{odd}(4.5\delta-0.2y_{PHV}+0.3\delta y_{PHV}+1)}$
$m_{s,feast}$	Maintenance	$\frac{2n_{even}n_{odd}m_{ATP}}{n_{even}n_{odd}(1+6\delta)+4n_{odd}(y+\delta y-1-\delta)-n_e y(5+4\delta)}$

3.4.1. Famine Phase Steady State Balancing of Intermediates

The famine phase is comprised of 8 metabolic reactions (R_5, R_8-R_{12}, R_{15}, R_{16}). For the case of PHA degradation, the model assumes the monomer stage is superseded [44]; therefore, R_6 and R_7 are not considered and there are only 4 intracellular metabolites in steady state. Assuming no net consumption or accumulation of these moieties results in the following linear equations:

Equation 3.15: Famine Phase Balance on Acetyl-CoA

$$r_5 - 1.27r_8 - r_{10} + R_{16} + 0.4R_{17} = 0$$

Equation 3.16: Famine Phase Balance on Propionyl-CoA

$$0.6r_{17} - 1.06r_9 - 1.5r_5 = 0$$

Equation 3.17: Famine Phase Balance on NADH

$$1.5r_5 + 0.43r_8 + 0.37r_9 + 2r_{10} - r_{11} + 0.25r_{16} + 0.2r_{17} = 0$$

Equation 3.18: Famine Phase Balance on ATP

$$0.5r_{10} - r_{12} - 0.25r_{16} - 0.2r_{17} + \delta r_{11} - K_1 r_8 - K_2 r_9 = 0$$

3.4.3. Famine Phase Yield and Maintenance Coefficients

Similar to the feast phase, the famine phase requires an additional constraint be made to reduce model complexity. To this end, the ratio of PHV consumption to total PHA consumption, y_f, is defined by Equation 3.19.

Equation 3.19: Ratio of PHV Degradation Flux to

$$y_f = \frac{r_{16}}{r_{15} + r_{16}} = \frac{r_{PHVf}}{r_{PHAf}}$$

Provided this relationship, PHA degradation can be defined by one stoichiometric reaction illustrated in Equation 3.20.

Equation 3.20: Lumped PHA Consumption

$$R_{PHAf}: PHA + \left(\frac{1}{4} - \frac{y_f}{20}\right)\text{ATP} \rightarrow \left(1 - \frac{3y_f}{5}\right) CHO_{0.5} + \frac{3y_f}{5}\, CH_{1.33}O_{0.33} + \left(\frac{1}{4} - \frac{y_f}{20}\right) NADH_2$$

Effectively, the famine phase is reduced to 7 unknown fluxes that are correlated with 4 algebraic relationships (Equations 3.15-3.18); moreover, if three fluxes are defined all of the remaining fluxes can be expressed in terms of the defined fluxes. By repeating the MFA methodology performed in the previous section for the famine phase, the vectors $\boldsymbol{v_1}$ and $\boldsymbol{v_2}$ become:

$$\boldsymbol{v_1} = \begin{bmatrix} r_8 \\ r_9 \\ r_{12} \end{bmatrix} \boldsymbol{v_2} = \begin{bmatrix} r_{PHAf} \\ r_5 \\ r_{10} \\ r_{11} \end{bmatrix}$$

Using Equation 3.13 with the input of the respective famine phase submatrices T_1 and T_2, the resultant PHA degradation rate, $\boldsymbol{v_2}(1)$, is defined as:

$$-r_{PHAf} = \frac{r_8}{Y_{\frac{X_{Ac}}{PHA}}} + \frac{r_9}{Y_{\frac{X_{Pr}}{PHA}}} + r_{12}$$

Similar to the feast phase, the model assumes growth on acetyl-CoA and propionyl-CoA is proportional to the ratio y_f; further substitution of $r_X = \mu C_X$, $r_S = q_S C_X$, and $r_{PHA} = q_{PHA} C_X$ followed by division by the biomass concentration C_X, results in a Herbert-Pirt type relationship for the famine phase, shown in Equation 3.21.

Equation 3.21: Famine Herbert-Pirt Relationship

$$-q_{PHA,f} = (1 - y_f)\frac{\mu_{famine}}{Y_{\frac{X_{Ac}}{PHA}}} + y_f \frac{\mu_{famine}}{Y_{\frac{X_{Pr}}{PHA}}} + m_{s,famine}$$

This relationship couples PHA consumption to growth and maintenance through defined yields derived from the steady-state balance. The expressions for the famine yield and maintenance coefficients are compiled in Table 3.3.

Table 3.3: Famine Yield and Maintenance Coefficients on PHA

Parameter	Description	Stoichiometry
$Y_{\frac{X_{Ac}}{PHA}}$	Growth on PHA degraded to Acetyl-CoA	$\frac{4.5\delta - 0.1y_f + 0.3\delta y_f + 0.5}{(2K_1 + 4.2\delta + 1.27)}$
$Y_{\frac{X_{Pr}}{PHA}}$	Growth on PHA degraded to Propionyl-CoA	$\frac{4.5\delta - 0.1y_f + 0.3\delta y_f + 0.5}{(2K_2 + 4.2\delta + 0.7)}$
$m_{s,famine}$	Maintenance	$\frac{2m_{ATP}}{4.5\delta - 0.1y_f + 0.3\delta y_f + 0.5}$

3.6. Kinetic Model

A kinetic model was developed to empirically describe the model's 'known' fluxes, biomass growth, PHA/VFA consumption, and maintenance, in order to calculate the entire network of fluxes. The kinetic equations used in this work are compiled in Table 3.4. Stoichiometric relations for O_2 and CO_2 were not included in the kinetic model due to a lack of accurate measurement; this would require precise reactor k_La estimation and DO probe calibration

while yielding minimal benefit, as the reactors in this work were excessively aerated throughout.

3.6.1. Feast Phase

For the model described herein, substrate uptake is assumed to occur at a maximum rate due to intracellular PHA concentrations observed in the enrichment stage being too low to inhibit VFA uptake; hence, VFA uptake, q_s , is modelled with saturation kinetics with a small half-saturation constant [131]. Similarly, the biomass specific growth rate, μ_{feast}, is modelled with a maximum growth rate, μ_{max}, and with Monod-like saturation terms for VFAs and ammonia [42]. The maintenance rate related to substrate, $m_{s,feast}$, is a function of the constant biomass specific ATP consumption rate, m_{ATP}, and the ATP yield on VFA (see Table 3.2). The conversion rate of PHA can then be obtained from rearranging Equation 3.14; furthermore, the model separates PHA into PHB and PHV by using the ratio of PHV flux to PHA flux y_{PHV} (Equation 3.11).

3.6.2. Famine Phase

Famine phase kinetics were applied when modelled concentration of VFAs was below 0.001 Cmmol/L, as suggested by Johnson et al. [42]. Under this condition, growth is a function of PHA degradation and maintenance as described by Equation 3.21. This approach assumes that growth on PHA is rate-limited by PHA consumption which is generally valid [37, 44, 132]. Murnleitner et al. [133] suggests the rate of PHA degradation is dependent on PHA surface area and can be expressed by a two-third order function of intracellular PHA content. This approach was adopted for this model; moreover, the degradation rate of PHB and PHV,$q_{PHB,famine}$ and $q_{PHV,famine}$, are individually specified by modeled biomass fraction of homopolymer, $f_{\frac{PHB}{X}}$ and $f_{\frac{PHB}{X}}$, as shown in Equation 3.22. The maintenance rate related to PHA consumption, $m_{s,famine}$, is a function of m_{ATP}, and the stoichiometric ATP yield on PHA (see Table 3.3).

Equation 3.22: Modelled Biomass Fraction of PHB or PHV

$$f_{\frac{PHB,PHV}{X}} = \frac{C_{PHB,PHV}}{C_X}$$

Table 3.4: Model Kinetics Equations

Feast Phase		
Parameter	**Description**	**Kinetic Rate Equation**
$q_{PHB,feast}$	PHB production	$[q_s(t) - \mu_{feast}(t)\left(\frac{1-y}{Y_{\frac{X_{Ac}}{S}}} + \frac{y}{Y_{\frac{X_{Pr}}{S}}}\right) - m_{s,feast}](Y_{\frac{PHA}{S}})(1 - y_{PHV})$
$q_{PHV,feast}$	PHV production	$[q_s(t) - \mu_{feast}(t)\left(\frac{1-y}{Y_{\frac{X_{Ac}}{S}}} + \frac{y}{Y_{\frac{X_{Pr}}{S}}}\right) - m_{s,feast}](Y_{\frac{PHA}{S}})(y_{PHV})$
q_s	Substrate uptake	$\Sigma(-q_{VFAi,max})\frac{C_i(t)}{K_i + C_i(t)}; of\ i^{th}\ VFA$
μ_{feast}	Growth	$\mu_{max}\frac{C_{NH_3}(t)}{K_{NH_3} + C_{NH_3}(t)}\frac{C_S(t)}{K_S + C_S(t)}$
$q_{NH_3,feast}$	NH_3 uptake	$\mu_{feast}(t)\ Y_{\frac{NH_3}{X}}$
Famine Phase		
μ_{famine}	Growth	$q_{PHB,f}(t)Y_{\frac{X_{Ac}}{PHA}} + q_{PHV,f}(t)Y_{\frac{X_{Pr}}{PHA}} - m_{s,famine}\left(\frac{1-y_f}{Y_{\frac{X_{Ac}}{PHA}}} + \frac{y_f}{Y_{\frac{X_{Pr}}{PHA}}}\right)$
$q_{PHB,famine}$	PHB degradation	$kf_{\frac{PHB}{X}}(t)^{2/3}\frac{C_{NH_3}(t)}{K_{NH_3} + C_{NH_3}(t)}$
$q_{PHV,famine}$	PHV degradation	$kf_{\frac{PHV}{X}}(t)^{2/3}\frac{C_{NH_3}(t)}{K_{NH_3} + C_{NH_3}(t)}$
$q_{NH_3,famine}$	NH_3 uptake	$\mu_{famine}(t)\ Y_{\frac{NH_3}{X}}$

3.6.3. Dynamic Material Balances

The transient material balances for all kinetically described compounds – acetate, propionate, butyrate, valerate, biomass, PHB, PHV, and ammonia – were modelled. The general form for the material balance equations is shown in Equation 3.23.

Equation 3.23: General Material Balance Form

$$\frac{dC_i(t)}{dt} = q_i(t)C_X(t)$$

Where $i = [Ac \quad Pr \quad Bu \quad Va \quad X \quad PHB \quad PHV \quad NH_3]$. Importantly, q_X, is represented by μ_{feast} or μ_{famine} depending on reactor phase. Initial concentrations of all materials were established by optimization.

3.7. Model Calibration

To calculate all rates and concentrations as a function of time, several parameters were held constant while others were estimated using measured data. A summary of model parameters is provided in Table 3.5.

Similar to the method of Johnson et al. [42] and Jiang et al. [44], half-saturation constants for each VFA and ammonia, and the P/O ratio (δ) were held constant. Half-saturation constants are such that beget near-zero order kinetics without causing numerical issues with integration. The P/O ratio, δ, and maintenance ATP requirement, m_{ATP}, are dependent of each other and therefore cannot be independently separated from measurements. A constant P/O ratio of 2 mmol ATP per mmol $NADH_2$ was chosen for this model, as is common for similar models [37, 42, 43]. Conversely, m_{ATP} is estimated by fitting, which is suggested to vary more significantly with differences in environmental conditions [42]. The maximum specific VFA uptake rate for each of the four VFAs, $q_{VFAi,max}$, maximum feast growth rate, μ_{max}, ratio of PHV to total PHA production flux, y_{PHV}, and PHA degradation constant, k, were estimated by the calibration procedure. The remaining parameters y and y_{fam} are calculated from the material balances as a function of time. As it was observed that y and y_{PHV} share collinearity, y_{PHV} was estimated as the product of a fitted constant and y (see Table 3.5).

Table 3.5: Model Parameters

Parameter	Value	Units	Estimated (Yes/No)
Substrate half-saturation	$K_S = 0.2$	$\frac{Cmmol}{L}$	N
Ammonia half-saturation	$K_{NH_3} = 0.0001$	$\frac{mmol}{L}$	N
Oxidative phosphorylation efficiency	$\delta = 2$	$\frac{mmol\ ATP}{mmol\ NADH_2}$	N
Maintenance ATP requirement	m_{ATP}	$\frac{mmol}{Cmmol * hr}$	Y
Max. acetate uptake rate	$q_{Ac,,max}$	$\frac{Cmmol}{Cmmol * hr}$	Y
Max. propionate uptake rate	$q_{Pr,max}$	$\frac{Cmmol}{Cmmol * hr}$	Y
Max. butyrate uptake rate	$q_{Bu,max}$	$\frac{Cmmol}{Cmmol * hr}$	Y
Max. valerate uptake rate	$q_{Va,max}$	$\frac{Cmmol}{Cmmol * hr}$	Y
Max. growth rate feast	μ_{max}	$\frac{Cmmol}{Cmmol * hr}$	Y
PHA degradation rate constant	k	$(\frac{Cmmol}{Cmmol})^{\frac{1}{3}} h^{-1}$	Y
Ratio of PHV to PHA storage feast	$y_{phv} = Cy$	$\frac{Cmmol}{Cmmol}$	Y
Ratio of odd carbon VFA to total VFA flux feast	y	$\frac{Cmmol}{Cmmol}$	N
Ratio of PHV to PHA degradation famine	y_{fam}	$\frac{Cmmol}{Cmmol}$	N
Yield of ammonia on biomass	$Y_{\frac{NH_3}{X}} = -0.2$	$\frac{mmol}{Cmmol}$	N; See biomass formula

3.7.2. Parameter Estimation

The kinetic parameters were estimated by a nonlinear least-squares solver, *lsqcurvefit or lsqnonlin* (MATLAB), which uses the Trust-Region-Reflective algorithm. The program minimizes the root mean squared error:

Equation 3.24: Root Mean Squared Error

$$RMSE = \sqrt{\frac{e^T e}{DOF}}$$

Where DOF is the difference between the number of measured values and number of parameters estimated, and e is the vector of residuals scaled by their maximum value [40]. This follows that all measurements are weighted equally.

Model concentrations of acetate, propionate, butyrate, valerate, PHB, PHV, X, and NH_3 were obtained from integrating respective transient material balances (Equation 3.23) using a 4th/5th order Runge-Kutta solver, *ode45* (MATLAB). The modelled values were subtracted from the time-respective data measurements to generate the residuals. This error is referred to as the relative error, E_R. In steady state the amount of biomass and PHA produced over an operational cycle is equal to the amount removed at the end of the cycle, as expressed in Equation 3.25.

Equation 3.25: SRT Definition for Biomass and PHA Conversions

$$C_{X,PHA}^{SRT}(t_{end}) = C_{X,PHA}(0)\frac{SRT}{SRT - t_{cycle}}$$

Therefore an additional error, an additional steady state error, E_{SS}, is included for solids agreement across cycles [42, 44]. Essentially, the difference between modelled PHA and biomass concentration at the end of the cycle and the concentrations produced from Equation 3.25 provide another set of residuals in which to minimize error. The kinetic rates and concentrations of modelled compounds can then be calculated by minimizing the total error defined by:

Equation 3.26: Total Model Error

$$E_T = E_R + E_{SS}$$

The confidence bounds for the estimated parameters were obtained using approximate standard deviations by performing a student's t-test with 95% confidence interval. Standard deviations were estimated using the covariance matrix generated from the Jacobian matrix produced at the RMSE.

4. Methods and Materials

4.1. Experimental Setup

4.1.1. Substrate

Dairy manure was obtained from the University of Idaho dairy farm approximately every two weeks and stored at 4°C until used. Collection took place in the loafing barns in order to avoid contaminating the manure with rocks and bedding material. For every new batch collected, Total solids (TS) and volatile solids (VS) was measured in triplicate, with average values (n=36) of 16.3% ± 1.6% and 80.8% ± 4.7%, respectively.

4.1.2. Bench-Scale Fermenter

Dairy manure fermenter operations employed in this research were a legacy from and a continuation of previous related investigations [50, 134, 135]. The bench-scale fermenter was operated as an SBR, with an operational volume of 16 L and an SRT/HRT of 4 days; hence, 4 L was decanted and 4 L of diluted dairy manure was added on a 24-hour cycle. Manure was added to maintain an organic loading rate of 11.0 gVSS/L*day. The substrate for the enrichment and production reactors (i.e., DFL) was obtained from the fermenter effluent, which was centrifuged at 9000 rpm for 60 min. The fermenter was equipped with a 3.75 inch diameter helical impeller powered by an Oriental Motor (San Jose, CA, USA) USM315-401W 15 W AC speed-control motor connected to a 3GN35SA reduction gearbox. Mixing speed was set to suspend material and ensure uniform reactor properties. VFAs were measured tri-weekly with average values (n=172) of 1553 ± 434 mg/L (acetate), 858 ± 202 mg/L (propionate), 231 ± 164 mg/L (butyrate), 87 ± 58 mg/L (iso-butyrate), 112 ± 59 mg/L (valerate), 92 ± 43 mg/L (iso-valerate), and 24 ± 19 mg/L (caproate). Total carboxylates were on average 4006 ± 790 as mg-COD/L and 112 ± 22 as Cmmol/L.

4.1.3. Source of Microorganisms

The inocula for the PHBV enrichment reactors used in this research was obtained from an existing fermented dairy manure fed ADF processes' enrichment reactor that had been in operation since August 2011 [50, 89].

4.1.4. Enrichment Reactors

Unless otherwise specified, the following experimental setup used in the factorial enrichment and production stage investigations was also used for the optimal operation evaluation.

4.1.4.1. Factorial Enrichment Reactor Setup

In the factorial investigation phase of this study, 3 reactors were operated over a span of 185 days to assess the effects of SRT and OLR on PHA production potential. The enrichment reactors were operated as SBRs in chemostat mode, such that SRT=HRT. Three enrichment reactors were online at any given time, operated as SBRs (identified by E.SRT.OLR) with working volumes of 2 L as shown in Figure 4.1. Each of the three SBRs was operated at a fixed SRT, with the OLR adjusted accordingly after a given SRT-OLR investigation was completed; the exception was for the 10 Cmmol/L-d OLR investigations. In total, 12 combinations of operating conditions were evaluated in the factorial (3 SRTs (2, 3, and 4 days) x 4 OLRs (10, 20, 25, and 30 Cmmol L^{-1} d^{-1})). The operation and sampling timeline for the factorial is shown in Table 4.1. A total cycle length of 1 day was maintained for all SBRs, with wasting and feeding occurring at the same time each day via two Watson Marlow model 323 peristaltic pumps operating on digital timers. The wasting time was set for 10 min, while the feed time was set at 5 min. The enrichment SBRs are shown in Figure 4.2. The volume of substrate fed to each SBR was adjusted daily to maintain the target OLR and was dependent on the measured concentration of VFAs in each DFL batch. Aeration was supplied through stainless steel diffusers at approximately 1-1.5 LPM (Key Instruments rotometer (0-2.5 LPM range), Hatfield, PA, USA) depending on reactor SRT and OLR. Dissolved oxygen (DO) was controlled at a maximum setpoint of 3 mg/L using a Hach (Loveland, CO, USA) sc100™ Controller equipped with a Hach LDO™ Dissolved Oxygen Sensor. The reactors were mixed with Teflon™-coated stir bars and magnetic stir plates. The reactors are covered but are vented to the atmosphere.

Table 4.1: Factorial Operation Timeline

Reactor	Start Date	Sample Date	SRT (d)	OLR (Cmmol/L)	V Before Feed (L)
E.4.20	1/21/2018	2/8/2019	4	20	1.5
E.4.20	1/21/2018	2/12/2019	4	20	1.5
E.4.20	1/21/2018	2/21/2019	4	20	1.5
E.4.25	1/21/2018	2/8/2019	4	25	1.5
E.4.25	1/21/2018	2/12/2019	4	25	1.5
E.4.25	1/21/2018	2/21/2019	4	25	1.5
E.4.30	1/21/2018	2/8/2019	4	30	1.5
E.4.30	1/21/2018	2/12/2019	4	30	1.5
E.4.30	1/21/2018	2/21/2019	4	30	1.5
E.3.20	3/4/2019	3/21/2019	3	20	1.33
E.3.20	3/4/2019	3/28/2019	3	20	1.33
E.3.20	3/4/2019	4/4/2019	3	20	1.33
E.3.20	3/4/2019	4/11/2019	3	20	1.33
E.3.25	3/4/2019	3/21/2019	3	25	1.33
E.3.25	3/4/2019	3/28/2019	3	25	1.33
E.3.25	3/4/2019	4/4/2019	3	25	1.33
E.3.25	3/4/2019	4/11/2019	3	25	1.33
E.3.30	3/4/2019	3/21/2019	3	30	1.33
E.3.30	3/4/2019	3/28/2019	3	30	1.33
E.3.30	3/4/2019	4/4/2019	3	30	1.33
E.3.30	3/4/2019	4/11/2019	3	30	1.33
E.2.20	4/17/2019	4/25/2019	2	20	1
E.2.20	4/17/2019	5/16/2019	2	20	1
E.2.20	4/17/2019	5/23/2019	2	20	1
E.2.20	4/17/2019	5/28/2019	2	20	1
E.2.20	4/17/2019	5/30/2019	2	20	1
E.2.25	4/17/2019	4/25/2019	2	25	1
E.2.25	4/17/2019	5/16/2019	2	25	1
E.2.25	4/17/2019	5/23/2019	2	25	1
E.2.25	4/17/2019	5/28/2019	2	25	1
E.2.25	4/17/2019	5/30/2019	2	25	1
E.2.30	4/17/2019	4/25/2019	2	30	1
E.2.30	4/17/2019	5/16/2019	2	30	1
E.2.30	4/17/2019	5/23/2019	2	30	1
E.2.30	4/17/2019	5/28/2019	2	30	1
E.2.30	4/17/2019	5/30/2019	2	30	1
E.4.10	6/3/2019	6/17/2019	4	10	1.5
E.4.10	6/3/2019	6/18/2019	4	10	1.5
E.4.10	6/3/2019	6/26/2019	4	10	1.5
E.4.10	6/3/2019	7/12/2019	4	10	1.5
E.3.10	6/3/2019	6/17/2019	3	10	1.33
E.3.10	6/3/2019	6/18/2019	3	10	1.33
E.3.10	6/3/2019	6/26/2019	3	10	1.33
E.3.10	6/3/2019	7/12/2019	3	10	1.33
E.2.10	6/3/2019	6/17/2019	2	10	1
E.2.10	6/3/2019	6/18/2019	2	10	1
E.2.10	6/3/2019	6/26/2019	2	10	1
E.2.10	6/3/2019	7/12/2019	2	10	1

Figure 4.1: Factorial Enrichment Reactor Setup E.2.10, E.3.10, and E.4.10 (left to right)

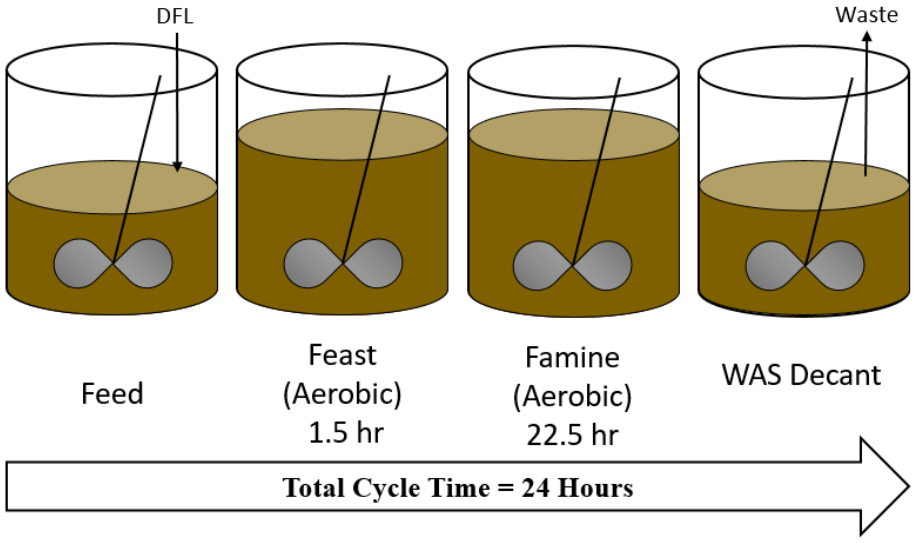

Figure 4.2: Enrichment Reactor Cycle Phases, adapted from [50]

4.1.4.2 “Optimum” Enrichment Reactor

Upon completing the factorial analysis, the “optimum” enrichment reactor operational condition was determined (see SRT & OLR Factorial: Results and Discussion). The enrichment reactor (identified as E.2.20) was operated as an SBR with a working volume of 8 L as depicted in Figure 4.3. The SRT and HRT were maintained at 2 days, with a total cycle length of 1 day. The reactor was decanted and fed (4 L) every day following the same method as described herein. The target OLR was set at 20 Cmmol L^{-1} d^{-1}. Aeration was achieved using a 9 inch diameter Sanitaire Silver Series II membrane fine bubble disc diffuser at approximately 8 LPM. A three-bladed, 6 inch diameter impeller was used for mixing, powered by an Oriental Motor Co., LTD. (1500 rpm max at 60 Hz), model 5GN3.6SA. The “optimum” reactor was operated from 7/12/19 to the date of this thesis, with sampling events on 8/17/19, 8/22/19, and 10/23/19.

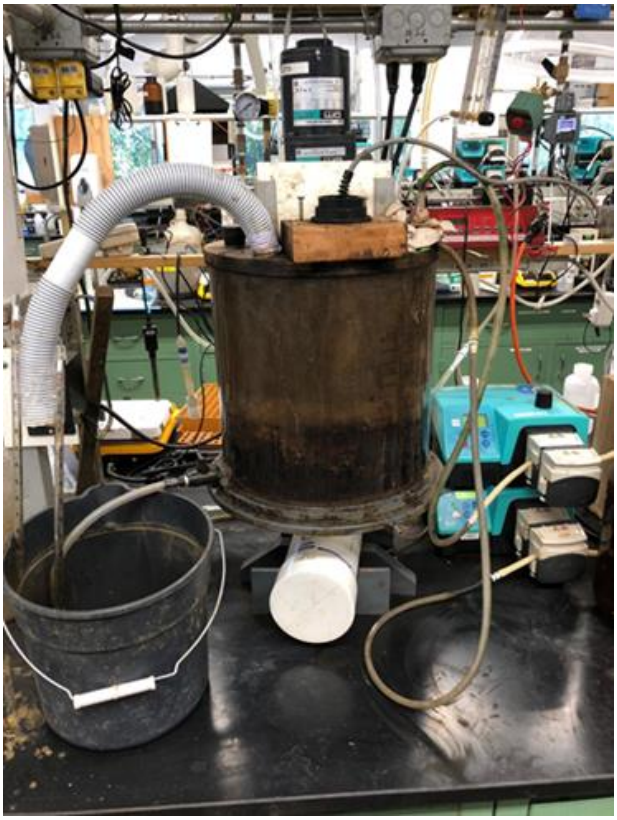

Figure 4.3: E.2.20 Enrichment Reactor

4.1.5. PHA Production Reactors

Production reactors were operated in batch mode with varying working volume (< 3 L); the base of each reactor was a Sanitaire Silver Series fine bubble diffuser. The waste of each production reactor's parent enrichment reactor was used as the inocula (e.g., E.2.20 provides inocula for P.2.20). All experiments were conducted using a pulse fed operation mode. Pulses of undiluted DFL were introduced manually every 45 min for the 4-day SRT evaluations and every 30 min for the remaining events; the operational strategy was selected to ensure that VFAs were never depleted (i.e., avoiding the onset of 'famine' conditions). The volume of DFL added for each pulse was determined based on the parent enrichment reactor specific VFA uptake rate (realized prior to sampling), the DFL VFA concentration, and volumetric dilution effects; the goal was to achieve the same OLR for each pulse as realized in the parent enrichment reactor. Dissolved oxygen, VFAs, PHA, TSS, and VSS were sampled prior to each pulse addition. A discrete mixer was not employed due to the fine bubble aeration providing sufficient mixing.

4.2. Analytical Techniques

Samples were collected to monitor pH, DO, TS, VS, TSS, VSS, soluble nutrients (NH_3-N, NO_3-N, and PO_4-P), VFAs, and PHA. Prior to analyzing soluble constituents, samples were centrifuged to remove biomass, from which the supernatant was filtered through a 0.22 µm syringe filter (Millipore Corp., Billerica, MA, USA). For the analysis of PHA, 10 mL samples were taken from the reactor and centrifuged at 5,000 rpm for 4 min. The resulting supernatant was then decanted before the samples were dried at 100ºC for at least 24 hours. Measurement of pH was accomplished using a Hach (Loveland, CO, USA) Intellical pHC101 pH Electrode. DO concentrations were measured using a Hach HQ40d Meter configured with a LDO101 DO probe. TS, VS, TSS, and VSS were measured in compliance with Standard Methods 2540 D and 2540 E [136].

4.2.1. Nutrient Analysis

Testing for soluble NH_3-N, NO_3-N, and PO_4-P was performed in accordance with Hach method 10031, 10020, and 8048 (equivalent method to Standard Methods 4500-PE [136]), respectively. Absorbance for each reacted sample was measured using a Thermo-Fisher Scientific Corp (Waltham, MA, USA) Spectronic® 20 Genesys ™ spectrophotometer at a

wavelength of 655 nm for NH_3-N, 410 nm for NO_3-N, and 890 nm for PO_4-P. Concentrations were calculated using linear standard curves ($R^2 > 0.99$).

4.2.2. VFA Analysis

VFAs (acetic, propionic, butyric, isobutyric, valeric, isovaleric, and caproic acids) were quantified using a Hewlett-Packard 6890 series gas chromatograph (Agilent Technologies, Inc., Santa Clara, CA, USA) equipped with a flame-ionization detector and a Hewlett-Packard 7679 series injector. The system was interfaced with the Hewlett-Packard GC ChemStation software version A.06.01. VFA separation was achieved using a capillary column (Zebron ZB-WAXplus 30 m x 0.25 mm ID, Phenomenex, Inc., Torrance, CA, USA) which was ramped from an initial 50°C to 200°C in three steps (2 min at 50°C, ramp to 95°C at 30°C/min then to 150°C at 10°C/min and hold for 3 min; lastly, ramp to 200°C at 25°C/min and hold for 12 min) with helium as the carrier gas (1.2 mL/min). The split/splitless injector and detector were operated isothermally at 210 and 300ºC, respectively. Prior to analysis, samples were acidified to a pH < 2 using nitric acid. After preparation, 0.5 μL of each sample was injected in 20:1 split mode. VFA concentrations were determined through retention time matching with known standards (Sigma-Aldrich Co., St. Louis, MO, USA; Thermo Fisher Scientific Inc., Waltham, MA, USA) and linear standard curves ($R^2 > 0.99$).

4.2.3. Intracellular PHA Analysis

Recovered solids (TSSr) PHA content was determined by gas chromatography/mass spectrometry (GC-MS) as described by Braunegg et al. [137]. Dried solids samples were digested for 4 hours at 100°C in 2 mL of acidified methanol (3% v/v sulfuric acid) and chloroform containing an internal standard of benzoic acid (0.25 mg/mL). Following digestion, 2 mL of deionized water was added and vortexed to separate into chloroform and water phases. The chloroform phase was extracted and filtered through sodium sulfate anhydrous to remove excess moisture and particulates. GC-MS was performed using a ThermoScientific ISQ7000-Trace1300 GC-MS instrument. Separation was achieved using a ZB1ms (30 m x 0.25 mm ID) capillary column (Phenomenex, Torrance, CA, USA) with an initial temperature of 40ºC ramped to 200ºC at 5ºC/min and using helium as the carrier gas (1.2 mL/min). 3-hydroxybutyrate (3HB) and 3-hydroxyvalerate monomers (3HV) were verified by retention time and mass spectral matching with PHA standards (Sigma-Aldrich

Co., St. Louis, MO, USA; Metabolix, Cambridge, MA, USA) as methyl ester derivatives, with quantification derived from the internal standard. The Xcalibur 4.0 software program (Thermo Electron Corporation) was used to facilitate PHA quantification. 3HB and 3HV were identified and quantified based on a m/z of 103. 3HB eluted at approximately 6.1-6.5 min, 3HV eluted at approximately 9.1-9.4 min, and the benzoic acid standard eluted at approximately 13.2-13.9 min. Total intracellular PHA content was determined on a percent dry weight basis (mass PHA per mass recovered solids, w/w).

4.3. Calculations

PHA, biomass, and VFAs were normalized to a Cmmol basis for calculations associated with carbon conversion and to compare quantities across varying operations and constituents. As assumed in the metabolic model, a biomass formula $C_1H_{1.8}O_{0.5}N_{0.2}$ (C-mole basis), with 0.0406 Cmmol/gVSS as the Cmmol/L equivalence, was used to normalize biomass VSS. The initial biomass concentration used in rate quantification was approximated using the VSS at the beginning of the cycle. PHA values determined on a Cmmol/L basis were calculated as a function of PHB and PHV mass (mg) and the recovered solids (TSSr) concentration (mg/L). The justification for using TSSr, rather than TSS, for the quantification of reactor PHA concentration is due to its increased accuracy in representing PHA content for the reactor solids not captured for PHA measurement. Calculation of PHA concentrations using reactor TSS was shown to overestimate carbon yields (> 1 $Cmmol_{VFA}/Cmmol_{PHA}$), presumably because PHA-rich biomass is preferentially captured in centrifugation compared to DFL solids which remain post-centrifugation.

PHA yield on substrate ($Y_{PHA/S}$) was calculated at the time point the maximum intracellular PHA concentration was realized, and uses the cumulative amount of VFAs depleted to that point. For enrichment reactor evaluations (high volume to sample event ratio), the effect of sampling on PHA yield calculation is negligible; conversely, production reactor evaluation (low reactor volume to sample event ratio) requires the volume removed for VFA, biomass, and PHA analysis be accounted for in calculations. PHA yield is a valuable metric that indicates the ADF metabolism's efficiency of the MMC during the feast phase. A higher $Y_{PHA/S}$ indicates less carbon is being used for growth and maintenance purposes, as shown in Equation 3.14.

The specific VFA uptake (q_{VFA}) and PHA storage (q_{PHA}) rates were calculated using linear regression on VFA and PHA data with respect to cycle duration, normalized by the initial biomass concentration. Thus, the rate of carbon uptake and PHA storage for a unit of MMC are estimated. Reactor feast lengths, and ultimately the F-F ratio (Equation 4.1), were calculated using the q_{VFA} to reduce error resulting from the feast phase ending in between sample times.

The active biomass concentration was calculated by subtracting PHA content from the VSS concentration, as shown in Equation 4.2. The PHB and PHV fraction of biomass was calculated by factoring the respective molecular weights, as shown in Equation 4.3, for which the summation of PHB and PHV fraction represents the total PHA fraction of biomass.

The calculations for the enrichment and production stage factorial were performed using Microsoft Excel® software; however, statistical analysis of variance utilized ANOVA1 and ANOVA2 packages in MATLAB®. For the optimal operation investigations and metabolic model, all calculations, including statistical calculations were performed using MATLAB®.

4.3.1. Equations

Equation 4.1: Feast-Famine Ratio

$$F/F\ Ratio = \frac{Time_{Feast}}{Time_{Famine}}$$

Equation 4.2: Active Biomass Estimation

$$X = VSS\left(1 - \frac{\%PHA}{100}\right)\left(\frac{1}{1000}\right);\ [\frac{g}{L}]$$

Equation 4.3: PHB or PHV Biomass Fraction

$$f_{PHB(V),X} = \frac{\%PHB(V)}{100 - \%PHB(V)}\frac{MW_X}{MW_{PHB(V)}};[\frac{Cmol}{Cmol}]$$

Equation 4.4: Fermenter Manure Loading

$$W_{Manure} = \frac{OLR(V_{fermenter})}{1000(TS)(VS)};[\frac{kg}{day}]$$

5. SRT & OLR Factorial: Results and Discussion

A primary focus of this research was to establish near-optimal operating criteria for the PHA Enrichment Reactor (Figure 2.7); to that end, an experimental design was executed focused on two of the most critical, and easily controllable, Enrichment Reactor operational parameters, SRT and OLR, with tested values of 2-4 days and 10-30 C-mmol/L-d, respectively. The following discussion presents results from these analyses, first comparing effects of SRT and OLR independently, then concluding with a discussion on the combined effect of SRT-OLR. The common thread in this discussion is PHA, and thus the dependent variables in this study, used to determine near-optimal operational criteria, were PHA yield and maximum intracellular PHA concentration.

5.1. Effect of SRT

5.1.1. Enrichment Reactors

Enrichment profiles are presented for all SRTs at constant OLR; the variable OLR for a given SRT prevents the compilation of all data for a given SRT on a single plot. An OLR of 10 Cmmol/L-d was chosen as minimum operating OLR. Figure 5.1 illustrates the average (n = 3; operational days 148, 156, and 172) VFA uptake and PHA accumulation profile for the 10 C-mmol/L-d reactors, by SRT.

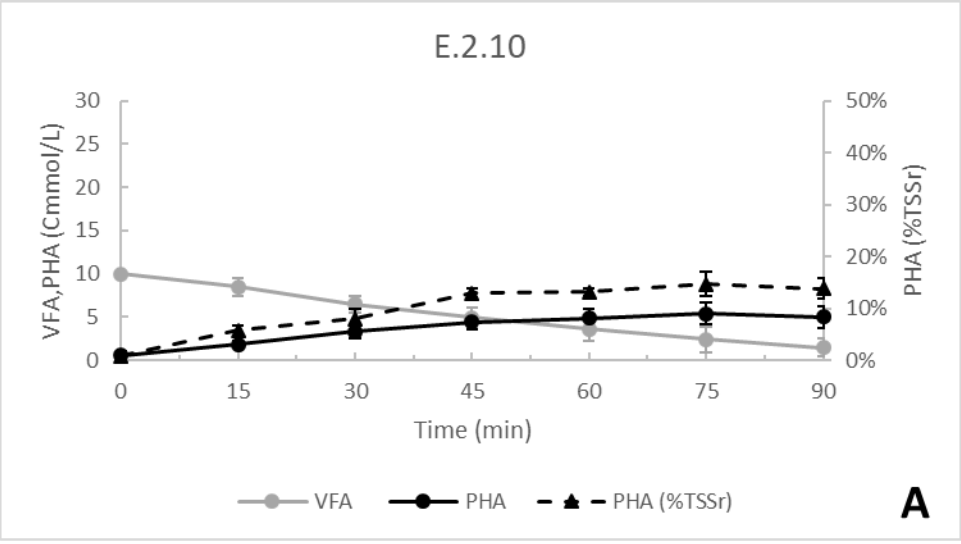

Figure 5.1: Average (n = 3) 10 Cmmol/L Enrichment Assessment by SRT (A, B, and C represent 2-, 3-, and 4-day SRT, respectively)

Figure continued on next page

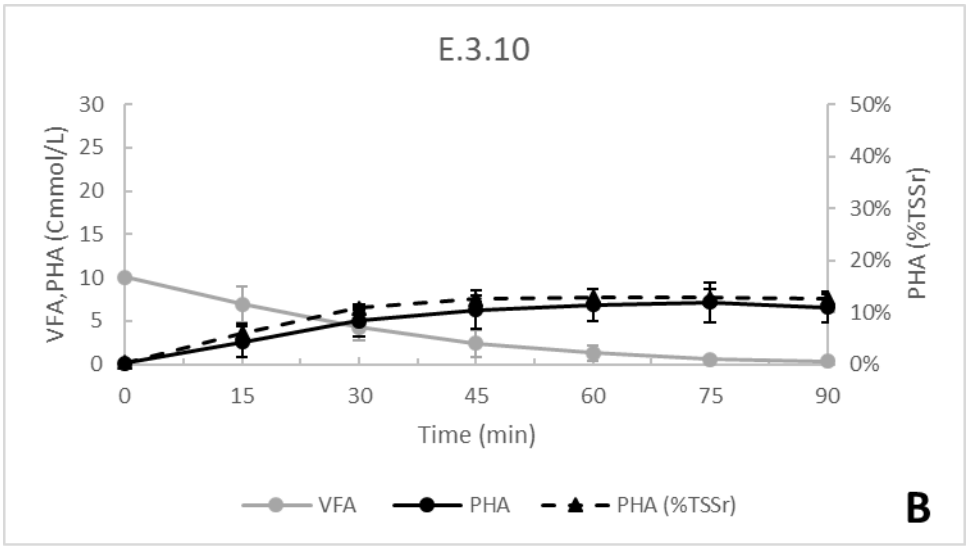

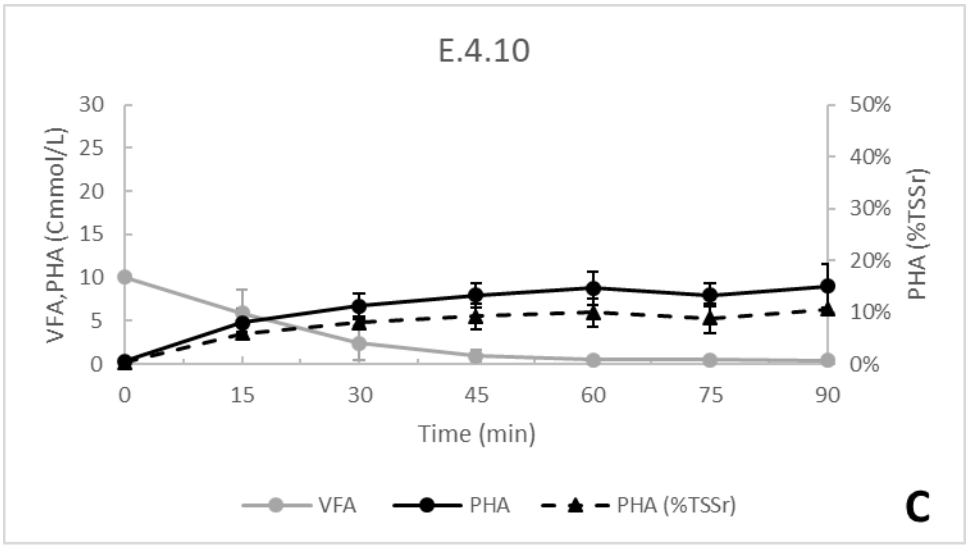

Figure 5.1: Average (n = 3) 10 Cmmol/L Enrichment Assessment by SRT (A, B, and C represent 2-, 3-, and 4-day SRT, respectively)

As shown, when operating at an OLR of 10 Cmmol/L-d, the average VFA uptake rate increases with SRT, and as a result the feast length decreases with increased SRT; the F-F ratios were 0.08, 0.05, and 0.04 for SRTs of 2, 3, and 4 days, respectively. Commensurately, a shorter feast length resulted in increased PHA yield on VFAs consumed. However, maximum intracellular PHA content was observed at the lowest SRT. Average yield values for E.2.10, E.3.10, and E.4.10 were 0.70, 0.78, and 0.84 $Cmmol_{PHA}/Cmmol_{VFA}$, while average peak PHA content were 14.9%, 13.6%, and 10.1% TSS_r (w/w), respectively. This contradictory response can be explained by accounting for biomass content; in other words, although VFA uptake

rates increased with SRT, the specific VFA uptake rate (q_{VFA}) for E.2.10, E.3.10, and E.4.10 were 0.33, 0.34, and 0.21 Cmmol/gVSS-min, respectively; thus as can be inferred, the shorter SRT MMC were ultimately more efficient in consuming VFAs and storing PHA.

Scaling up from a low OLR, 20 Cmmol/L-d was chosen as an intermediate OLR to be evaluated. Figure 5.2 shows the average (n = 3; operational days 94, 127, and 129 for 2-day, 66, 73, and 80 for 3-day, and 18, 22, and 31 for 4-day SRT) VFA uptake and PHA accumulation profile for the 20 C-mmol/L-d reactors, by SRT.

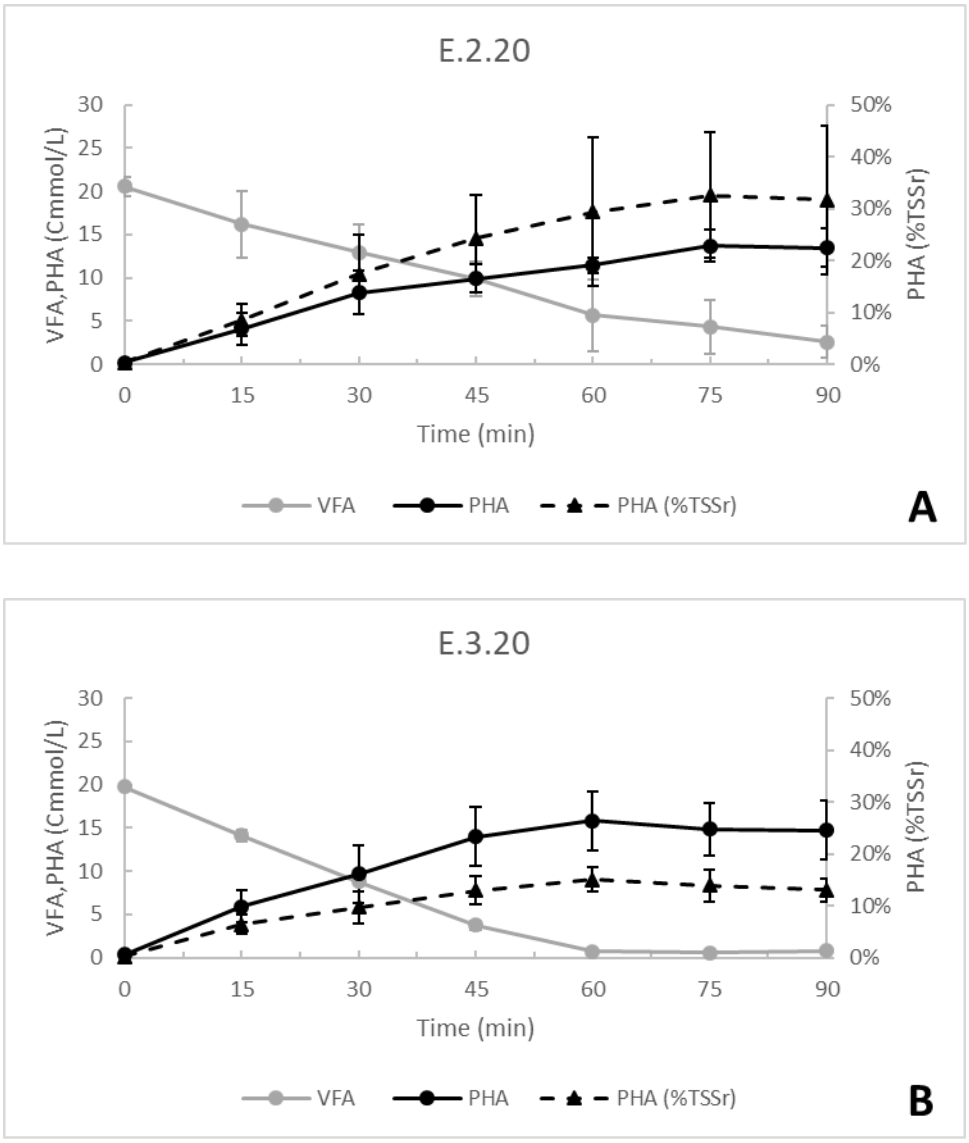

Figure 5.2: Average (n = 3) 20 Cmmol/L Enrichment Assessment by SRT (A, B, and C represent 2-, 3-, and 4-day SRT, respectively)

Figure continued

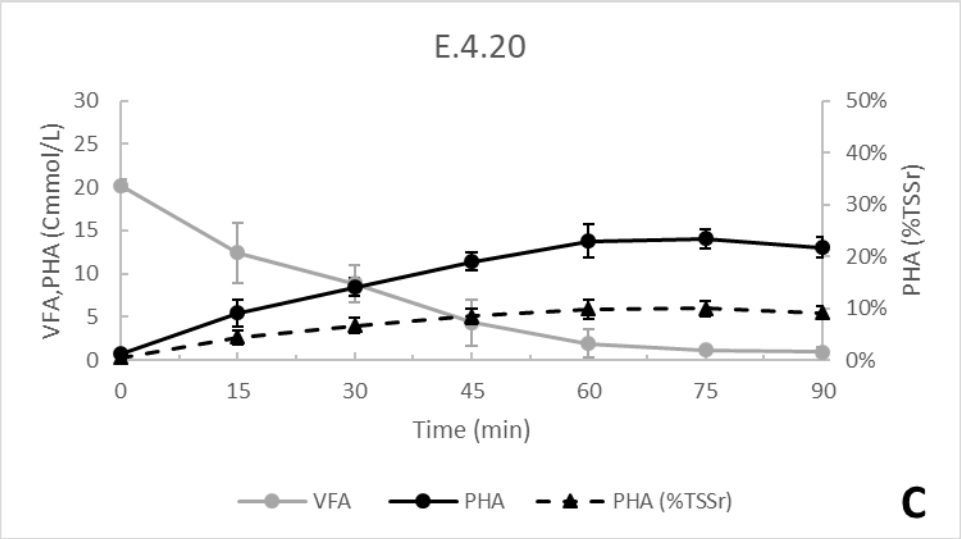

Figure 5.2: Average (n = 3) 20 Cmmol/L Enrichment Assessment by SRT (A, B, and C represent 2-, 3-, and 4-day SRT, respectively)

Under an organic loading rate of 20 Cmmol/L-day, E.3.20 and E.4.20 experienced similar feast lengths of roughly 70 min, sharing an average F-F ratio of 0.05. In contrast, E.2.20 only reached complete VFA consumption once within 90 min, averaging a F-F ratio of 0.07. However, contrary to the 10 Cmmol/L-day findings, decreased feast-length did not result in higher PHA yield (Y_{PHA}), as E.2.20, E.3.20, and E.4.20 averaged 0.82, 0.82, and 0.73 $Cmmol_{PHA}/Cmmol_{VFA}$, respectively. As shown, peak intracellular PHA content increased with lower SRTs, particularly for the 2-day operation, where E.2.20 averaged a peak PHA content of 33% TSS_r (w/w); this result was more than double that observed by the E.3.20 MMC, and triple the E.4.20 MMC. As a caveat to these observations, the large variation in intracellular PHA content is due to a small sample size, coupled with the 2-day reactors seeing their best performance on operational day 127, where E.2.20 reached an intracellular PHA content of 48% TSS_r (w/w). This PHA content is remarkably high for the enrichment stage of this PHA production process, as compared to, for example, a maximum achieved by Chua et al. [108] of 31%. Commensurate with elevated PHA productivity, specific VFA uptake rates (q_{VFA}) increased with shorter SRTs, as E.2.20, E.3.20, and E.4.20 averaged rates of 0.47, 0.22, and 0.18 Cmmol/gVSS-min, respectively. This aligns with the comparison at an OLR of 10 Cmmol/L-day, as the lower SRTs saw increased efficiency in VFA consumption and storage.

Figure 5.3 shows the average (n = 3; operational days 94, 127, and 129 for 2-day, 66, 73, and 80 for 3-day, and 18, 22, and 31 for 4-day SRT) VFA uptake and PHA accumulation profile for the 25 C-mmol/L-d reactors, by SRT.

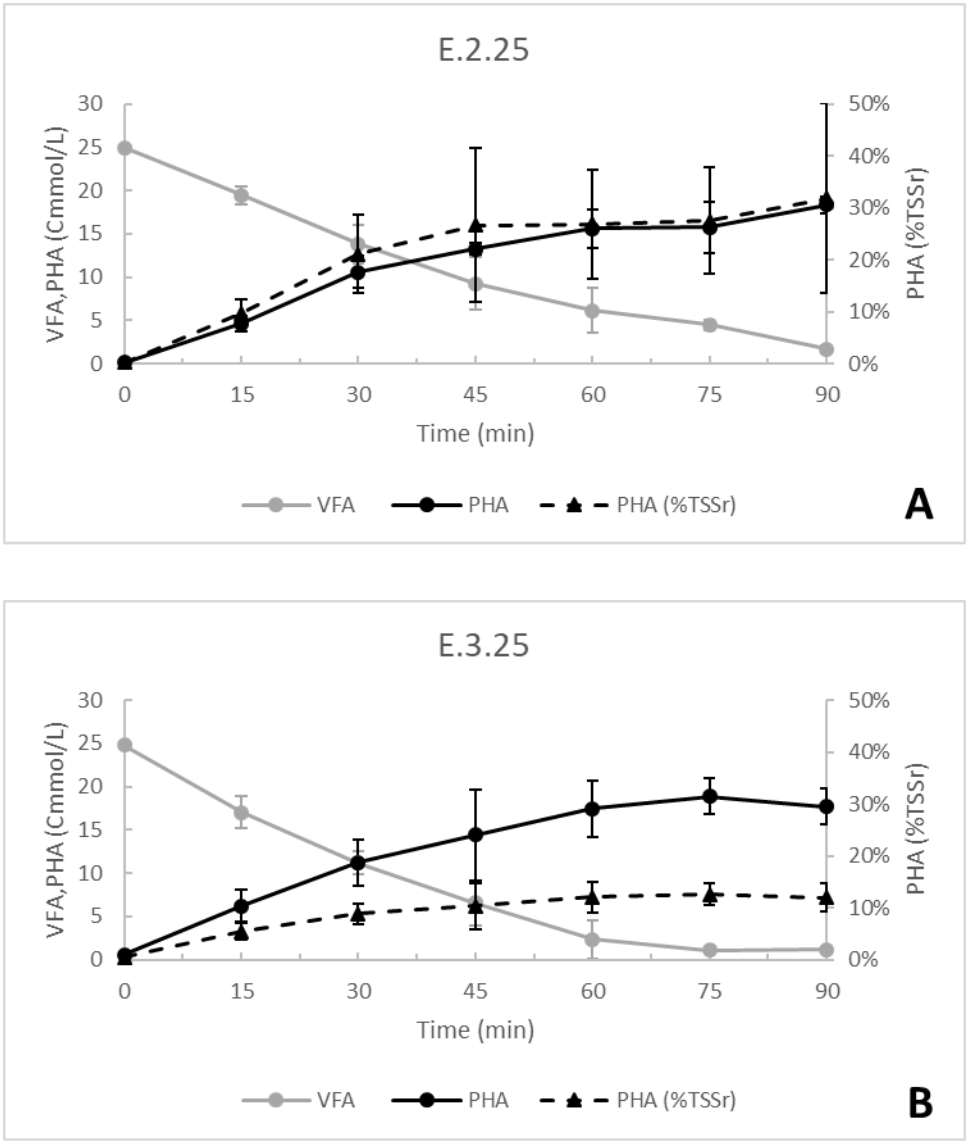

Figure 5.3: Average (n = 3) 25 Cmmol/L Enrichment Assessment by SRT (A, B, and C represent 2-, 3-, and 4-day SRT, respectively)

Figure continued on next page

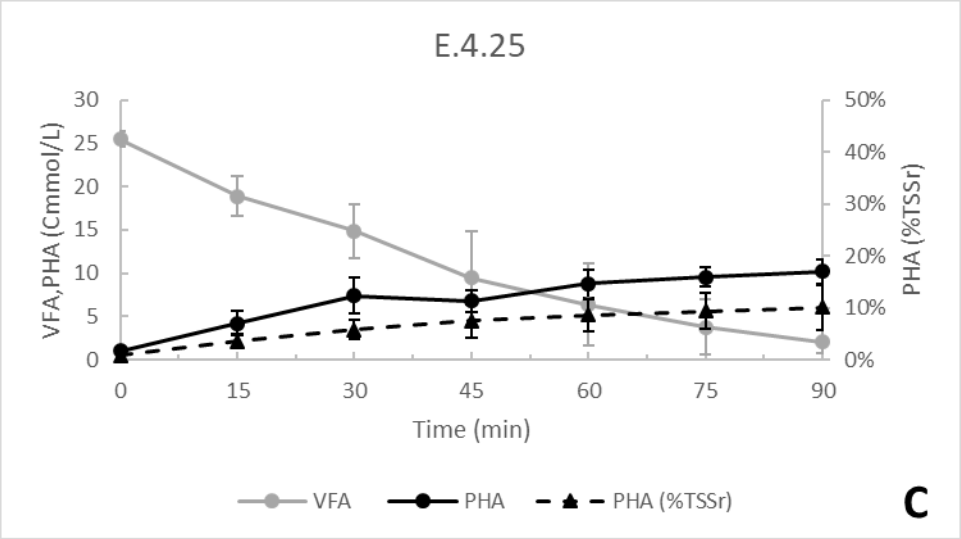

Figure 5.3: Average (n = 3) 25 Cmmol/L Enrichment Assessment by SRT (A, B, and C represent 2-, 3-, and 4-day SRT, respectively)

The 20 and 25 Cmmol/L-d enrichment profiles are remarkably similar, with the exception of E.4.25 exhibiting a longer feast period and significantly lower PHA yield of 0.43 $Cmmol_{PHA}/Cmmol_{VFA}$, indicating a decrease in the MMC's efficiency regarding the uptake and conversion of VFAs to PHA. The specific VFA uptake rate, PHA yield, F-F ratio, and intracellular PHA content for E.2.25 and E.3.25 are comparable to those of E.2.20 and E.3.20, suggesting PHA production is a linear function of VFAs added within an SRT range of 2 to 3 days and OLR range of 20 to 25 Cmmol/L-d. Similar MMC behavior for various operational ranges was observed in other SRT vs OLR studies [27, 37, 96]. Of note, E.2.25 achieved an intracellular PHA content of 52.8% TSS_r (w/w) on operational day 127, the highest content observed in the enrichment reactor factorial.

Following the evaluation of SRT effect on the 25 Cmmol/L-d reactors, reactor sampling assessments for the 30 Cmmol/L-d reactors, deemed the maximum operational OLR, were evaluated. Figure 5.4 shows the average (n = 3; operational days 94, 127, and 129 for 2-day, 66, 73, and 80 for 3-day, and 18, 22, and 31 for 4-day SRT) VFA uptake and PHA accumulation profile for the 30 C-mmol/L-d reactors, by SRT.

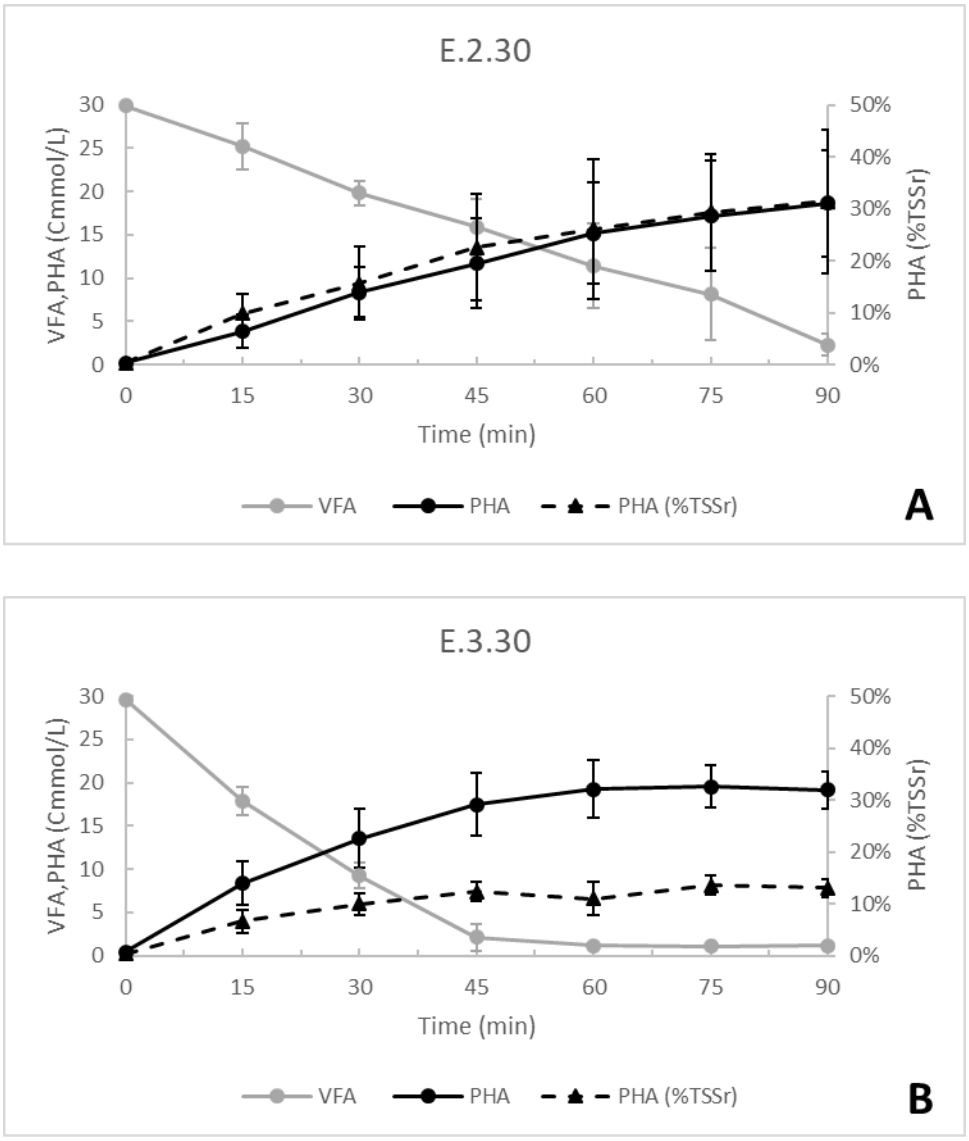

Figure 5.4: Average (n = 3) 30 Cmmol/L Enrichment Assessment by SRT (A, B, and C represent 2-, 3-, and 4-day SRT, respectively).

Figure continued on next page

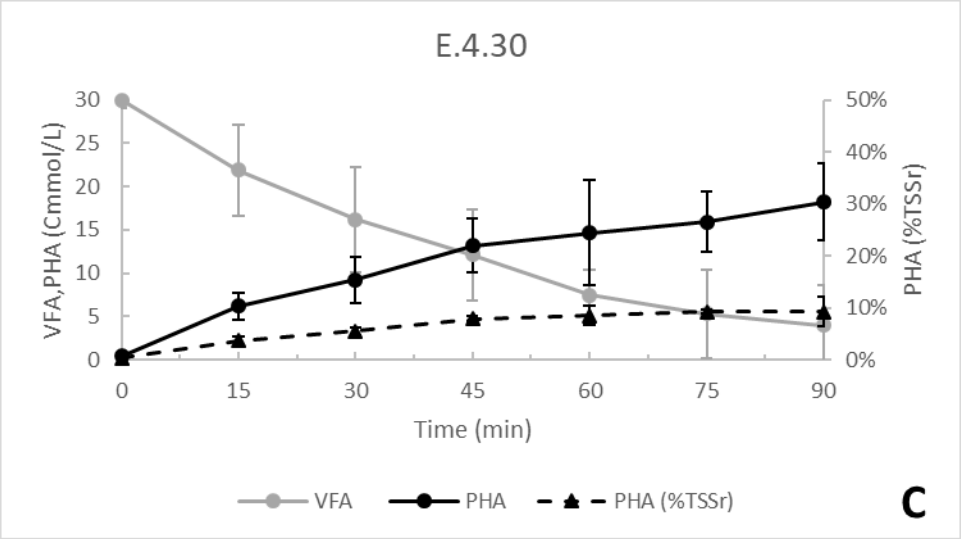

Figure 5.4: Average (n = 3) 30 Cmmol/L Enrichment Assessment by SRT (A, B, and C represent 2-, 3-, and 4-day SRT, respectively)

As can be seen, the primary difference between SRTs is the intracellular PHA content increasing with decreased SRT, especially from a 3-day to a 2-day SRT. Interestingly, E.3.30 exhibits a much shorter feast length than E.2.30 and E.4.30, despite the high organic loading. This is attributed to E.3.30 having an average specific VFA uptake rate of 0.37 compared to 0.17 Cmmol/gVSS-min for the E.4.30 MMC, with only 18% less biomass. Regardless of feast length, all three SRTs exhibit relatively equal PHA storage efficiency, with average PHA yields for E.2.30, E.3.30, and E.4.30 being 0.67, 0.69, and 0.67 $Cmmol_{PHA}/Cmmol_{VFA}$, respectively.

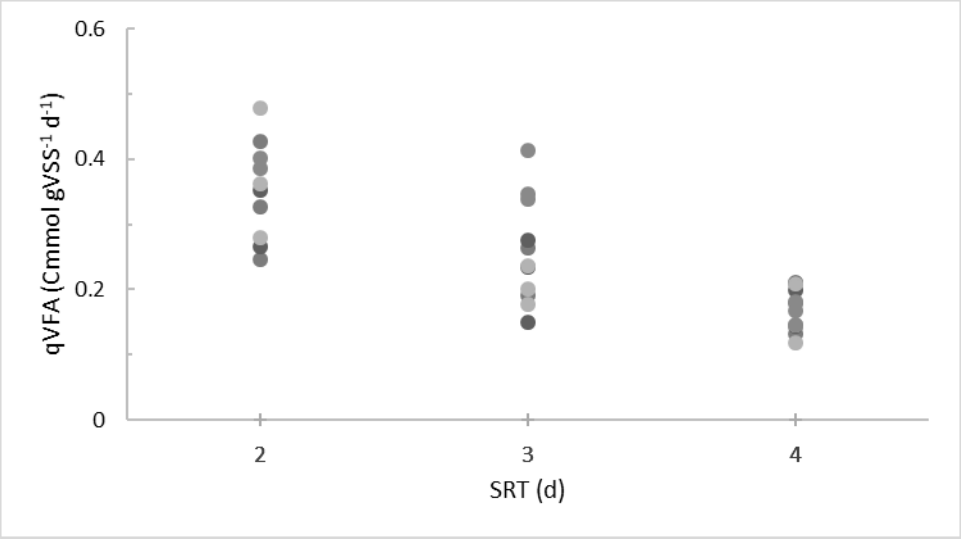

Figure 5.5: Enrichment q_{VFA} vs SRT (n=10, n=11, and n=11 for 2-,3-, and 4-day SRT, respectively)

One of the more pronounced differences observed between SRTs was the specific VFA uptake rate (q_{VFA}). Figure 5.5 shows the difference in specific VFA uptake rate for the 2-, 3-, and 4-day enrichment assessments; average specific VFA uptake rates were 0.35 ± 0.07, 0.26 ± 0.08, and 0.18 ± 0.03, respectively (n = 10). Generally, such a response aligns with microbial growth theory for suspended growth systems; specifically, the microbial specific growth rate, μ, is inversely proportional to SRT, and thus the rate of substrate utilization (r_s; i.e., VFA consumption) and the specific rate are inversely proportional to SRT (see Equation 5.1; Y = yield, X = MLVSS).

Equation 5.1: SRT's Relationship to Specific Growth Rate and Substrate Utilization

$$r_s = \frac{\mu}{Y} * X = \frac{1}{SRT * Y} * X; \;\; q_s = \frac{r_s}{X} = \frac{1}{SRT * Y}$$

However, conventional microbial theory links r_{su} to microbial growth, not PHA storage. Yet, lower SRT and increased specific VFA uptake rates did correlate with higher intracellular PHA content. Similarly, Chua et al. [108] observed a roughly 30% higher PHA content when operating at a 3-day SRT as compared to a 10-day SRT. Conversely, Dias et al. [28] suggests that greater PHA storage occurs with increasing SRT, although it is also suggested that SRTs less than 2 days beget great PHA accumulation. Ultimately the data suggests a metabolic disconnection between VFA uptake and growth under F-F conditions; clearly the induced feast metabolism and associated overloading of VFAs at t=0 yields a temporary non-growth,

"energy spilling" [69] metabolic response. Indeed, higher growth rates have been shown to yield decreased intracellular PHB content, as observed in pure cultures and MMC by van Aalst-van Leeuwen et al. [39] and Beun et al. [38]. Ultimately the relationship between substrate uptake rate, specific growth rate, and polymer storage remains poorly understood and requires further study. Nevertheless, this research suggests a shorter SRT – 2 days – enriches for a MMC with a larger PHA-storing capacity.

As previously mentioned, SRT generally shares a positive relationship with reactor solids concentration, a metric that has profound implications on performance and design of a PHA production process. Solids concentrations were evaluated for each reactor at the beginning of the operation cycle and evaluated over the feast period to track changes over time. Solids at t = 0 represents WAS concentrations at the end of the previous cycle, assuming the added solids from the DFL are hydrolyzed as substrate. The decision to ignore the relatively small solids addition from the diluted DFL purposefully allows for data analysis on the basis of just the potential PHA producing microorganisms in the MMC. Figure 5.6 illustrates the average enrichment mixed liquor solids inventory by SRT during each OLR assessment as well as the TSS recovery efficiency. As shown, SRT has a pronounced effect on reactor solids concentration; the average increase in t = 0 solids concentration from 2- to 3-day SRT and from 3- to 4-day SRT is 42% and 18%. The average VSS/TSS ratio for the 2-, 3-, and 4-day SRT configurations were 0.83, 0.81, and 0.80, respectively, indicating that longer SRTs increased inert solids minimally. This primarily has implications on volumetric productivity, which is the product of intracellular PHA content ($\%TSS_r$) and the concentration of recovered solids.

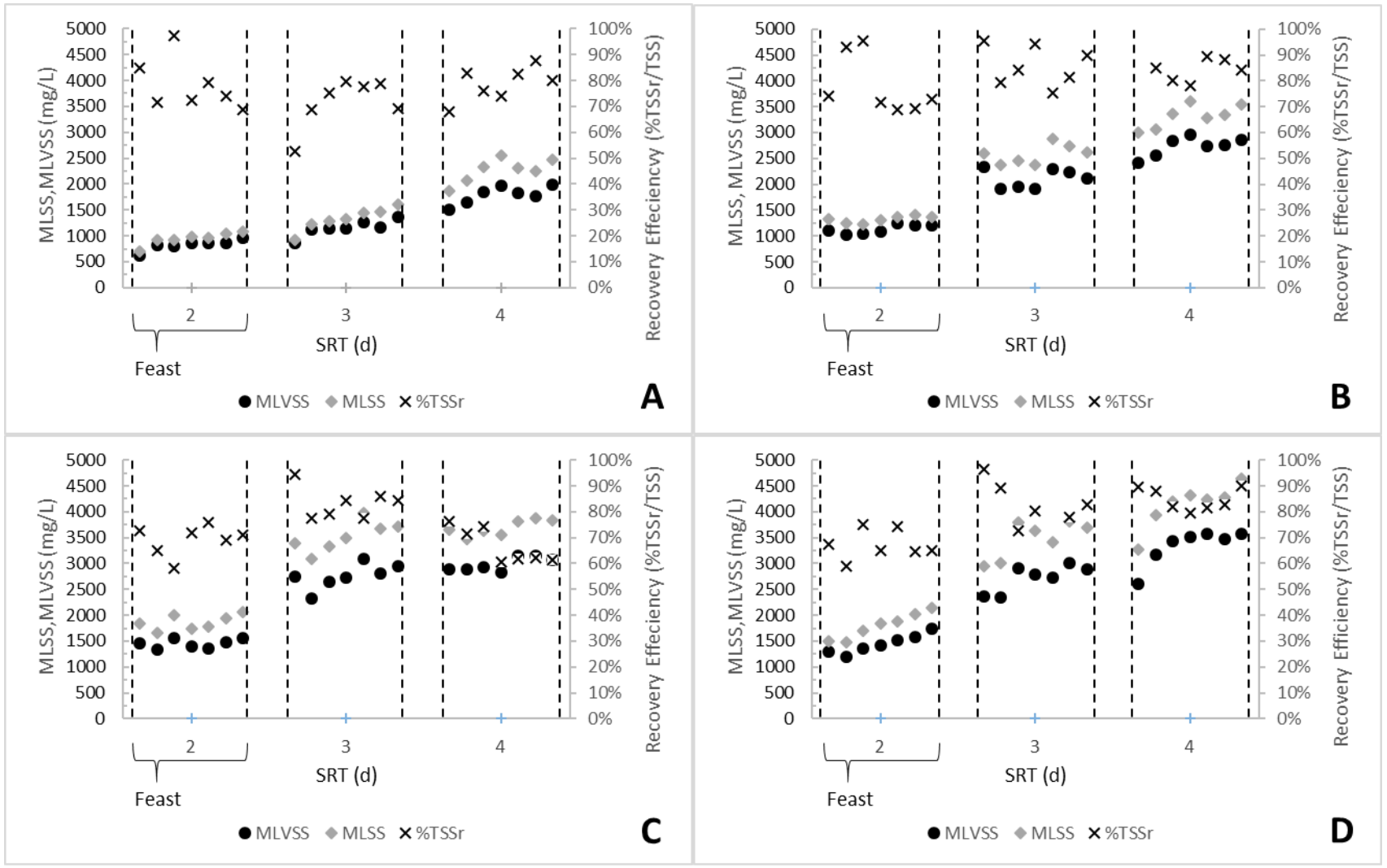

Figure 5.6: Average Enrichment Reactor Solids Inventory by SRT (A, B, C, and D represent OLRs of 10, 20, 25, and 30 Cmmol/L, respectively)

5.1.2. Production Reactors

Each of the aforementioned enrichment reactors provided biomass for same-day fed-batch production assessments. Initial production reactor volume, sourced from the enrichment WAS, was always 0.45-0.5 L for consistency; however, due to varying initial VSS concentrations, DFL VFA concentrations, specific uptake rates, and rate of dilution, the volume of DFL added with each pulse varied. The average production reactor carbon profiles for each reactor are shown in Figure 5.7. Predicted VFA profiles represent the pulse-feeding strategy employed for each reactor, assuming a constant substrate uptake after every pulse. More information on the pulse-feeding is found in Chapter 4.

Similar to the enrichment stage, a prominent difference between SRTs is the specific VFA uptake rate. Average specific VFA uptake rates for the 2-, 3-, and 4-day reactors were 0.17, 0.16, and 0.12 Cmmol/gVSS-min, respectively (n = 12). These values are substantially lower than their enrichment reactor counterparts due to being averages of specific uptake over all the substrate pulse additions (substrate uptake generally decreased with every pulse added). This is discussed further in the effects of OLR.

As can be observed in Figure 5.7, production results are remarkably similar between the 3-day and 4-day reactors; however, a significant increase in peak intracellular PHA content on a weight basis was observed for the 2-day reactors. Average peak percent PHA for the 2-, 3-, and 4-day production reactors were 30.5, 22.5, and 22.4% TSS_r (w/w). Similarly, higher PHA yield was generally observed for the 2-day reactors, with average values for the 2-, 3-, and 4-day reactors of 0.91, 0.72, and 0.74 $Cmmol_{PHA}/Cmmol_{VFA}$. The highest obtained value of 55.2% TSS_r – 73.2% on a VSS basis – was achieved by P.2.30 on operational day 127. Similar values of 75 and 77% VSS basis were achieved by Albuquerque et al. [103] and Jiang et al. [123]. Interestingly, unlike the research presented herein, these cited studies were performed under growth limiting conditions (namely ammonia limitation) favoring PHA storage. Although performance matched growth-limited studies, this peak PHA content was only achieved one time. Excluding the best performance achieved by the 2-day reactors on operational day 127, P.2.20 achieved peak intracellular PHA contents of 36% and 26% TSSr and 41% and 33% VSS basis, the highest performing OLR for the 2-day reactors.

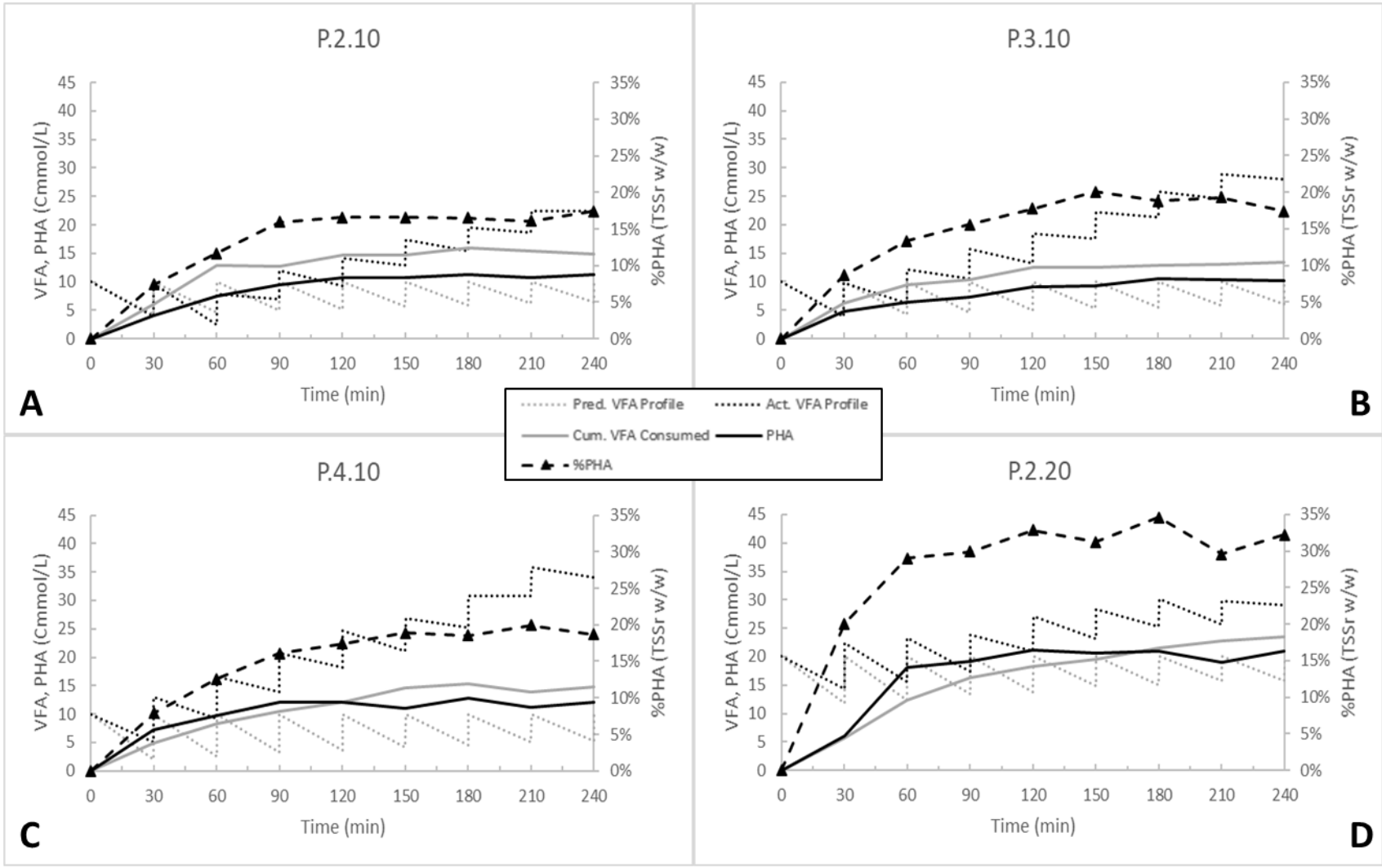

Figure 5.7: Production Reactor Carbon Conversion Assessment (A, B, C, and D represent P.2.10, P.3.10, P.4.10, and P.2.20, respectively). ***Figure continued on next page***

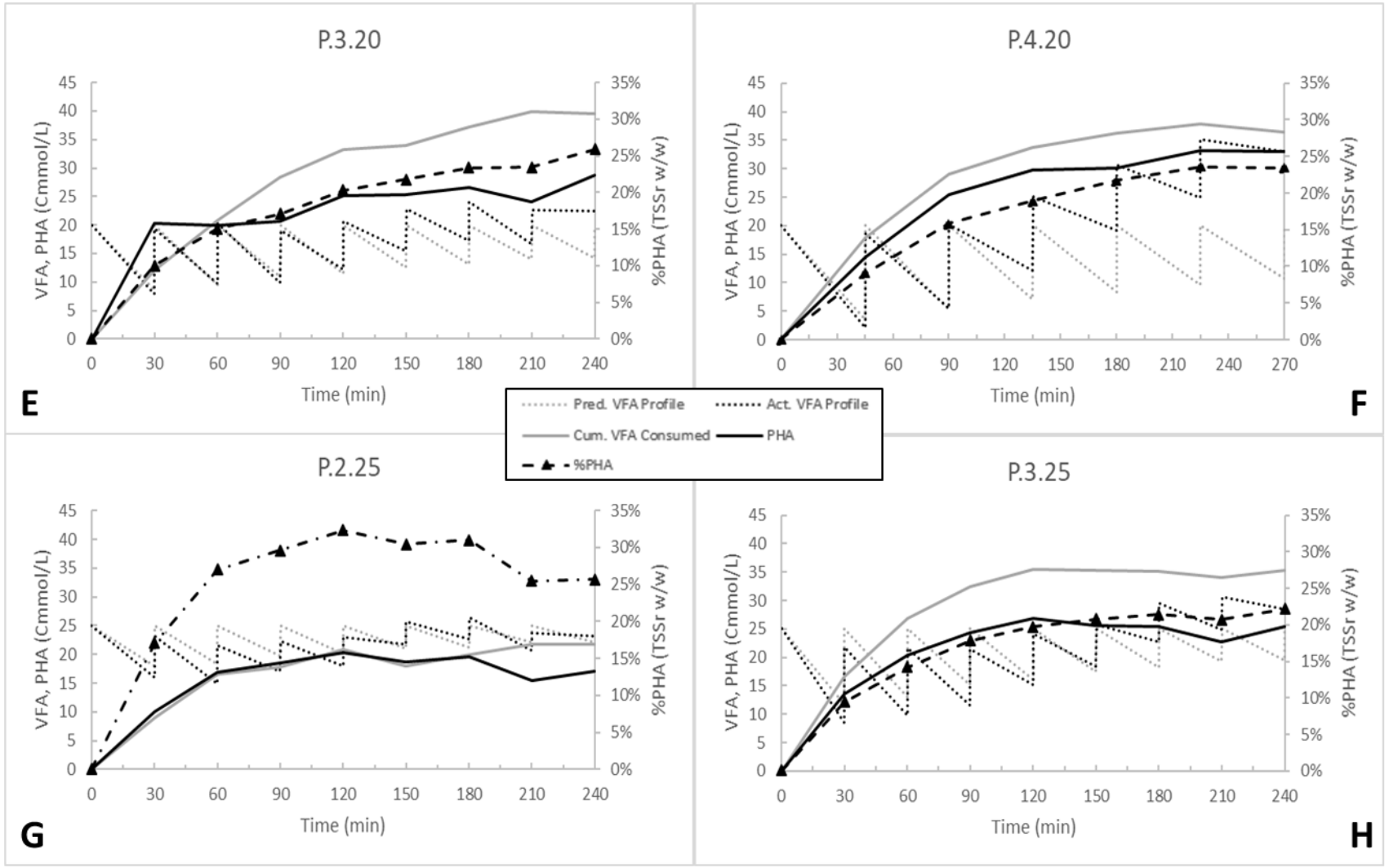

Figure 5.7: Production Reactor Carbon Conversion Assessment (E, F, G, and H represent P.3.20, P.4.20, P.2.25, and P.3.25, respectively). ***Figure continued on next page***

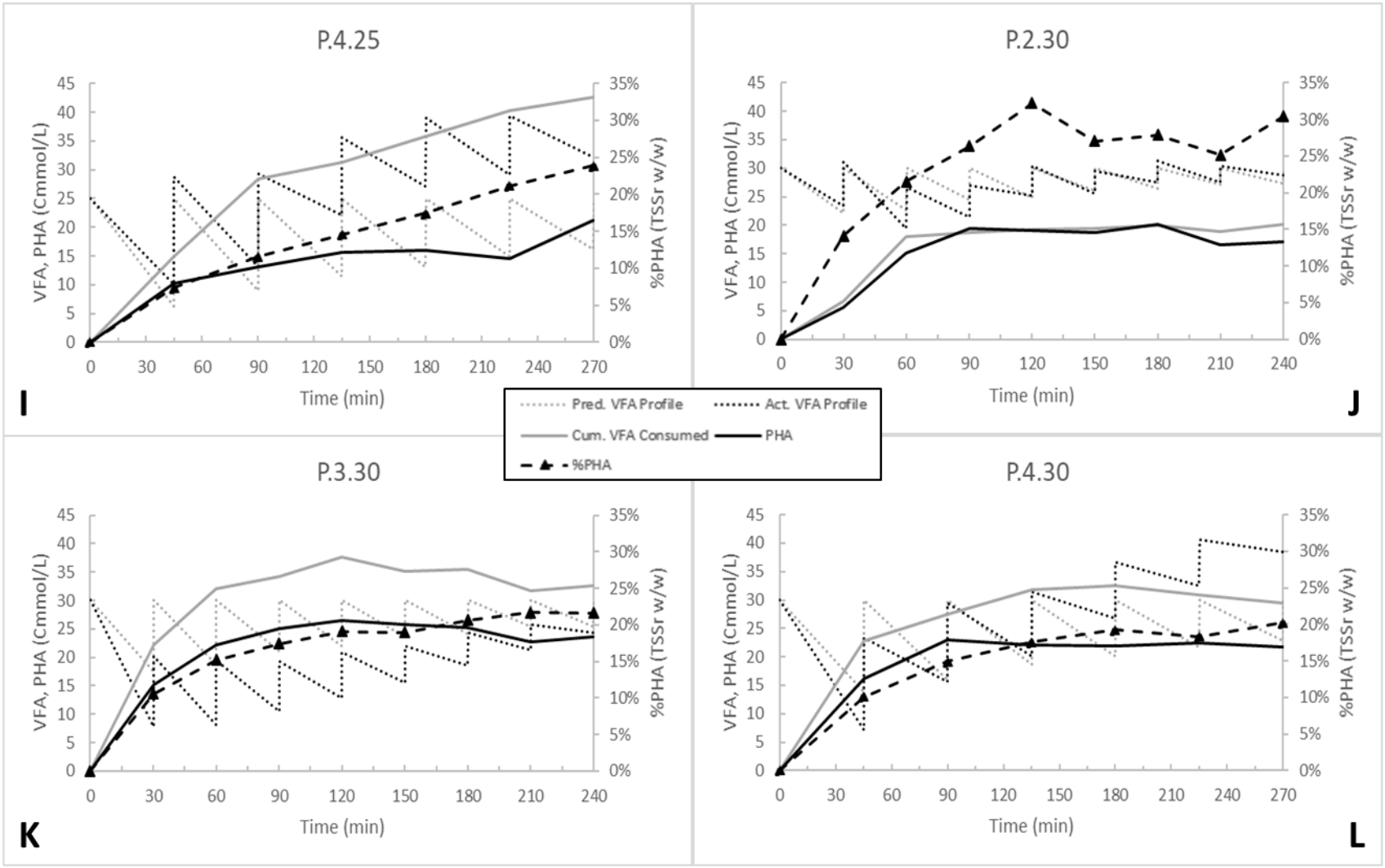

Figure 5.7: Production Reactor Carbon Conversion Assessment (I, J, K, and L represent P.4.25, P.2.30, P.3.30, and P.4.30, respectively).

5.2. Effect of OLR

5.2.1. Enrichment Reactors

As previously shown in Figure 5.6, higher applied OLR resulted in an increase in reactor solids concentration, as more carbon for growth and residual DFL solids were being supplied to the system. Average VSS and TSS concentrations increased 3.5% and 4% per additional Cmmol/L-d loaded, except from the 25 to 30 Cmmol/L-d configurations where solids increase was negligible. Of note, q_{VFA} and feast length were relatively constant across all OLRs for a given SRT, indicating an increase in solids with OLR did not result in decreased substrate uptake efficiency.

While peak PHA content on a $\%TSS_r$ basis was generally constant across OLRs for a given SRT, the maximum PHA produced (g) was a function of OLR, as depicted in Figure 5.8. Average peak weight of PHA for the 10-, 20-, 25-, and 30 Cmmol/L-d reactors were 0.3, 0.61, 0.67, and 0.79 grams, respectively. This indicates that, for the OLR ranges in question, net PHA produced is a linear function of carbon supplied, roughly 0.014 gPHA/Cmmol.

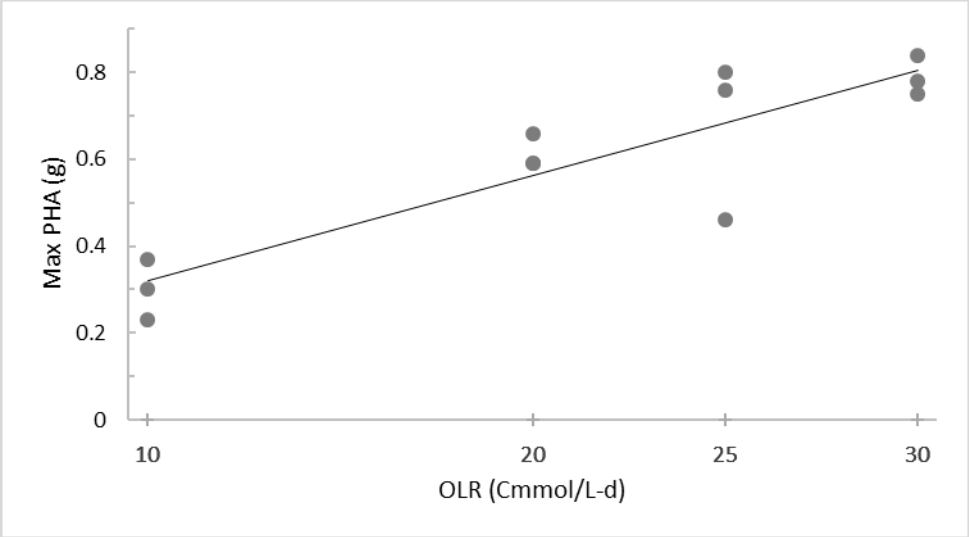

Figure 5.8: Maximum PHA (g) as Related to OLR

5.2.2 Production Reactors

The independent impacts of OLR for the production reactors were similar to that of the enrichment. Uniquely, as on can see in Figure 5.7, as the OLR decreases, the amount the rate of substrate uptake generally decreases between pulses is intensified (i.e. at lower OLRs the MMC have a low propensity for maintaining a constant rate of substrate uptake). This

indicates the MMC are more susceptible to high PHA concentrations inhibiting substrate uptake.

5.3. Combined SRT & OLR Assessment

Bivariate statistical analysis of the combined effects of SRT and OLR on PHA yield, intracellular PHA content, and total PHA produced was performed to identify potential optimal operational parameters. Additionally, contour plots were developed for enhanced visualization of SRT and OLR ranges relative to performance.

5.3.1 Enrichment Reactors

5.1.3.1. Feast-Famine

The F-F ratio was relatively consistent across all OLRs for each SRT, suggesting it is independent of OLR within a range of 10-30 Cmmol/L-d. The average F-F ratios for the 2-, 3-, and 4-day SRT operations were 0.05, 0.05, and 0.07, respectively. All reactor F-F ratios were below the suggested maximum F-F of 0.20 necessary to achieve process success [112]; therefore, sufficient famine lengths for inducing a stressful microbial environment suitable for a PHA-producing MMC were maintained throughout the factorial.

5.1.3.2. PHA Yield on Substrate

PHA yield is analogous to PHA production efficiency and aids in quantifying the degree of enrichment of PHA-producing microorganisms within an enrichment reactor. For said reasons, it is a parameter that is heavily valued in optimal operation determination. Figure 5.9 depicts the results of a two-way analysis of variance (ANOVA2) performed with PHA yield as the response variable, and SRT and OLR as the two factors.

Statistical tests on the effects of SRT and OLR regarding PHA yield verified that there is no correlation between the two operational parameters and PHA yield, independently; however, the interaction between SRT and OLR is significant within a 97% confidence interval. As can be inferred, there is no optimal SRT or OLR with respect to PHA yield, but there exists an optimal combination(s) of the two parameters, identified by E.2.20, E.2.25, E.3.20, E.3.25, and E.4.10.

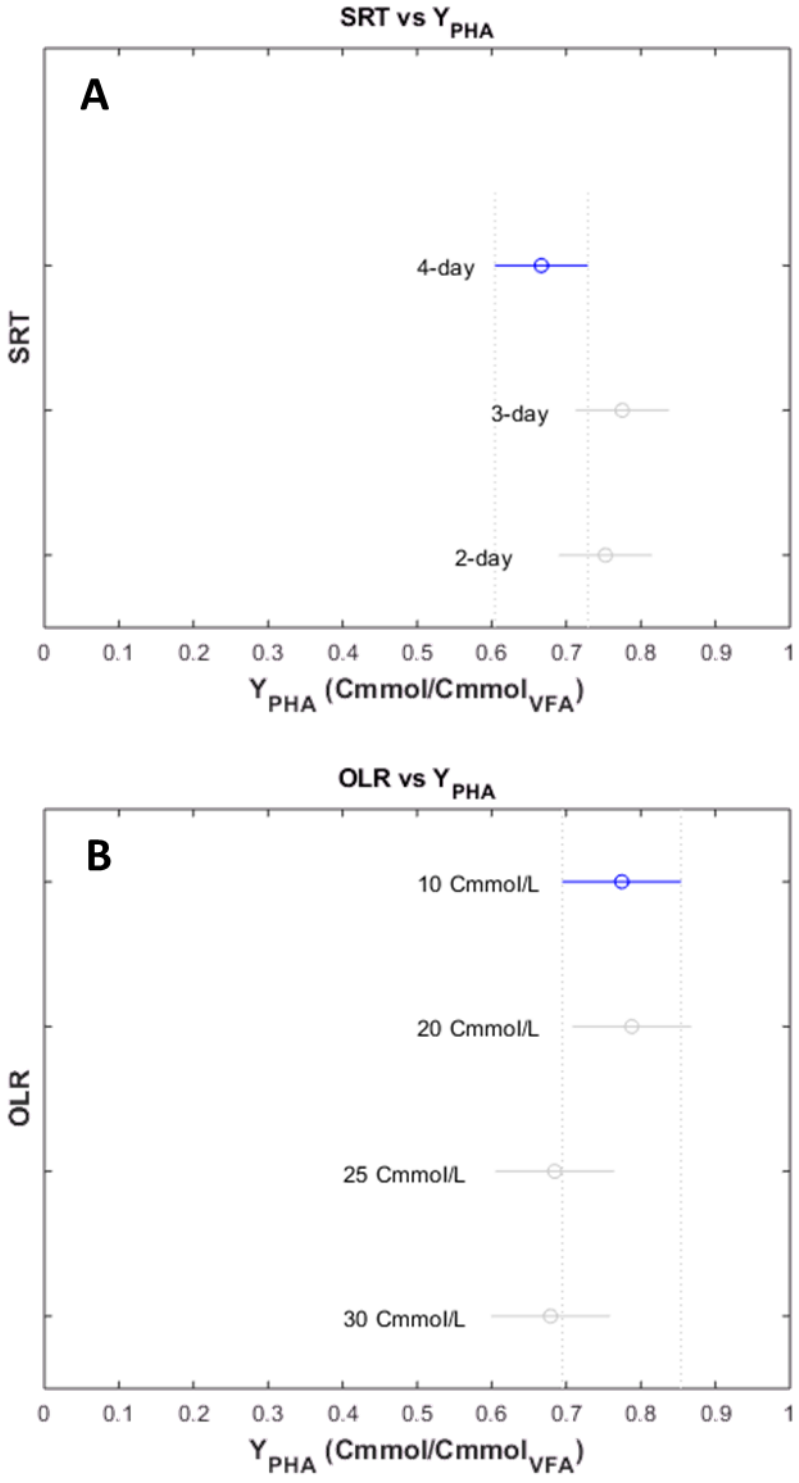

Figure 5.9: Factorial Operational Criteria vs. PHA Yield on Substrate (A and B represent SRT and OLR).

Figure 5.10 illustrates average PHA yields over the SRT and OLR ranges evaluated.

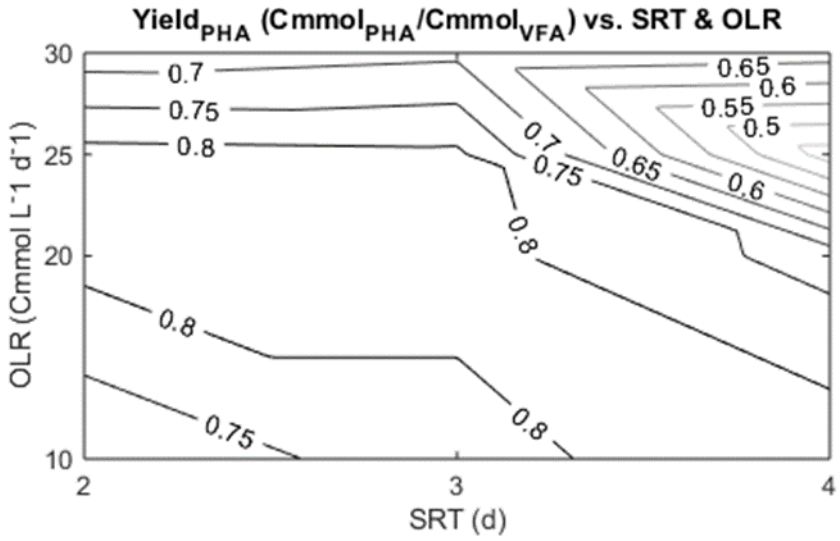

Figure 5.10: SRT & OLR vs PHA Yield on Substrate

As shown, PHA yield is at a maximum within an OLR range of 20 to 25 C-mmol/L-d and an SRT range of 2 to 3 days; additionally, a 10 Cmmol/L-d OLR and 4-day SRT exhibited similar yields. The average PHA yield for the reactors operating within said ranges is 0.82 $Cmmol_{PHA}/Cmmol_{VFA}$ (n = 15), indicating a substantial fraction of carbon being stored as PHA.

5.1.3.3. Maximum PHA Content

For a commercial PHA production process, intracellular PHA content is of utmost importance – specifically, the weight percent PHA reported on TSS_r basis. This metric represents the PHA in the effluent solids, prior to extraction, and has profound implications on economic feasibility – specifically, low intracellular PHA content equates to increased chemical usage per gram of PHA recovered for extraction. Referring to Figure 5.6, no correlation between in-reactor solids content and that recovered from centrifuging and drying methods was observed; therefore, quantification of PHA recovered on a $\%TSS_r$ is consistent across all reactors. Figure 5.11 shows the ANOVA2 results for the two factors, SRT and OLR, with maximum intracellular PHA content as the response variable.

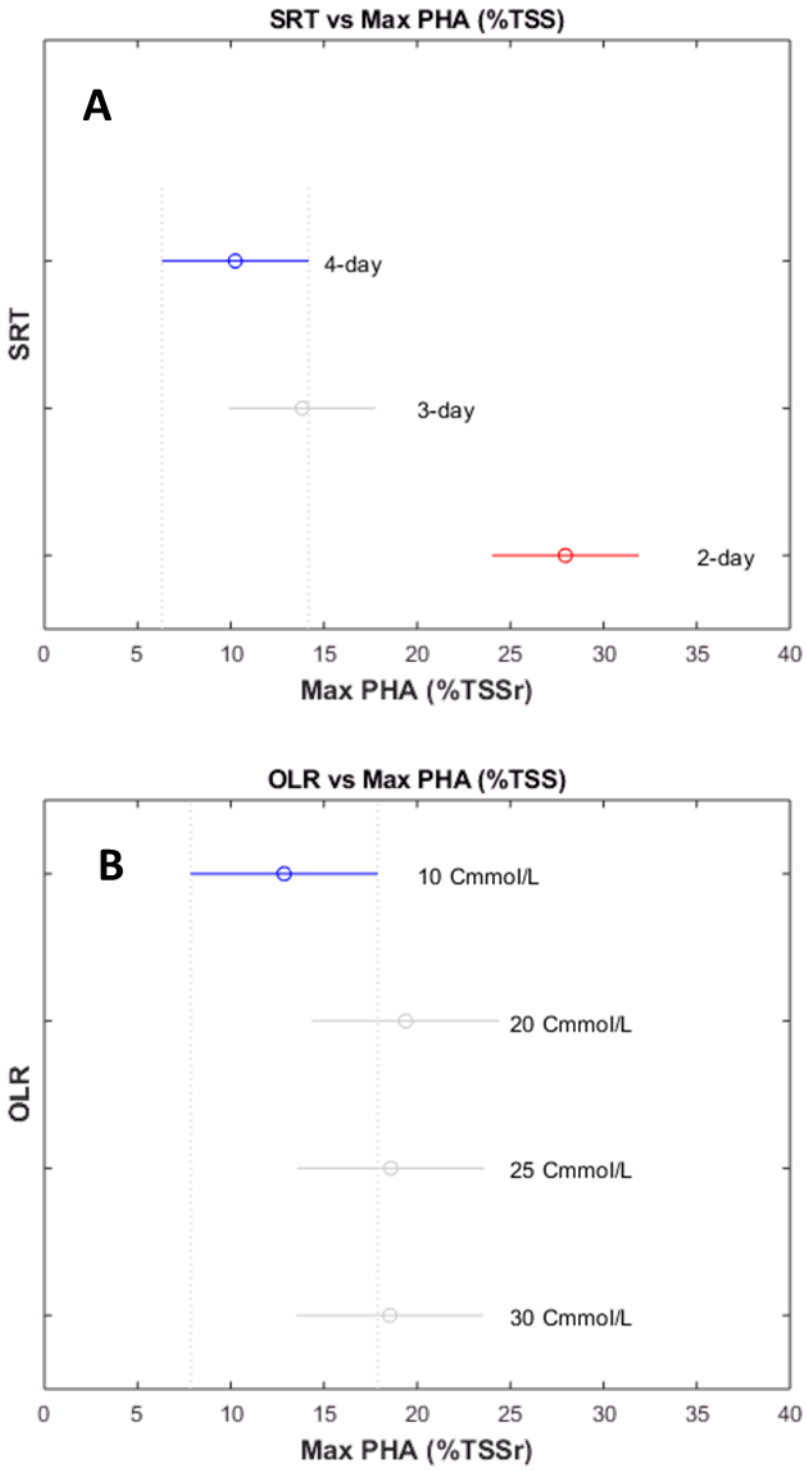

Figure 5.11: Factorial Operational Criteria vs. Intracellular PHA Content (A and B represent SRT and OLR).

Bivariate analysis of the effect SRT and OLR have on maximum intracellular PHA content showed a 2-day SRT is statistically superior from the 3- and 4-day SRT reactors; however,

no correlation between both the interaction of SRT and OLR, nor OLR independently, on PHA content was observed. In other words, increased OLR did not result in increased PHA produced per unit of recovered solids. Average peak PHA content on a $\%TSS_r$ (w/w) basis for the 2-, 3-, and 4-day SRT configurations were 28.0, 13.8, and 10.2%, respectively. As suggested by the results, PHA accumulation efficiency increases substantially as SRT decreases from 3- to 2-days. This is visualized in Figure 5.12, which depicts average peak PHA content for the SRT and OLR ranges evaluated.

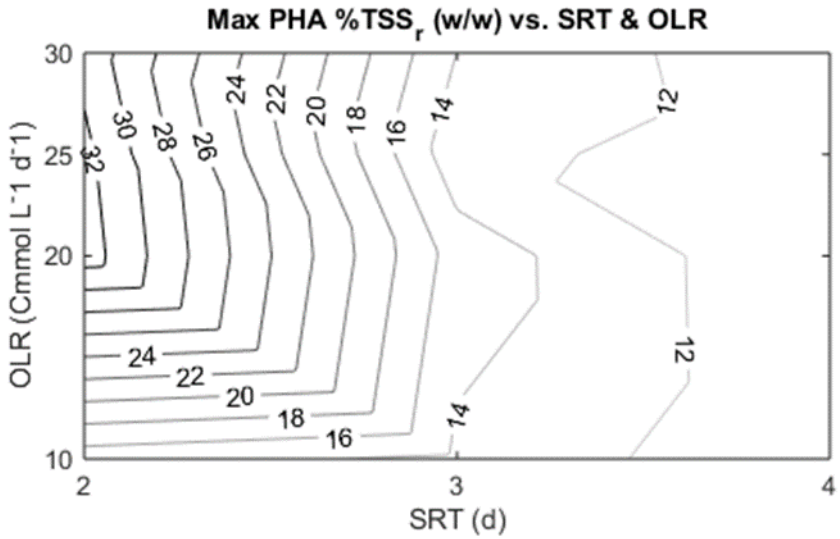

Figure 5.12: SRT & OLR vs Maximum Intracellular PHA Content

Maximum PHA content was observed within an OLR range of 20 to 25 Cmmol/L-d for the 2-day SRT operation, with an average of 32.8% TSS_r on a weight basis (n = 6); results align with analysis of PHA yield (Figure 5.9).

Comparable to peak intracellular PHA content on a TSS_r basis is the peak PHA to inocula solids (VSS) ratio. The VSS basis is more indicative of MMC performance compared to a TSS basis, as inocula VSS better represents the viable, PHA-producing, microbial population. Figure 5.13 illustrates the average peak PHA to VSS ratio (g/g) over the SRT and OLR ranges evaluated.

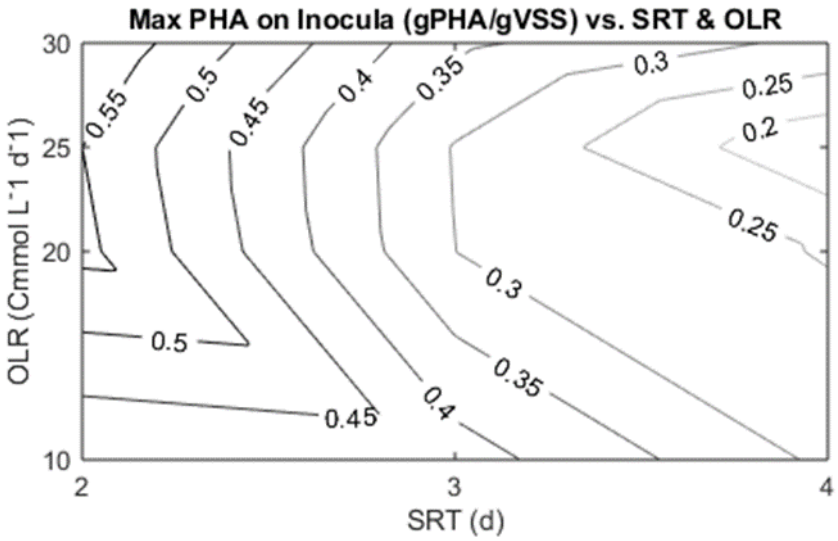

Figure 5.13: SRT & OLR vs PHA Production Efficiency

Results shown follow similar behavior to the peak PHA content on a weight basis, as the ratio of PHA produced to inocula VSS is maximized within an OLR range of 20 to 25 Cmmol/L-d for the 2-day SRT. Average ratios observed for E.2.20 and E.2.25 were 0.56 and 0.55 (n = 3).

Table 5.1 summarizes the parameters evaluated to access enrichment reactor performance for the various SRT and OLR configurations.

Table 5.1: Enrichment Factorial Results

Enrichment Results: 2-day SRT (n = 3)					
Parameter	**Units**	**E.2.10**	**E.2.20**	**E.2.25**	**E.2.30**
qVFA	Cmmol/ gVSS*min	0.33 ± 0.09	0.47 ± 0.28	0.37 ± 0.1	0.51 ± 0.21
Y_{PHA}	$Cmmol_{PHA}$/ $Cmmol_{VFA}$	0.7 ± 0.08	0.82 ± 0.09	0.82 ± 0.07	0.67 ± 0.23
Max %PHA	%TSSr w/w	14.9% ± 2.1%	33% ± 13%	32.5% ± 17.7%	31.4% ± 13.8%
Max PHA	g	0.23 ± 0.04	0.59 ± 0.07	0.76 ± 0.04	0.78 ± 0.26
F-F	$time_{feast}$/ $time_{famine}$	0.08 ± 0.02	0.07 ± 0.02	0.07 ± 0.001	0.07 ± 0.004
MLVSS	mg/L	831 ± 206	1133 ± 151	1443 ± 56	1444 ± 469

Enrichment Results: 3-day SRT (n = 3)					
Parameter	**Units**	**E.3.10**	**E.3.20**	**E.3.25**	**E.3.30**
qVFA	Cmmol/ gVSS*min	0.34 ± 0.2	0.22 ± 0.06	0.2 ± 0.03	0.37 ± 0.04
Y_{PHA}	$Cmmol_{PHA}$/ $Cmmol_{VFA}$	0.78 ± 0.2	0.82 ± 0.17	0.81 ± 0.09	0.69 ± 0.09
Max %PHA	%TSSr w/w	13.6% ± 1.3%	15.1% ± 2.5%	12.7% ± 2.3%	13.9% ± 2%
Max PHA	g	0.3 ± 0.08	0.66 ± 0.14	0.8 ± 0.09	0.84 ± 0.12
F-F	$time_{feast}$/ $time_{famine}$	0.05 ± 0.01	0.05 ± 0.001	0.05 ± 0.01	0.04 ± 0.01
MLVSS	mg/L	1151 ± 504	2102 ± 95	2752 ± 425	2718 ± 297

Enrichment Results: 4-day SRT (n = 3)					
Parameter	**Units**	**E.4.10**	**E.4.20**	**E.4.25**	**E.4.30**
qVFA	Cmmol/ gVSS*min	0.21 ± 0.1	0.18 ± 0.04	0.16 ± 0.05	0.17 ± 0.02
Y_{PHA}	$Cmmol_{PHA}$/ $Cmmol_{VFA}$	0.84 ± 0.12	0.73 ± 0.08	0.43 ± 0.05	0.67 ± 0.05
Max %PHA	%TSSr w/w	10.1% ± 2.4%	10.1% ± 1.6%	10.5% ± 3.6%	10.3% ± 1.1%
Max PHA	g	0.37 ± 0.07	0.59 ± 0.06	0.46 ± 0.02	0.75 ± 0.18
F-F	$time_{feast}$/ $time_{famine}$	0.04 ± 0.02	0.05 ± 0.01	0.06 ± 0.02	0.07 ± 0.02
MLVSS	mg/L	1789 ± 613	2730 ± 246	2985 ± 164	3332 ± 481

5.3.2 Production Reactors

5.3.2.1. PHA Yield on Substrate

Production reactor PHA yields were comparable to those of their respective parent (enrichment) reactors, with the exception of P.2.20, P.2.30, and P.4.20 exhibiting roughly a 15% increase; this is attributed to numerous factors including the production stage having an increased margin of error due to varying solution volume, lack of DO control, use of undiluted DFL, and increased sample to total volume ratio. However, the data suggests enrichment reactor PHA yield is nonetheless indicative of 'downstream' production reactor performance. This observation aligns with the findings of Carleton [89], also utilizing dairy manure feedstock. Figure 5.14 illustrates the average PHA yield for the production reactors over the SRT and OLR ranges evaluated.

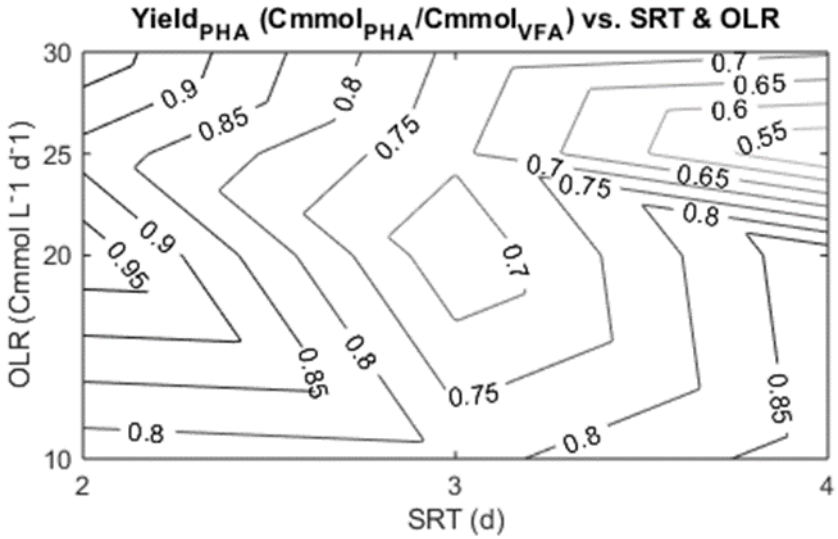

Figure 5.14: Production - SRT & OLR vs. PHA Yield

As shown, maximum PHA yield was observed within an OLR range of 20 to 30 Cmmol/L-d for the 2-day configuration, with an average yield of 0.95 $Cmmol_{PHA}/Cmmol_{VFA}$ (n = 9); importantly, nearly all of the VFAs consumed are directly converted to PHA. The subsequent highest average PHA yield of 0.88 $Cmmol_{PHA}/Cmmol_{VFA}$ (n = 6), was observed for an OLR range of 10 to 20 Cmmol/L-d for the 4-day configuration.

5.3.2.2. Maximum PHA Content

As with PHA yield, higher enrichment reactor intracellular PHA content generally translated to higher PHA content in the production stage. Figure 5.15 shows the average PHA content (%TSS_r w/w) for the production reactors over the SRT and OLR ranges evaluated.

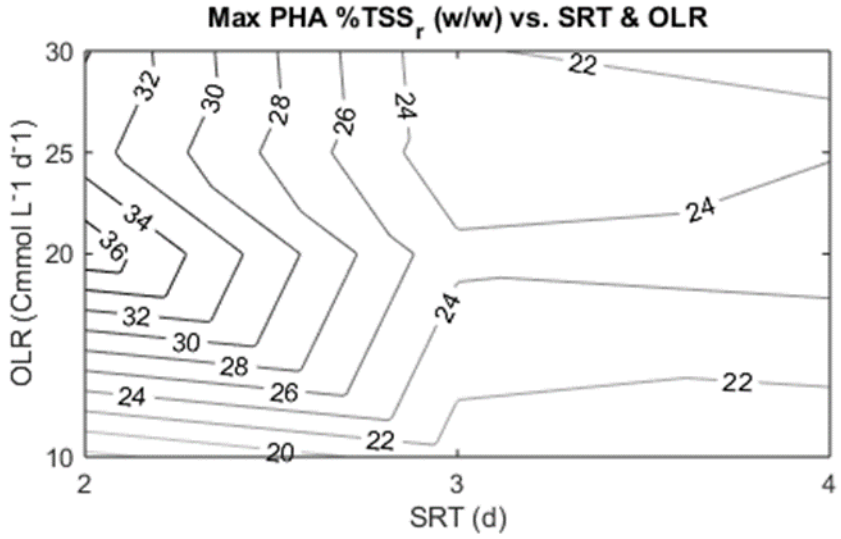

Figure 5.15: Production – SRT & OLR vs. Max Intracellular PHA Content

As can be seen, the highest peak intracellular PHA content on a weight basis was observed for a 20 Cmmol/L-d OLR and 2-day SRT (P.2.20), averaging a value of 37.6% (n = 3); furthermore, the 3- and 4-day SRT reactors remained in the 20-25% range regardless of OLR. Overall, the peak PHA content achieved in the production reactors were in agreement with reported ranges when using dairy waste substrate, albeit on the low end [1, 50, 68, 89, 116].

With regards to commercial PHA production, the maximum PHA accumulated in the production reactor, less extraction losses, represents the net PHA produced; therefore, evaluating the maximum weight of PHA produced at lab scale for each operational scheme is valuable for scaling purposes. Figure 5.16 illustrates the average maximum PHA harvestable in the production stage across the SRT and OLR ranges evaluated.

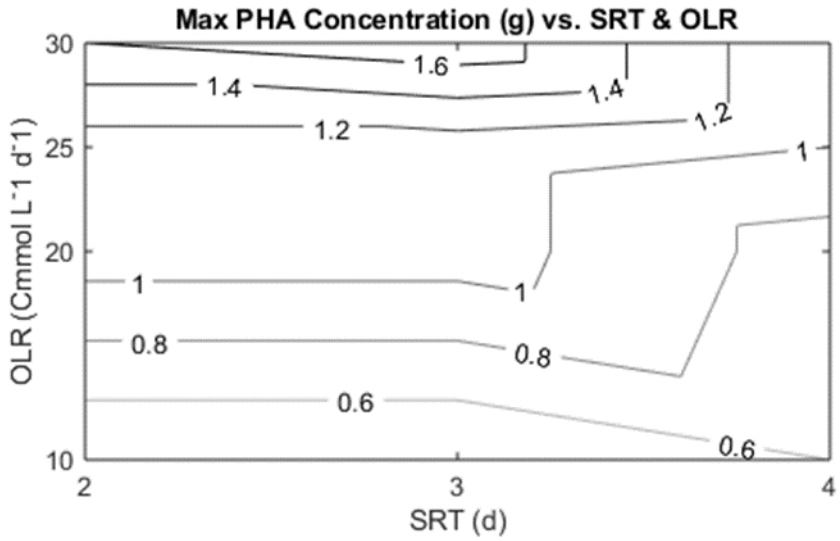

Figure 5.16: Production – SRT & OLR vs. Max PHA Concentration

Perhaps of no surprise, regardless of accumulation efficiencies the peak PHA produced is primarily a function of OLR. A maximum of 2.08g PHA was produced by P.3.30 on operational day 80. Production reactor volume at peak PHA accumulation varied substantially due to change in DFL strength and inocula VSS concentrations, thus volume of DFL required to meet said maximums were not reported. The values depicted represent the PHA output that roughly 0.5L of WAS (inoculum) is capable of producing.

Table 5.2 summarizes the parameters evaluated to access production reactor performance for the various SRT and OLR configurations.

Table 5.2: Production Factorial Results

Production Results: 2-day SRT (n = 3)					
Parameter	**Units**	**P.2.10**	**P.2.20**	**P.2.25**	**P.2.30**
qVFA	Cmmol/ gVSS*min	0.12 ± 0.04	0.17 ± 0.03	0.19 ± 0.02	0.21 ± 0.05
qPHA	Cmmol /gVSS*min	0.08 ± 0.03	0.16 ± 0.01	0.19 ± 0.02	0.19 ± 0.04
Y_{PHA}	$Cmmol_{PHA}/Cmmol_{VFA}$	0.77 ± 0.07	0.99 ± 0.02	0.88 ± 0.11	0.99 ± 0.02
Max PHA	%TSSr w/w	17.5% ± 1.8%	37.6% ± 12.6%	32.8% ± 17.2%	34.2% ± 19.5%
VFA Consumed	Cmmol	13 ± 2	28 ± 5	34 ± 6	39 ± 10
Max PHA	g	0.4 ± 0.1	1.1 ± 0.1	1.1 ± 0.3	1.6 ± 0.6
MLVSS	mg/L	1534 ± 181	1792 ± 322	1924 ± 409	2086 ± 393
Production Results: 3-day SRT (n = 3)					
Parameter	**Units**	**P.3.10**	**P.3.20**	**P.3.25**	**P.3.30**
qVFA	Cmmol/ gVSS*min	0.12 ± 0.07	0.16 ± 0.01	0.17 ± 0.05	0.2 ± 0.06
qPHA	Cmmol /gVSS*min	0.07 ± 0.01	0.13 ± 0.03	0.17 ± 0.04	0.15 ± 0.03
Y_{PHA}	$Cmmol_{PHA}/Cmmol_{VFA}$	0.78 ± 0.37	0.66 ± 0.12	0.71 ± 0.07	0.74 ± 0.17
Max PHA	%TSSr w/w	21% ± 2.2%	24.5% ± 2.5%	22.5% ± 5.3%	22.2% ± 1.8%
VFA Consumed	Cmmol	11 ± 4	46 ± 6	54 ± 10	58 ± 3
Max PHA	g	0.4 ± 0.2	1.1 ± 0.1	1.1 ± 0.3	2 ± 0.5
MLVSS	mg/L	1333 ± 739	2894 ± 597	3151 ± 632	3510 ± 741
Production Results: 4-day SRT (n = 3)					
Parameter	**Units**	**P.4.10**	**P.4.20**	**P.4.25**	**P.4.30**
qVFA	Cmmol/ gVSS*min	0.08 ± 0.03	0.12 ± 0.01	0.15 ± 0.04	0.13 ± 0.03
qPHA	Cmmol /gVSS*min	0.08 ± 0.01	0.1 ± 0.01	0.15 ± 0.02	0.09 ± 0.03
Y_{PHA}	$Cmmol_{PHA}/Cmmol_{VFA}$	0.87 ± 0.21	0.89 ± 0.1	0.5 ± 0.08	0.71 ± 0.21
Max PHA	%TSSr w/w	20.4% ± 1.2%	25% ± 2.3%	23.9% ± 5.6%	20.3% ± 2.4%
VFA Consumed	Cmmol	14 ± 8	28 ± 6	47 ± 8	35 ± 15
Max PHA	g	0.6 ± 0.3	0.7 ± 0.1	1 ± 0.3	1 ± 0.1
MLVSS	mg/L	2425 ± 530	3193 ± 198	3135 ± 358	3439 ± 728

5.3. Optimal Enrichment Reactor Operational Criteria

To preface the selection of the optimal enrichment reactor operation scheme, a 2-day SRT reactor is inherently favored over increased SRTs, independent of OLR and PHA production performance. A 2-day SRT has the highest rate of turnover from the enrichment to the production stage – half of the enrichment reactor volume per day as compared to 33% and 25% for the 3- and 4-day. Furthermore, the 2-day SRT has the shortest acclimatization time for returning to steady state if a process upset were to occur. These benefits of decreased SRT played were factored in the selection of optimal operational criteria.

The 2-day SRT configurations elicited substantial increases in intracellular PHA concentration and conversion of VFAs to PHA, indicative of a more active, PHA-accumulating MMC. Of note, the maximum intracellular PHA concentrations observed in this study were achieved under a CL:SRT ratio of 0.5 (2-day SRT), the same CL:SRT ratio used to achieve the record high 89% intracellular PHA content from MMC [73]. Maximum PHA storage was observed for the 3-day SRT configuration, which averaged roughly 15% more PHA (g) produced than corresponding 2-day SRT reactors; however, 3-day SRT intracellular PHA concentrations were roughly 35% lower in comparison to 2-day reactors. Assuming extraction costs are scalable by PHA content, the increase in net PHA production is unjustifiable for suggestion of a 3-day SRT as optimal. The question then became one of OLR, specifically, between 20-, 25-, and 30-Cmmol/L-d, as the 10-Cmmol/L-d saw diminished F-F metabolism. For E.2.20, E.2.25, and E.2.30 and their respective production reactors, net PHA production was a function of the amount of carbon supplied; however, E.2.20 averaged slightly higher PHA yield on substrate and intracellular PHA content. Ultimately, the choice of optimal OLR amongst the three becomes the highest OLR that you can afford given the limitations of the upstream fermentation stage. Within the scope of this research, optimization of the ADF process aims to conserve carbon usage across the enrichment and production stages; therefore, E.2.20 is the near-optimal operational criteria as the lower OLR does not negatively impact MMC enrichment or PHA production performance.

5.4. Conclusions

The objective of this research was to determine the optimal combination of enrichment stage operational parameters, SRT and OLR, through factorial based evaluation of Enrichment and Production Reactor carbon conversion assessments. Commercial viability of PHA production requires maximizing net PHA quantities while minimizing extraction costs; furthermore, optimal operation further pursues exaggeration of volumetric productivity and efficient use of limited carbon supply (DFL) in both stages. Twelve enrichment reactors were operated and evaluated at SRTs of 2-, 3-, and 4-days, and OLRs of 10-, 20-, 25-, and 30 Cmmol/L-d, along with their corresponding production reactors. It was hypothesized that within said ranges there exists a combination of SRT and OLR such that maximum PHA production is achieved.

Conclusions based on this study include the following:

i. Near-optimal Enrichment Reactor operation was achieved for an SRT of 2-days and an OLR of 20 Cmmol/L-d.
ii. Decreased SRT resulted in enhanced ADF metabolism characterized by increased intracellular PHA storage and PHA yield on substrate in both the enrichment and production stages. Moreover, decreased SRT did not result in more carbon being shunted to growth, rather it increased the overall enrichment and activity of PHA-accumulating MMC.
iii. OLR shared a positive linear relationship with net PHA produced for the OLR ranges evaluated, suggesting F-F selective pressure is maintained up to 30 Cmmol/L-d. As evidenced by E.2.10, decreased SRT in conjunction with decreased OLR can result in a negative metabolic impact characterized by reduced intracellular PHA storage.

5.4.1. Future Research

This research evaluated and determined the optimal combination of ADF enrichment reactor operational parameters, SRT and OLR; however, the impacts of additional easily-controlled enrichment reactor operational parameters on ADF metabolism have yet to be assessed, including: HRT, CL, and volume. Future investigations for the advancement of this research include:

i. Investigation of the impacts of CL and HRT on F-F metabolism and PHA production for the enrichment and production stages, independent of SRT.

ii. Elucidation of production stage VFA uptake kinetics for conditions of PHA inhibition, ideally through metabolic modeling. As shown in Figure 5.7, employing a pulse-feed strategy can result in large quantities of VFAs remaining in bulk solution after PHA stores have reached saturation. Proper estimation of required substrate per pulse addition could potentially save significant amounts of fermenter liquor with no consequence on productivity.

6. Metabolic Modeling: Results and Discussion

6.1. Model Calibration

Three E.2.20 sampling events, performed on operational days 36, 41, and 103, were leveraged in model calibration. Due to the tolerances of the nonlinear least-squares solver, the minimization of error between modelled and measured concentrations, E_R, and steady state error, E_R, were performed individually. The model incorporates the theoretical yield and maintenance coefficients, as previously described, which are a function of the modelled VFA and PHA flux.

6.1.1. Calibration to Measurements

The estimation of kinetic parameters for each sampling event and the concentration profiles thereof are shown in Figure 6.1 and Figure 6.2. For operational days 41 and 103, the relative error decreased significantly when measured biomass concentrations were excluded from the model fitting procedure; moreover, this exclusion was required for maintaining non-negative concentrations during simulation of operational day 103. This suggests a discrepancy in measured material concentrations, a topic that is further discussed below. As shown in Figure 6.1, the fitting procedure results in accurate representation of the metabolism observed on operational day 36. Conversely, for operational day 41 the fitted model overpredicts the initial concentration of PHV and falsely shows negligible changes in ammonia concentration. This deviation from measured values was reduced by fitting kinetic parameters independent of solids concentrations, as shown in Figure 6.2. In doing so the model adequately describes the observed concentrations for operational days 41 and 103 at the expense of accurate biomass representation. In both cases, the biomass concentration behaves in an implausible manner. The reactor appears to experience sporadic periods of growth and decay despite availability of carbon throughout (e.g., VFAs, PHA); moreover, the magnitude of decay is far too large for a microbial system of this time scale. The results from this stage of model calibration were sufficient in denying the adequacy of using measurements obtained on operational days 41 and 103 as a basis for the model. However, the kinetic parameters obtained do offer insight on overall process behavior.

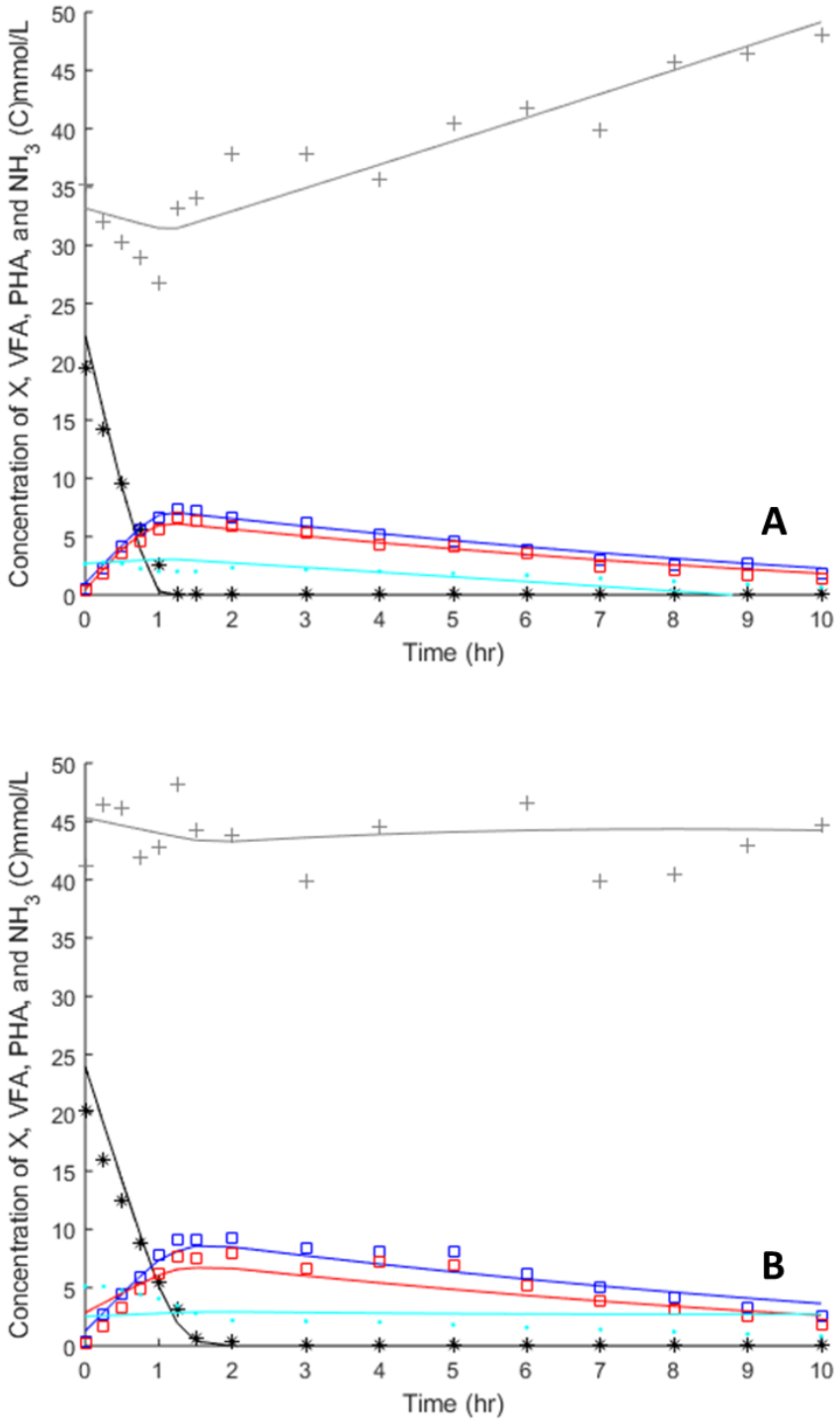

Figure 6.1: Model Parameter Estimation Respective to Measurements (A and B represent Operational Day 36 and 41). Symbols indicate experimental data and full lines indicate the modelled results. (*) VFAs, (□, blue) PHB, (□. red) PHV, (+) active biomass, and (.) ammonia.

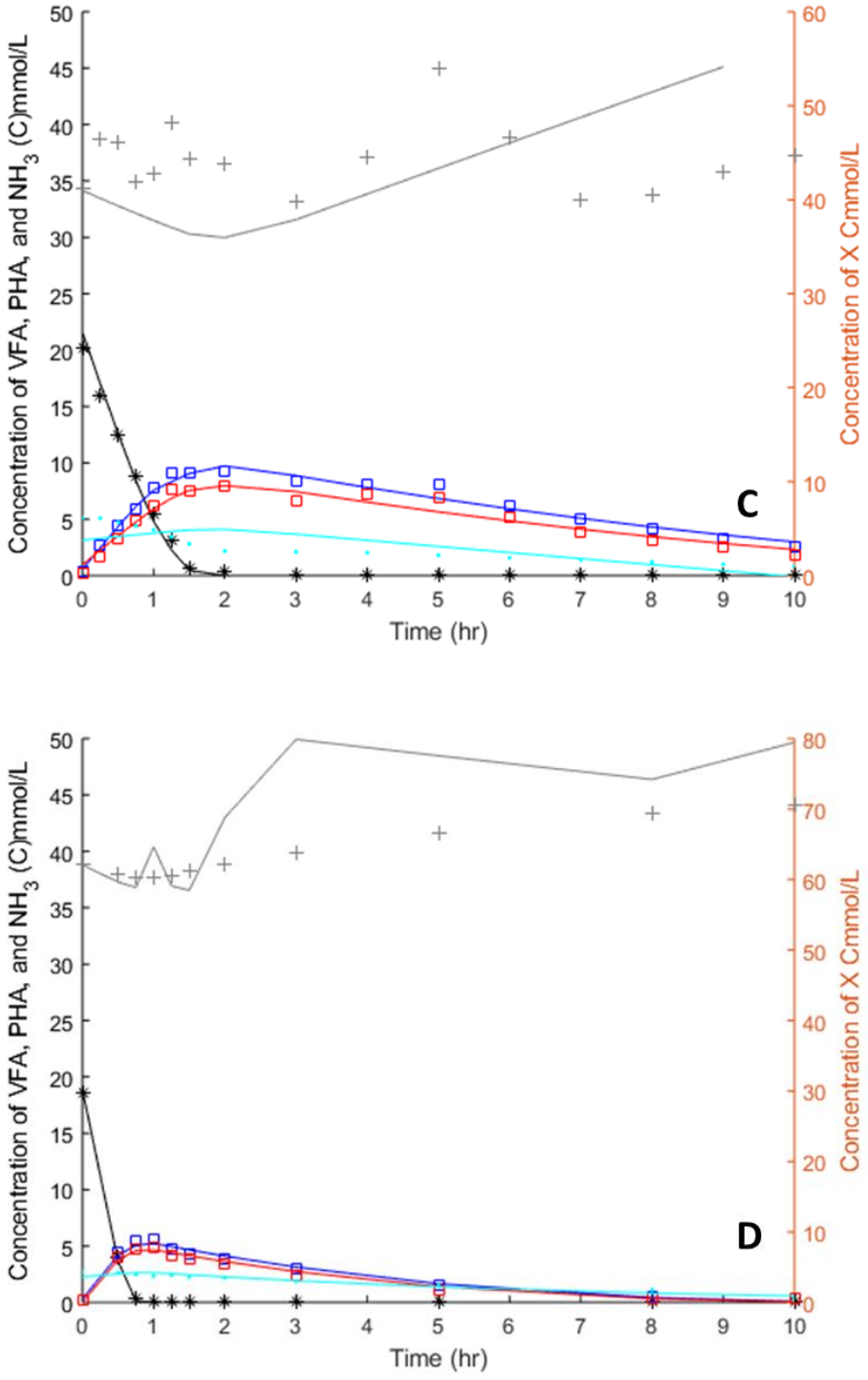

Figure 6.2: Model Parameter Estimation Respective to Measurements, Excluding Biomass (C and D represent Operational Day 41[a] and 103[a]). Symbols indicate experimental data and full lines indicate the modelled results. (*) VFAs, (□, blue) PHB, (□, red) PHV, (+) active biomass, and (.) ammonia.

6.1.2. Steady State Calibration

For steady state calibration, the fitted kinetic parameters from the previous step were initialized for subsequent adjustment in the steady state error minimization step. The resultant adjusted kinetic parameters were then used for model simulation and verification of steady state. Figure 6.3 depicts the calibrated steady state model representative of the initial material concentrations observed on operational day 36. In all experiments used for model calibration, the concentration of PHA at the end of the cycle was negligible, and thus biomass concentration was the sole criteria for steady state realization (see Equation 3.26). With a CL of 24 hours and an effective SRT/HRT of 2 days, E.2.20 is theoretically in steady state when the concentration of biomass at the end of the cycle is double the concentration at the beginning of the cycle.

Steady state conditions were verified by performing model simulation over a model time of 288 hours, equivalent to 3 times the target SRT of E.2.20, with negligible changes in material concentrations cycle to cycle. This simulation time is generally viewed as the minimum operation time for an SBR to achieve sufficient stability [102]. Of the three sampling events, operational day 36 was the only dataset capable of steady state calibration within acceptable integration tolerances. This limitation is primarily attributed to insignificant changes in solids concentration over the course of a cycle, commonly observed in this study (see Figure 5.6, Figure 6.1, and Figure 6.2). Presumably, the active biomass are growing throughout the feast-famine cycle (as witnessed by ammonia concentrations), however, the biomass measurements do not support this for reasons that remain unknown. A possible explanation is that the solids inherent in the DFL are being hydrolyzed simultaneously with biomass growth; thus, if the rate of solids hydrolysis is equal or greater than the growth rate, anabolism will not be presented in the TSS/VSS measurements. Modeled ammonia concentrations are in good agreement with measured values, suggesting ammonia depletion more reliably represents biomass growth than biomass concentrations; however, this does not aid in determining initial biomass concentration, for which the rate change of state variables are all effectively scaled by.

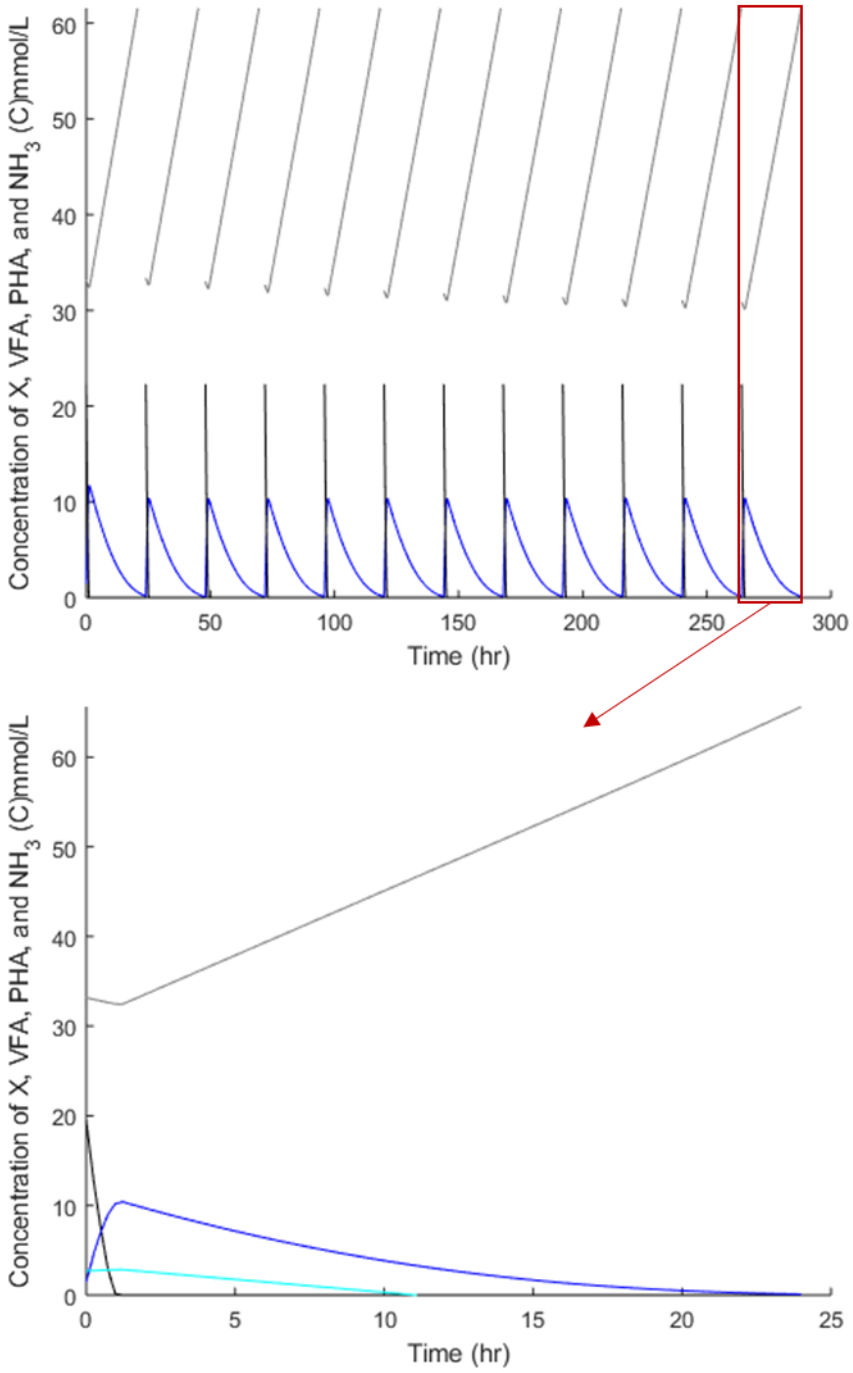

Figure 6.3: Steady State Feast-Famine Model (gray = biomass, black = VFAs, and blue = PHA; produced using initial concentrations identified by optimization of operational day 36).

6.1.3. Model Kinetic Parameters

The kinetic parameters determined from the calibration procedure are shown in Table 6.1. The calibrated model's kinetic parameters are listed for operation day 36. Importantly, the estimated butyrate and valerate specific uptake rates include iso-butyric and iso-valeric acid. This inclusion increases the accuracy of the carbon and electron balance of the measured data while obeying the model framework, being 4 and 5 carbon VFAs.

Table 6.1: Estimated Kinetic Parameters

E.2.20	Operational Day 36		Operational Day 41[c]		Operational Day 41[a,c]		Operational Day 103[a,c]		
Parameter	**Value**	**95% CI**	**Value**	**95% CI**	**Value**	**95% CI[b]**	**Value**	**95% CI**	**Units**
$q_{Ac,,max}$	-0.27	± 0.03	-0.12	± 0.05	-0.13	-	-0.13	± 0.04	$\frac{Cmmol}{Cmmol * hr}$
$q_{Pr,max}$	-0.22	± 0.04	-0.13	± 0.07	-0.13	-	-0.21	± 0.06	$\frac{Cmmol}{Cmmol * hr}$
$q_{Bu,max}$	-0.17	± 0.06	-0.14	± 0.10	-0.15	-	-0.14	± 0.03	$\frac{Cmmol}{Cmmol * hr}$
$q_{Va,max}$	-0.23	± 0.10	-0.07	± 0.04	-0.05	-	-0.07	± 0.02	$\frac{Cmmol}{Cmmol * hr}$
μ_{max}	-0.02	± 0.01	-0.03	± 0.03	-0.08	-	-0.04	± 0.02	$\frac{Cmmol}{Cmmol * hr}$
m_{ATP}	-0.16	± 0.03	0.10	± 0.04	-0.21	-	-0.04	± 0.02	$\frac{mmol}{Cmmol * hr}$
k	-0.05	± 0.02	-0.05	± 0.01	-0.07	-	-0.10	± 0.05	$(\frac{Cmmol}{Cmmol})^{\frac{1}{3}} h^{-1}$
y_{phv}	1.1	± 0.2	0.80	± 0.3	1.07	-	0.96	± 0.06	$\frac{Cmmol}{Cmmol}$

[a] Calibration procedure excluded measured biomass concentration.

[b] Confidence interval extrapolated by large changes in modelled biomass.

[c] Model could not estimate steady state within allowable tolerances.

As shown, the specific uptake rates for each VFA are quite variable between experiments except for butyrate, principally due to being highly sensitive to measured biomass concentrations. The calibrated model incorporates the upper limit of estimated VFA uptake rates as operational day 36, the sole experiment to exhibit near steady state conditions, was the most efficient regarding substrate uptake.

The ratio of PHV to total PHA flux, y_{PHV}, was relatively consistent across all experiments and resulted in good agreement between modelled and measured PHA composition. As y_{PHV} is estimated as a linear function of the ratio of odd carbon flux to total VFA flux, y, the range of 0.8 to 1.1 indicates that uptake of even and odd carbon VFA is highly correlated with PHB and PHV storage. This presents the concern of inaccurate parameter estimation between y_{PHV} and each of the specific VFA uptake rates due to collinearity; however, some enrichment cultures exhibit little correlation between VFA distribution and condensed PHA composition [40, 49].

The reaction order of 2/3 for PHB degradation, represented by k, described famine phase PHA consumption well across all experiments. The observed range of -0.05 to -0.07 is relatively similar to the range identified by Johnson et al. [42] and Beun et al. [38] of -0.09 to -0.14 and -0.09.

For all evaluations, the maximum growth rate in the feast phase, μ_{max} , was negative; similarly, the biomass specific ATP consumption rate, m_{ATP} , was negative for two of the experiments. The negative specific growth rate can be explained by the aforementioned hydrolysis of DFL solids; however, a negative maintenance coefficient implies ATP is being synthesized from an energy source other than PHA or VFAs. This was still the case even after increasing the oxidative phosphorylation efficiency constant, δ, from 2 (the assumed value) to its theoretical maximum of 3 mole ATP per mole $NADH_2$ [40]. For perspective, modelled values of the specific ATP consumption rate are typically in the range of 0-0.227 mmol/Cmmol-hr [42, 44], with a set value of 0.02 mmol/Cmmol-hr commonly employed in relevant modeling efforts [37, 43]. In the initial parameter estimation attempts, the growth rate and maintenance term were each given non-negative lower bounds; however, this resulted in significant underprediction of PHA storage. Further investigation led to the evaluation of the model yield and maintenance coefficients as depicted in Figure 6.4.

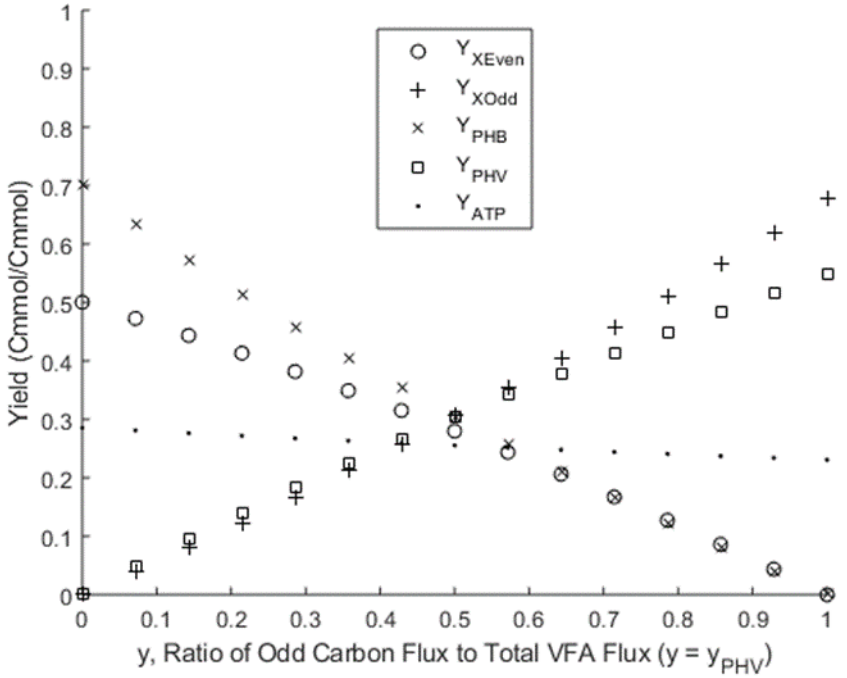

Figure 6.4: Model Yield and Maintenance Coefficients as a Function of VFA and PHA Flux Distribution

In the case that the theoretical yields are underpredicted, the unbounded calibration would compensate by using a negative maintenance term to fit PHA measurements. However, all yield coefficients are comparable to that of Dias et al. [40], and the theoretical PHA yield on substrate is in agreement with experimental true yields of 0.74 and 0.75 from literature [37, 131]. Being that the model stoichiometry is derived from a balance of conserved moieties and degree of reduction, the findings suggest an additional carbon source is contributing to ATP production and ultimately PHA synthesis therefrom. This was reaffirmed after performing a check where PHA yield on substrate was set to 1 Cmmol/Cmmol and the result was the same.

6.2. Model Results

6.2.1 Model Performance against E.2.20

Evaluation of the calibrated model was performed by comparing the ability of the model to represent the performance of E.2.20 for each of the sampling events. Famine phase comparisons are excluded from this section due to being highly reliant on accurate feast phase simulation; moreover, the famine phase kinetics were consistent across the individual calibration results.

The comparison between modelled and measured VFA concentrations is shown in Figure 6.5. The coefficients for a linear fit of the model outputs to measured values, and the associated coefficient of determination (R^2), are included to quantify modelling accuracy. As shown by R^2 values and slope terms (m) close to 1, VFA uptake is adequately described for operational days 36 and 103. For all comparisons the model overpredicts the rate of VFA uptake, and to a significantly higher degree for operational day 41. This can be attributed to having roughly 20% higher measured biomass concentrations compared to the other two sampling events.

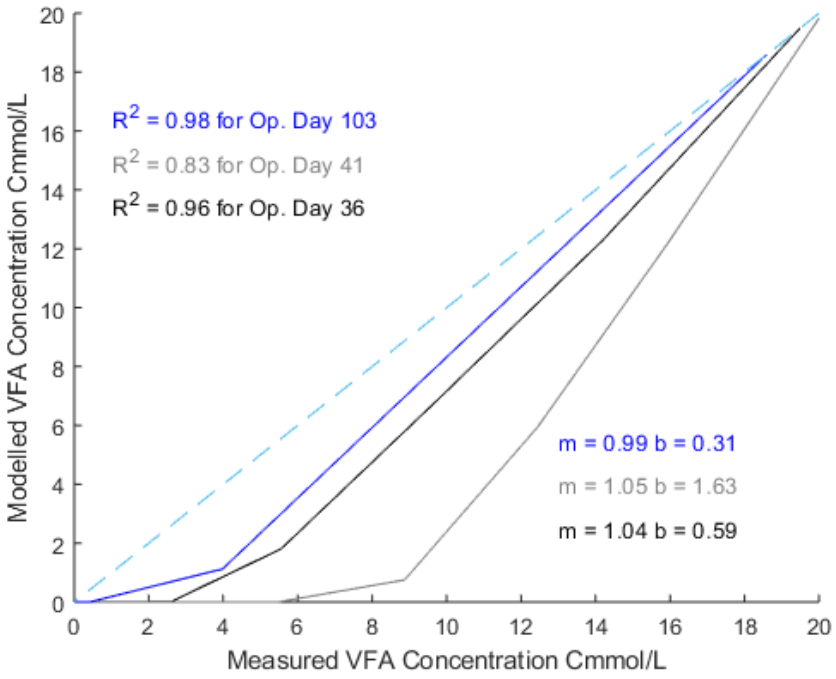

Figure 6.5: Modelled vs Measured: VFA Uptake

With respect to commercial PHA production, the most important quality of a model is its ability to accurately predict the maximum PHA content and the monomeric composition of the 'end-product'. The comparison between modelled and measured feast phase PHB and PHV concentrations are illustrated in Figure 6.6 and Figure 6.7. The tailing of the PHB and PHV curves at higher PHA concentrations is indicative of kinetic saturation terms taking effect at low VFA concentrations, resulting in a reduced PHA storage rate. Furthermore, the overall predictive accuracy of the model compared to each sampling event is summarized in Table 6.2.

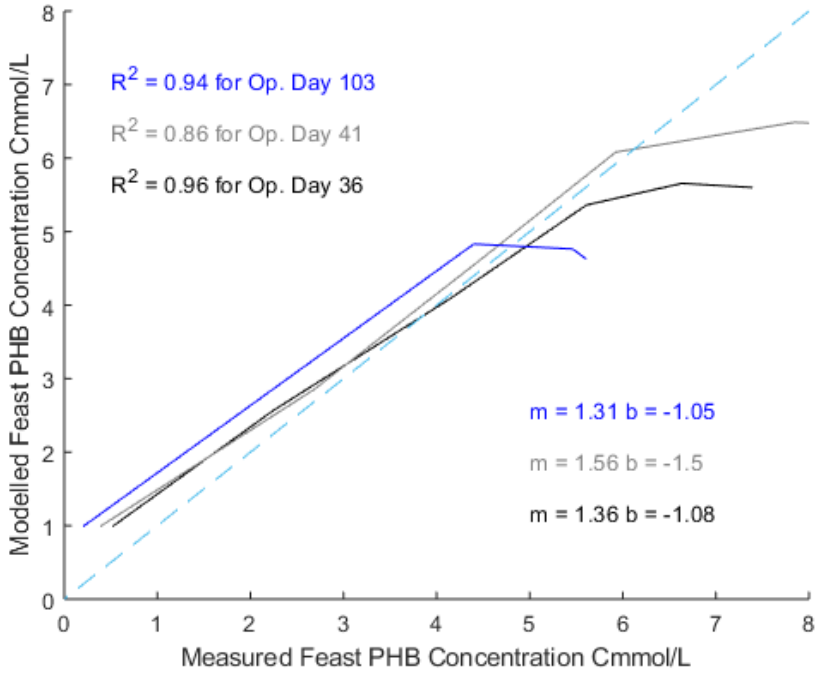

Figure 6.6: Modelled vs Measured: PHB Storage

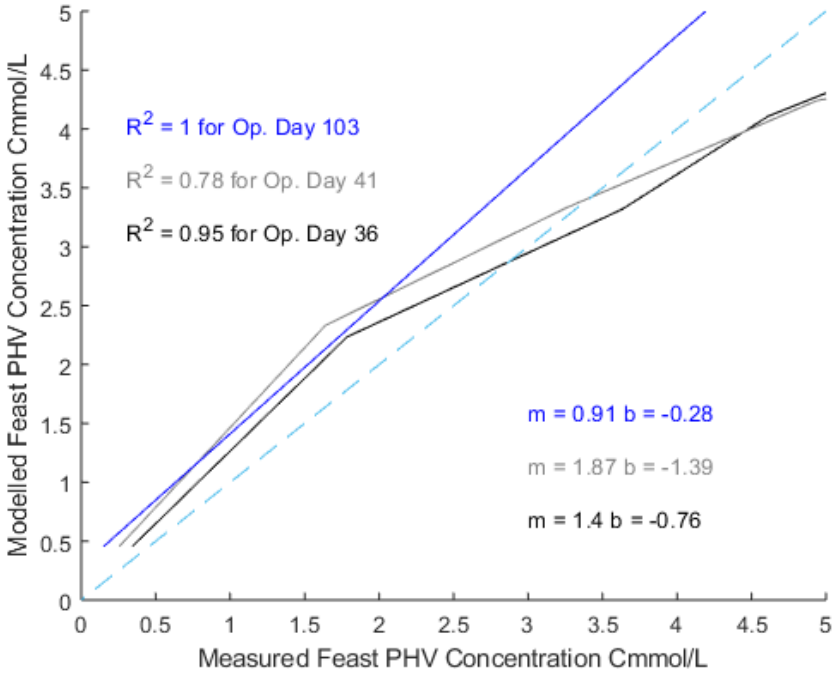

Figure 6.7: Modelled vs Measured: PHV Storage

Table 6.2: Model Results: Intracellular PHA Content and HV Fraction

Sampling Event	**VFA Content (Cmmol/L)**	**Max. PHA (%w/w)**		**HV Fraction (gHV/ gPHA)**	
Operational Day	Total*(Ac:Pr:(i)Bu:(i)Va)	Measured	Modelled	Measured	Modelled
36	19.5 (0.36,0.33, 0.2,0.11)	19.3	14.3	0.45	0.44
41	20.2 (0.36,0.32, 0.24,0.08)	23.7	15.2	0.44	0.39
103	18.6 (0.29,0.4,0.19,0.12)	14.5	14.3	0.44	0.52

As shown, the model slightly overpredicts PHA storage during the period of VFA saturation while underpredicting PHA storage in the latter period of the feast phase. The modelled maximum PHA content was underpredicted by 26% and 36% for operational days 36 and 41. As a result, the coefficients of linear regression between modelled and measured concentrations are not indicative of a good fit; however, visual inspection suggests accurate model prediction of the rate of PHA storage, albeit until near-zero VFA concentrations are reached. Interestingly, the model accurately predicted the maximum PHA content for operational day 103 although this comparison was the source of the largest deviation in monomeric composition. The model was capable of accurately representing the relative HV fraction for operational days 36 and 41, while the odd carbon dominant VFA feed greatly influenced modelled HV fraction for operational day 103. This is likely the case due to the model assuming steady state is achieved using the VFA distribution observed for each sampling event; thus, using an average VFA distribution for simulation would yield a constant HV fraction in agreement with measured values close to 0.44. As witnessed by the model results for operational day 36, minimization of the steady state error causes the model outputs to stray from observed measurements. Prior to the steady state calibration step (Figure 6.1), the estimated kinetic parameters fit maximum PHA concentration within 5% of the measured value.

6.2.2. Model Performance against PHA Pilot

For pseudo-validation and additional insight on the metabolic model's potential application, the model was vetted against a pilot-scale PHA production enrichment reactor not previously used for parameter estimation. The 680 L enrichment reactor was operated as an SBR under similar conditions to that of E.2.20; the primary differences in operation (excluding scale) being the reactor was operated with a target SRT/HRT of 4 days and fed uncentrifuged DFL diluted with tap water with a 1:1 ratio.

The modelled versus measured concentration profiles and the overall model performance are shown in Figure 6.8 and Table 6.3.

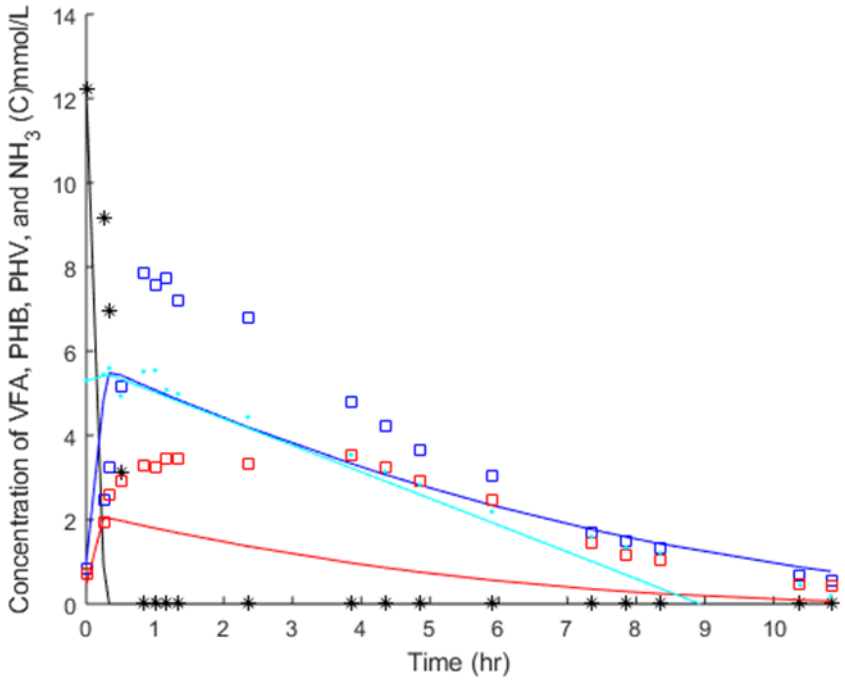

Figure 6.8: Model Results against PHA Pilot. Symbols indicate experimental data and full lines indicate the modelled results. (*) VFAs, (□, blue) PHB, (□, red) PHV, and (*) ammonia.

Table 6.3: PHA Pilot Model Results: Intracellular PHA Content and HV Fraction

Sampling Event	VFA Content (Cmmol/L)	Max. PHA (%w/w)		HV Fraction	
Date	Total*(Ac:Pr:(i)Bu:(i)Va)	Measured	Modelled	Measured	Modelled
8-22-19	12.2 (0.60,0.17, 0.17,0.06)	9.4	6.3	0.30	0.26

As shown, the modelled VFAs were depleted much faster than measured concentrations, and thus the famine phase and ensuing PHA consumption commence significantly earlier in the cycle. This result comes as no surprise due to model kinetic parameters being tailored for a 2 day versus a 4 day SRT configuration. While kinetic rates will change with variable SRT, the primary impact on modelling is the increased solids content with SRT; moreover, in the case of the PHA pilot being fed uncentrifuged DFL biomass concentrations are increasingly overestimated. The calibrated model is designed for initial biomass concentrations in the range of 35 to 62 Cmmol/L, whereas the PHA Pilot is roughly 104 Cmmol/L.

The PHA pilot system and E.2.20 vary significantly with operation and scale, enough so as to warrant low expectations for the model's ability to predict pilot performance; however, the model shows promising results. While maximum intracellular PHA content was under predicted by roughly 30%, the monomeric composition was described quite well. More impressively, the relative HV fraction was within 15% of the quantified fraction while the substrate composition differed substantially from the VFA composition used to calibrate the model. Ammonia concentrations, the rate of PHA storage, and the rate of PHA degradation were all in good agreement with respective experimental values. This suggests the model is, at its core, capable of describing feast-famine metabolism for both lab-scale and pilot processes; however, the issue of a potential uncharacterized source of carbon contributing to PHA storage is evidenced in both cases.

6.3. Conclusions

Modeling the dynamics of a biological system using real complex waste is a difficult endeavor, increasingly so for SBRs where natural environmental deviations occur cycle to

cycle. An SBR's cyclic nature can cause measurement error or parameter sensitivities to be compounded over many cycles and result in large discrepancies between real and modelled values. This imperfect reality lends itself as an explanation for the large error in model prediction of peak intracellular PHA content. For a model to even begin to drive design decisions accurate representation of experimental data is required, especially for key outputs such as intracellular PHA. Fortunately, initial parameter estimation disregarding the steady state condition described PHA production very well. This finding gives rise to a possible avenue of model error reduction. Ultimately, more datasets for E.2.20 are required for adequate calibration and smoothing of natural 'quasi-steady state' variations between sampling events. It was hypothesized that the model would be capable of driving optimization studies to further inform optimal Enrichment Reactor operation (RQ3), however, this is not the case for the developed model. The sheer scope of work involved in determination of near-optimal operational criteria (RQ1) for the basis of developing a metabolic model (RQ2) did not allow further model refinement. Indeed, the model described herein provides direction and empirical insight for future research of ADF process optimization.

Conclusions based on this study include the following:

i. The metabolic model developed in this research adequately describes ADF metabolism for MMC enriched on complex mixtures of VFAs. Net PHA produced was underpredicted for 2 of the 3 modelled experiments; however, computed rates of VFA uptake, PHA production, biomass growth (as related to ammonia measurements), and PHA degradation were in good agreement with measured data. As a result, the model presents itself as a valuable tool for regulation of PHA production and degradation for complex systems.
ii. A benefit of the developed metabolic model is that material, carbon, and degree of reduction balances close. Model simulations in this study yielded negative (although near-zero) feast phase growth rates and maintenance ATP requirements. While the values themselves do not reflect their actual rates, they are an indication of an additional source of ATP not accounted for by the model framework (e.g., carbon from VFAs).

a. The approach of using a constant P/O ratio, δ, and determining the MMC's ATP consumption rate, m_{ATP} , through fitting was ideal in this case. The quantity of unknown COD (Cmmol) contributing to PHA consumption can be estimated through model values of m_{ATP}.

iii. Model prediction of PHA monomeric composition was in good agreement for both lab-scale and pilot-scale evaluation. It was shown that polymer composition was strongly dependent on the composition of substrate; for all experiments, the linear relationship between the odd carbon fraction of VFA uptake to HV fraction of PHA storage was roughly 0.96-1.1 to 1. This carries important design implication for optimization of a 3-stage ADF process to beget desired polymer composition, particularly for the fermentation stage.

6.3.1. Future Research

While results presented in this research offer a promising foundation for further model-based optimization studies for ADF metabolism relative to dairy waste fed MMC systems, future refinements would be of value. Specifically, further advancement of model accuracy to add value to its application include:

i. Refining the method of determining active biomass concentration. In particular, consideration should be given to developing an approach for quantifying hydrolysis of DFL solids so as to separate MMC from general solids measurements. The enhanced speciation of solids in the bioreactor would drastically improve the accuracy of model kinetics, and as a result, the prediction of PHA production for a given process.

ii. Expansion of the model to include a COD component and to determine the yield coefficients thereof. The results from this research indicate the assumption that VFAs are the only carbon source utilized for PHA synthesis is not valid for accurate prediction of peak PHA content.

iii. Incorporating a feast-phase kinetic relationship for substrate uptake that accounts for PHA inhibition. This would allow the model to simulate fed-batch experiments that follow the kinetics describe herein until PHA saturation is reached and as a result substrate uptake and subsequent PHA storage stagnate.

References

1. Guho, N., *Polyhydroxyalkanoate production coupled with waste treatment using a three-stage sequencing batch reactor system fed dairy manure*, in *Civil Engineering*. 2010, University of Idaho. p. 89.
2. Senior, P.J. and E.A. Dawes, *The regulation of poly-beta-hydroxybutyrate metabolism in Azotobacter beijerinckii.* Biochem J, 1973. **134**(1): p. 225-38.
3. Steinbüchel, A., *Polyhydroxyalkanoic acids*, in *Biomaterials: Novel Materials from Biological Sources*, D. Byrom, Editor. 1991, Palgrave Macmillan UK: London. p. 123-213.
4. Reinecke, F. and A. Steinbuchel, *Ralstonia eutropha strain H16 as model organism for PHA metabolism and for biotechnological production of technically interesting biopolymers.* J Mol Microbiol Biotechnol, 2009. **16**(1-2): p. 91-108.
5. Kawaguchi, Y. and Y. Doi, *Kinetics and mechanism of synthesis and degradation of poly(3-hydroxybutyrate) in Alcaligenes eutrophus.* Macromolecules, 1992. **25**(9): p. 2324-2329.
6. Haywood, G.W., et al., *The role of NADH- and NADPH-linked acetoacetyl-CoA reductases in the poly-3-hydroxybutyrate synthesizing organism Alcaligenes eutrophus.* FEMS Microbiology Letters, 1988. **52**(3): p. 259-264.
7. Gottschalk, G., *Bacterial Metabolism*. Springer Series in Microbiology. 1979: Springer-Verlag.
8. Braunegg, G., G. Lefebvre, and K.F. Genser, *Polyhydroxyalkanoates, biopolyesters from renewable resources: Physiological and engineering aspects.* Journal of Biotechnology, 1998. **65**(2): p. 127-161.
9. Advisors, D., *Solving Plastic Pollution Through Accountability*, in *WWF International*. 2019. p. 46.
10. *Advancing Sustainable Materials Management: 2015 Fact Sheet*, in *Assessing Trends in Material Generation, Recycling, Composting, Combustion with Energy Recovery and Landfilling in the United States*. 2018, United States Environmental Protection Agency. p. 4.
11. Webb, H., et al., *Plastic Degradation and Its Environmental Implications with Special Reference to Poly(ethylene terephthalate)*. Vol. 5. 2012. 1-18.
12. Jambeck, J.R., et al., *Plastic waste inputs from land into the ocean.* Science, 2015. **347**(6223): p. 768.
13. Derraik, J.G.B., *The pollution of the marine environment by plastic debris: a review.* Marine Pollution Bulletin, 2002. **44**(9): p. 842-852.
14. Rios, L.M., C. Moore, and P.R. Jones, *Persistent organic pollutants carried by synthetic polymers in the ocean environment.* Marine Pollution Bulletin, 2007. **54**(8): p. 1230-1237.
15. Sivan, A., *New perspectives in plastic biodegradation.* Current Opinion in Biotechnology, 2011. **22**(3): p. 422-426.
16. McDonough, W. and M. Braungart, *Cradle to cradle: remaking the way we make things*. 2002, New York: North Point Press. 193.
17. Kumar, S., N. Prakash, and D. Datta, *Biopolymers Based on Carboxylic Acids Derived from Renewable Resources.* Biopolymers, 2011.
18. Pardelha, F., et al., *Dynamic metabolic modelling of volatile fatty acids conversion to polyhydroxyalkanoates by a mixed microbial culture.* New Biotechnology, 2014. **31**(4): p. 335-344.
19. Tamis, J., et al., *Modeling PHA-producing microbial enrichment cultures--towards a generalized model with predictive power.* N Biotechnol, 2014. **31**(4): p. 324-34.
20. U. Gerngross, T. and S. C. Slater, *How Green are Green Plastics?* Vol. 283. 2000. 37-41.
21. DiGregorio, B.E., *Biobased Performance Bioplastic: Mirel.* Chemistry & Biology, 2009. **16**(1): p. 1-2.

22. Gerngross, T.U., *Can biotechnology move us toward a sustainable society?* Nat Biotechnol, 1999. **17**(6): p. 541-4.
23. Dionisi, D., et al., *Biodegradable polymers from organic acids by using activated sludge enriched by aerobic periodic feeding.* Biotechnology and Bioengineering, 2004. **85**(6): p. 569-579.
24. Majone, M., et al., *Influence of storage on kinetic selection to control aerobic filamentous bulking.* Water Science and Technology, 1996. **34**(5): p. 223-232.
25. Majone, M., K. Dircks, and J.J. Beun, *Aerobic storage under dynamic conditions in activated sludge processes. The state of the art.* Water Science and Technology, 1999. **39**(1): p. 61-73.
26. Lemos, P.C., L.S. Serafim, and M.A.M. Reis, *Synthesis of polyhydroxyalkanoates from different short-chain fatty acids by mixed cultures submitted to aerobic dynamic feeding.* Journal of Biotechnology, 2006. **122**(2): p. 226-238.
27. Serafim, L.S., et al., *Optimization of polyhydroxybutyrate production by mixed cultures submitted to aerobic dynamic feeding conditions.* Biotechnology and Bioengineering, 2004. **87**(2): p. 145-160.
28. Dias, J.M.L., et al., *Recent Advances in Polyhydroxyalkanoate Production by Mixed Aerobic Cultures: From the Substrate to the Final Product.* Macromolecular Bioscience, 2006. **6**(11): p. 885-906.
29. Serafim, L.S., et al., *Strategies for PHA production by mixed cultures and renewable waste materials.* Applied Microbiology and Biotechnology, 2008. **81**(4): p. 615-628.
30. Albuquerque, M.G.E., et al., *Strategies for the development of a side stream process for polyhydroxyalkanoate (PHA) production from sugar cane molasses.* Journal of Biotechnology, 2007. **130**(4): p. 411-421.
31. Md Din, M.F., et al., *Optimization of nitrogen and phosphorus limitation for better biodegradable plastic production and organic removal using single fed-batch mixed cultures and renewable resources.* Water science and technology : a journal of the International Association on Water Pollution Research, 2006. **53**: p. 15-20.
32. Salmiati, et al., *Intracellular biopolymer productions using mixed microbial cultures from fermented POME.* Water Science and Technology, 2007. **56**(8): p. 179-185.
33. Dionisi, D., et al., *Effect of Feed Length on Settleability, Substrate Uptake and Storage in a Sequencing Batch Reactor Treating an Industrial Wastewater.* Environmental Technology, 2006. **27**(8): p. 901-908.
34. Liu, H.-Y., et al., *Production of Polyhydroxyalkanoate During Treatment of Tomato Cannery Wastewater.* Water Environment Research, 2008. **80**(4): p. 367-372.
35. Bengtsson, S., et al., *Production of polyhydroxyalkanoates by activated sludge treating a paper mill wastewater.* Bioresource Technology, 2008. **99**(3): p. 509-516.
36. Mato, T., et al. *PHA production using brewery wastewater*.
37. Beun, J.J., et al., *Poly-beta-hydroxybutyrate metabolism in dynamically fed mixed microbial cultures.* Water Res, 2002. **36**(5): p. 1167-80.
38. Beun, J.J., et al., *Stoichiometry and kinetics of poly-β-hydroxybutyrate metabolism in aerobic, slow growing, activated sludge cultures.* Biotechnology and Bioengineering, 2000. **67**(4): p. 379-389.
39. van Aalst-van Leeuwen, M.A., et al., *Kinetic modeling of poly(β-hydroxybutyrate) production and consumption by Paracoccus pantotrophus under dynamic substrate supply.* Biotechnology and Bioengineering, 1997. **55**(5): p. 773-782.
40. Dias, J.M.L., et al., *Metabolic modelling of polyhydroxyalkanoate copolymers production by mixed microbial cultures.* BMC Systems Biology, 2008. **2**(1): p. 59.

41. Pardelha, F., *Constraint-based modelling of mixed microbial populations: Application to polyhydroxyalkanoates production*, in *Chemistry Department*. 2013, Universidade Nova de Lisboa: Faculdade de Ciências e Tecnologia. p. 101.
42. Johnson, K., R. Kleerebezem, and M.C.M. van Loosdrecht, *Model-based data evaluation of polyhydroxybutyrate producing mixed microbial cultures in aerobic sequencing batch and fed-batch reactors.* Biotechnology and Bioengineering, 2009. **104**(1): p. 50-67.
43. Wang, X., et al., *Metabolic modeling of the substrate competition among multiple VFAs for PHA production by mixed microbial cultures.* Journal of Biotechnology, 2018. **280**: p. 62-69.
44. Jiang, Y., et al., *Metabolic modeling of mixed substrate uptake for polyhydroxyalkanoate (PHA) production.* Water Research, 2011. **45**(3): p. 1309-1321.
45. Lenz, R.W. and R.H. Marchessault, *Bacterial Polyesters: Biosynthesis, Biodegradable Plastics and Biotechnology.* Biomacromolecules, 2005. **6**(1): p. 1-8.
46. Raza, Z.A., S. Abid, and I.M. Banat, *Polyhydroxyalkanoates: Characteristics, production, recent developments and applications.* International Biodeterioration & Biodegradation, 2018. **126**: p. 45-56.
47. Sudesh, K., H. Abe, and Y. Doi, *Synthesis, structure and properties of polyhydroxyalkanoates: biological polyesters.* Progress in Polymer Science, 2000. **25**(10): p. 1503-1555.
48. Chen, G.-Q. and M.K. Patel, *Plastics Derived from Biological Sources: Present and Future: A Technical and Environmental Review.* Chemical Reviews, 2012. **112**(4): p. 2082-2099.
49. Wei, L., et al., *Characterization of poly(3-hydroxybutyrate-co-3-hydroxyvalerate) biosynthesized by mixed microbial consortia fed fermented dairy manure.* Journal of Applied Polymer Science, 2014. **131**(11).
50. Sprague, C.A., *Assessment of Operationally Effected Metabolic Conditions to Achieve Enhanced Polyhydroxyalkanoate Production on Fermented Dairy Manure*, in *Civil and Environmental Engineering*. 2018, University of Idaho: Moscow, ID. p. 120.
51. Albuquerque, M.G., et al., *Mixed culture polyhydroxyalkanoate (PHA) production from volatile fatty acid (VFA)-rich streams: effect of substrate composition and feeding regime on PHA productivity, composition and properties.* J Biotechnol, 2011. **151**(1): p. 66-76.
52. Koning, G., *Physical properties of bacterial poly((R)-3-hydroxyalkanoates).* Canadian Journal of Microbiology, 2011. **41**: p. 303-309.
53. Madison, L.L. and G.W. Huisman, *Metabolic engineering of poly(3-hydroxyalkanoates): from DNA to plastic.* Microbiol Mol Biol Rev, 1999. **63**(1): p. 21-53.
54. Luzier, W.D., *Materials derived from biomass/biodegradable materials.* Proceedings of the National Academy of Sciences of the United States of America, 1992. **89**(3): p. 839-842.
55. Fuhs, G.W. and M. Chen, *Microbiological basis of phosphate removal in the activated sludge process for the treatment of wastewater.* Microb Ecol, 1975. **2**(2): p. 119-38.
56. Oehmen, A., et al., *Advances in enhanced biological phosphorus removal: From micro to macro scale.* Water Research, 2007. **41**(11): p. 2271-2300.
57. Probst, D., *Polyhydroxyalkanoate Production within a Novel WRRF Configuration*, in *Civil and Environmental Engineering*. 2016, University of Idaho: Moscow, ID. p. 81.
58. Bengtsson, S., et al., *Production of polyhydroxyalkanoates from fermented sugar cane molasses by a mixed culture enriched in glycogen accumulating organisms.* J Biotechnol, 2010. **145**(3): p. 253-63.
59. Winkler, M., E.R. Coats, and C.K. Brinkman, *Advancing post-anoxic denitrification for biological nutrient removal.* Water Res, 2011. **45**(18): p. 6119-30.
60. Coats Erik, R., et al., *Toward Polyhydroxyalkanoate Production Concurrent with Municipal Wastewater Treatment in a Sequencing Batch Reactor System.* Journal of Environmental Engineering, 2011. **137**(1): p. 46-54.

61. Appel, F.J., *Advancing a Post-Anoxic Biological Nutrient Removal Process Selecting for Nitritation*, in *Civil and Environmental Engineering*. 2015, University of Idaho: Moscow, ID. p. 75.
62. Coats, E.R., et al., *Synthesis of Polyhydroxyalkanoates in Municipal Wastewater Treatment.* Water Environment Research, 2007. **79**(12): p. 2396-2403.
63. Choi, J.-i. and S.Y. Lee, *Process analysis and economic evaluation for Poly(3-hydroxybutyrate) production by fermentation.* Bioprocess Engineering, 1997. **17**(6): p. 335-342.
64. Laycock, B., et al., *The chemomechanical properties of microbial polyhydroxyalkanoates.* Progress in Polymer Science, 2013. **38**(3): p. 536-583.
65. Lee, S.Y., *Plastic bacteria? Progress and prospects for polyhydroxyalkanoate production in bacteria.* Trends in Biotechnology, 1996. **14**(11): p. 431-438.
66. Salehizadeh, H. and M.C.M. Van Loosdrecht, *Production of polyhydroxyalkanoates by mixed culture: recent trends and biotechnological importance.* Biotechnology Advances, 2004. **22**(3): p. 261-279.
67. Hanson, A.J., et al., *Community proteomics provides functional insight into polyhydroxyalkanoate production by a mixed microbial culture cultivated on fermented dairy manure.* Applied Microbiology and Biotechnology, 2016. **100**(18): p. 7957-7976.
68. Coats, E.R., B. Watson, and C.K. Brinkman, *Polyhydroxyalkanoate Synthesis by Mixed Microbial Consortia cultured on Fermented Dairy Manure: Effect of Oxygen Mass Transfer on Process Rates/Yields and Microbial Ecology.* Water Res., 2016. **106**: p. 26-40.
69. Guho, N., *Advancing bioplastic production from waste feedstocks using mixed microbial consortia by reconsidering the underlying biochemical basis: One step back, two steps forward*, in *Civil and Environmental Engineering*. 2014, University of Idaho. p. 27.
70. Russell, J.B., *The energy spilling reactions of bacteria and other organisms.* J Mol Microbiol Biotechnol, 2007. **13**(1-3): p. 1-11.
71. Russell, J.B. and G.M. Cook, *Energetics of bacterial growth: balance of anabolic and catabolic reactions.* Microbiological reviews, 1995. **59**(1): p. 48-62.
72. Morgan-Sagastume, F., et al., *Production of polyhydroxyalkanoates in open, mixed cultures from a waste sludge stream containing high levels of soluble organics, nitrogen and phosphorus.* Water Res, 2010. **44**(18): p. 5196-211.
73. Johnson, K., et al., *Enrichment of a mixed bacterial culture with a high polyhydroxyalkanoate storage capacity.* Biomacromolecules, 2009. **10**(4): p. 670-6.
74. Choi, J. and S.Y. Lee, *Factors affecting the economics of polyhydroxyalkanoate production by bacterial fermentation.* Applied Microbiology and Biotechnology, 1999. **51**(1): p. 13-21.
75. Metcalf, amp, and I. Eddy, *Wastewater engineering : treatment and reuse*. 2003: Fourth edition / revised by George Tchobanoglous, Franklin L. Burton, H. David Stensel. Boston : McGraw-Hill, [2003] ©2003.
76. Westerhoff, H.V. and K. van Dam, *Thermodynamics and control of biological free-energy transduction*. 1987: Elsevier.
77. Cherrington, C.A., et al., *Organic Acids: Chemistry, Antibacterial Activity and Practical Applications*, in *Advances in Microbial Physiology*, A.H. Rose and D.W. Tempest, Editors. 1991, Academic Press. p. 87-108.
78. Stephanopoulos, G., A.A. Aristidou, and J. Nielsen, *Metabolic Engineering: Principles and Methodologies*. 1998: Elsevier Science.
79. Russell, J.B. and F. Diez-Gonzalez, *The effects of fermentation acids on bacterial growth.* Adv Microb Physiol, 1998. **39**: p. 205-34.
80. Stouthamer, A.H., *A Theoretical Study on the Amount of ATP Required for Synthesis of Microbial Cell Material*. Vol. 39. 1973. 545-65.

81. Villadsen, J., J. Nielsen, and G. Lidén, *Bioreaction Engineering Principles*. 2011.
82. Lemos, P.C., et al., *Metabolic pathway for propionate utilization by phosphorus-accumulating organisms in activated sludge: 13C labeling and in vivo nuclear magnetic resonance.* Appl Environ Microbiol, 2003. **69**(1): p. 241-51.
83. Steinbüchel, A., *Biodegradable plastics.* Current Opinion in Biotechnology, 1992. **3**(3): p. 291-297.
84. Berg, J.M., J.L. Tymoczko, and L. Stryer, *Biochemistry, Fifth Edition*. 2002: W.H. Freeman.
85. Madigan, M.T., et al., *Brock Biology of Microorganisms, Books a la Carte Edition*. 2017: Pearson Education.
86. Frederick Carl, N., J.L. Ingraham, and M. Schaechter, *Physiology of the Bacterial Cell: A Molecular Approach*. 1990: Sinauer Associates.
87. Third, K.A., M. Newland, and R. Cord-Ruwisch, *The effect of dissolved oxygen on PHB accumulation in activated sludge cultures.* Biotechnology and Bioengineering, 2003. **82**(2): p. 238-250.
88. Kleerebezem, R. and M.C.M. Van Loosdrecht, *A Generalized Method for Thermodynamic State Analysis of Environmental Systems.* Critical Reviews in Environmental Science and Technology, 2010. **40**(1): p. 1-54.
89. Carleton, B.S., *Toward Maximal Polyhydroxyalkanoate Production from Dairy Manure: Controlling and Optimizing Biosynthesis with Implications for Design*, in *Chemical Engineering*. 2016, University of Idaho. p. 118.
90. Haywood, G.W., et al., *Characterization of two 3-ketothiolases possessing differing substrate specificities in the polyhydroxyalkanoate synthesizing organism Alcaligenes eutrophus.* FEMS Microbiology Letters, 1988. **52**(1-2): p. 91-96.
91. Haywood, G.W., A.J. Anderson, and E.A. Dawes, *The importance of PHB-synthase substrate specificity in polyhydroxyalkanoate synthesis by Alcaligenes eutrophus.* FEMS Microbiology Letters, 1989. **57**(1): p. 1-6.
92. Oeding, V. and H.G. Schlegel, *Beta-ketothiolase from Hydrogenomonas eutropha H16 and its significance in the regulation of poly-beta-hydroxybutyrate metabolism.* Biochem J, 1973. **134**(1): p. 239-48.
93. Doi, Y., et al., *Biosynthesis of copolyesters in Alcaligenes eutrophus H16 from carbon-13 labeled acetate and propionate.* Macromolecules, 1987. **20**(12): p. 2988-2991.
94. Doi, Y., et al., *Biosynthesis of terpolyesters of 3-hydroxybutyrate, 3-hydroxyvalerate, and 5-hydroxyvalerate in alcaligenes eutrophus from 5-chloropentanoic and pentanoic acids.* Die Makromolekulare Chemie, Rapid Communications, 1987. **8**(12): p. 631-635.
95. Jendrossek, D., *Polyhydroxyalkanoate Granules Are Complex Subcellular Organelles (Carbonosomes).* Journal of Bacteriology, 2009. **191**(10): p. 3195.
96. Dionisi, D., et al., *Sequencing Batch Reactor: Influence of Periodic Operation on Performance of Activated Sludges in Biological Wastewater Treatment.* Industrial & Engineering Chemistry Research, 2001. **40**(23): p. 5110-5119.
97. Dionisi, D., et al., *Effect of the applied organic load rate on biodegradable polymer production by mixed microbial cultures in a sequencing batch reactor.* Biotechnology and Bioengineering, 2006. **93**(1): p. 76-88.
98. Beccari, M., et al., *Exploiting olive oil mill effluents as a renewable resource for production of biodegradable polymers through a combined anaerobic–aerobic process.* Journal of Chemical Technology & Biotechnology, 2009. **84**(6): p. 901-908.
99. Dionisi, D., et al., *Storage of biodegradable polymers by an enriched microbial community in a sequencing batch reactor operated at high organic load rate.* Journal of Chemical Technology & Biotechnology, 2005. **80**(11): p. 1306-1318.

100. Romenesko, T. and E.R. Coats, *Cofermenting Algal Biomass with Municipal Primary Solids to Enhance Carboxylate Production.* Water Environ. Res., 2018. **90**(11): p. 1997-2007.
101. Smith, S.A., et al., *Toward Sustainable Dairy Waste Utilization: Enhanced VFA and Biogas Synthesis via Upcycling Algal Biomass Cultured on Waste Effluent.* J. Chem. Technol. Biotechnol., 2016. **91**(1): p. 113-121.
102. Grady, C.P.L., *Biological wastewater treatment*. 2011: Third edition. Boca Raton, FL : CRC Press : IWA Pub., [2011] ©2011.
103. Albuquerque, M., C.A.V. Torres, and M. Reis, *Polyhydroxyalkanoate (PHA) production by a mixed microbial culture using sugar molasses: Effect of the influent substrate concentration on culture selection.* Water research, 2010. **44**: p. 3419-33.
104. Albuquerque, M.G., et al., *Mixed culture polyhydroxyalkanoates production from sugar molasses: the use of a 2-stage CSTR system for culture selection.* Bioresour Technol, 2010. **101**(18): p. 7123-33.
105. Marang, L., M.C. van Loosdrecht, and R. Kleerebezem, *Modeling the competition between PHA-producing and non-PHA-producing bacteria in feast-famine SBR and staged CSTR systems.* Biotechnol Bioeng, 2015. **112**(12): p. 2475-84.
106. Fernández-Dacosta, C., et al., *Microbial community-based polyhydroxyalkanoates (PHAs) production from wastewater: Techno-economic analysis and ex-ante environmental assessment.* Bioresource Technology, 2015. **185**: p. 368-377.
107. Carta, F., et al., *Simultaneous storage and degradation of phb and glycogen in activated sludge cultures.* Water Research, 2001. **35**(11): p. 2693-2701.
108. Chua, A.S., et al., *Production of polyhydroxyalkanoates (PHA) by activated sludge treating municipal wastewater: effect of pH, sludge retention time (SRT), and acetate concentration in influent.* Water Res, 2003. **37**(15): p. 3602-11.
109. Johnson, K., R. Kleerebezem, and M.C. van Loosdrecht, *Influence of the C/N ratio on the performance of polyhydroxybutyrate (PHB) producing sequencing batch reactors at short SRTs.* Water Res, 2010. **44**(7): p. 2141-52.
110. Valentino, F., et al., *Polyhydroxyalkanoate (PHA) storage within a mixed-culture biomass with simultaneous growth as a function of accumulation substrate nitrogen and phosphorus levels.* Water Res, 2015. **77**: p. 49-63.
111. Villano, M., et al., *Effect of pH on the production of bacterial polyhydroxyalkanoates by mixed cultures enriched under periodic feeding.* Process Biochemistry, 2010. **45**(5): p. 714-723.
112. Jiang, Y., et al., *Effect of temperature and cycle length on microbial competition in PHB-producing sequencing batch reactor.* Isme j, 2011. **5**(5): p. 896-907.
113. Morgan-Sagastume, F., et al., *Polyhydroxyalkanoate (PHA) production from sludge and municipal wastewater treatment.* Water Sci Technol, 2014. **69**(1): p. 177-84.
114. Garcia-Ochoa, F. and E. Gomez, *Bioreactor scale-up and oxygen transfer rate in microbial processes: an overview.* Biotechnol Adv, 2009. **27**(2): p. 153-76.
115. Coats, E.R., B.S. Watson, and C.K. Brinkman, *Polyhydroxyalkanoate synthesis by mixed microbial consortia cultured on fermented dairy manure: Effect of aeration on process rates/yields and the associated microbial ecology.* Water Res, 2016. **106**: p. 26-40.
116. Watson, B., *Optimization of a Dairy Manure Based Polyhydroxyalkanoates Production through Reduced Aeration on Enrichment Cultures*, in *Civil Engineering*. 2015, University of Idaho: Moscow, ID. p. 112.
117. Fang, F., et al., *Identifying the influential priority of the factors governing PHB production by activated sludge with integration of uniform design and grey relational analysis.* Separation and Purification Technology, 2014. **136**: p. 111–114.

118. Venkata Mohan, S. and M. Venkateswar Reddy, *Optimization of critical factors to enhance polyhydroxyalkanoates (PHA) synthesis by mixed culture using Taguchi design of experimental methodology.* Bioresource Technology, 2013. **128**: p. 409-416.
119. Wei, Y.H., et al., *Screening and evaluation of polyhydroxybutyrate-producing strains from indigenous isolate Cupriavidus taiwanensis strains.* Int J Mol Sci, 2011. **12**(1): p. 252-65.
120. Liu, Z., et al., *Optimization of polyhydroxybutyrate (PHB) production by excess activated sludge and microbial community analysis.* J Hazard Mater, 2011. **185**(1): p. 8-16.
121. Bren, A., et al., *The last generation of bacterial growth in limiting nutrient.* BMC Syst Biol, 2013. **7**: p. 27.
122. Venkateswar Reddy, M. and S. Venkata Mohan, *Effect of substrate load and nutrients concentration on the polyhydroxyalkanoates (PHA) production using mixed consortia through wastewater treatment.* Bioresour Technol, 2012. **114**: p. 573-82.
123. Jiang, Y., et al., *Waste to resource: Converting paper mill wastewater to bioplastic.* Water Res, 2012. **46**(17): p. 5517-5530.
124. Henze, M., et al., *Activated Sludge Models ASM1, ASM2, ASM2D, ASM3*. Vol. 5. 2000.
125. Pardelha, F., et al., *Flux balance analysis of mixed microbial cultures: Application to the production of polyhydroxyalkanoates from complex mixtures of volatile fatty acids.* Journal of Biotechnology, 2012. **162**(2): p. 336-345.
126. Zeng, R.J., et al., *Metabolic model for glycogen-accumulating organisms in anaerobic/aerobic activated sludge systems.* Biotechnology and Bioengineering, 2002. **81**(1): p. 92-105.
127. Filipe, C.D., G.T. Daigger, and C.P. Grady, Jr., *A metabolic model for acetate uptake under anaerobic conditions by glycogen accumulating organisms: Stoichiometry, kinetics, and the effect of pH.* Biotechnol Bioeng, 2001. **76**(1): p. 17-31.
128. Roels, J.A., *Energetics and kinetics in biotechnology*. 1983: Elsevier Biomedical Press.
129. Verduyn, C., et al., *A theoretical evaluation of growth yields of yeasts.* Antonie van Leeuwenhoek, 1991. **59**(1): p. 49-63.
130. Gommers, P.J.F., et al., *Biochemical limits to microbial growth yields: An analysis of mixed substrate utilization.* Biotechnology and Bioengineering, 1988. **32**(1): p. 86-94.
131. Dias, J.M., et al., *Mathematical modelling of a mixed culture cultivation process for the production of polyhydroxybutyrate.* Biotechnol Bioeng, 2005. **92**(2): p. 209-22.
132. van Loosdrecht, M.C.M. and J.J. Heijnen, *Modelling of activated sludge processes with structured biomass.* Water Science and Technology, 2002. **45**(6): p. 13-23.
133. Murnleitner, E., et al., *An integrated metabolic model for the aerobic and denitrifying biological phosphorus removal.* Biotechnology and Bioengineering, 1997. **54**(5): p. 434-450.
134. Stowe, E.J., *Dairy Waste Treatment Utilizing a Two-Phase Anaerobic Digestion System: Evaluation of Parallel Reactor Configuration and Mixing Intensity*, in *Civil Engineering*. 2014, University of Idaho: Moscow, ID. p. 114.
135. Stowe, E.J., E.R. Coats, and C.K. Brinkman, *Dairy Manure Resource Recovery utilizing Two-stage Anaerobic Digestion - Implications of Solids Fractionation.* Bioresour. Technol., 2015. **198**: p. 237-245.
136. Association, A.P.-A.P.H., *Standard methods for the examination of water and wastewater.* USA: APHA, 1998.
137. Braunegg, G., B. Sonnleitner, and R.M. Lafferty, *A rapid gas chromatographic method for the determination of poly-β-hydroxybutyric acid in microbial biomass.* European journal of applied microbiology and biotechnology, 1978. **6**(1): p. 29-37.

Appendix A: Model

Reducing Equivalents

Specify Biomass Composition

```
clc, clear
syms C H N O P S

deg_red=[4 1 -3 -2 5 6];       %redox levels for NH3 as reference compound

C=1;
H=1.8;
N=0.2;
O=0.5;
P=0;
S=0;

X=[C H N O P S];               %biomass content of each element on C-mol basis

AcSCoA=[1 1 0 0.5 0 0];        %biomass content AcSCoA less H-S-CoA on C-mol basis
PropCoA=[1 4/3 0 1/3 0 0];     %biomass content PropCoA less H-S-CoA on C-mol basis

lambda_x = deg_red*X';         %degree of reduction of biomass w/NH3 as N source
lambda_A = deg_red*AcSCoA';    %degree of reduction of AcSCoA
lambda_P = deg_red*PropCoA';   %degree of reduction of PropCoA
lambda_NADH = 2;               %degree of reduction of NADH_2
```

Metabolism Parameters from Literature

```
deltaAc_x = 0.267;             %C-mol CO2 proced per C-mol X on Acetate (Gommers et al., 1988)
deltaPr_x = 1.409*0.75-1;      %C-mol CO2 produced per C-mol X on Prop from Succ (Zeng et al.,
alpha_x = 1.5;                 %mol ATP for active biomass/C-mol X (Verduyn et al., 1991)
alpha_m = 0.66;                %mol ATP for biomass precursor/C-mol X (Stouthamer et al., 1973
```

Biomass Growth on Acety-CoA

```
alphaAc_ATP = C*(alpha_x+alpha_m)                          %Balance on ATP
```

```
alphaAc_ATP = 2.1600
```

```
alpha_N = N;                                                %Balance on N
alpha_P = P;                                                %Balance on P
alpha_O = (1+deltaAc_x)*AcSCoA(4)+4*alpha_P-O-2*deltaAc_x   %Balance on O
```

```
alpha_O = -0.4005
```

```
alpha_NADH = ((1+deltaAc_x)*lambda_A-lambda_x)/lambda_NADH    %Balance on NADH2
```

```
alpha_NADH = 0.4340
```

Figure A. 1: Determination of R_8

```
%Reaction 8
syms AcSCoA NH_3 ATP H_2O X NADH_2 CO_2
E_Ac=[AcSCoA NH_3 ATP H_2O X NADH_2 CO_2];
Stoich_AcAnab=[-(1+deltaAc_x) -alpha_N -alphaAc_ATP alpha_O 1 alpha_NADH deltaAc_x];  %Stoi
```

Biomass Growth on Propionyl-CoA

```
alphaPr_ATP = alphaAc_ATP-(1+deltaAc_x)*0.25                %Balance on ATP AcCoA-PropCoA
```

```
alphaPr_ATP = 1.8433
```

```
alphaPr_N = N;                                               %Balance on N
alphaPr_P = P;                                               %Balance on P
alphaPr_O = (1+deltaPr_x)*PropCoA(4)+4*alpha_P-O-2*deltaPr_x  %Balance on O
```

```
alphaPr_O = -0.2613
```

```
alphaPr_NADH = ((1+deltaPr_x)*lambda_P-lambda_x)/lambda_NADH  %Balance on NADH2
```

```
alphaPr_NADH = 0.3658
```

```
%Reaction 9
syms PropCoA
E_Pr=[PropCoA NH_3 ATP H_2O X NADH_2 CO_2];
Stoich_PrAnab=[-(1+deltaPr_x) -alphaPr_N -alphaPr_ATP alphaPr_O 1 alphaPr_NADH deltaPr_x];
```

Figure A. 2: Determination of R_9

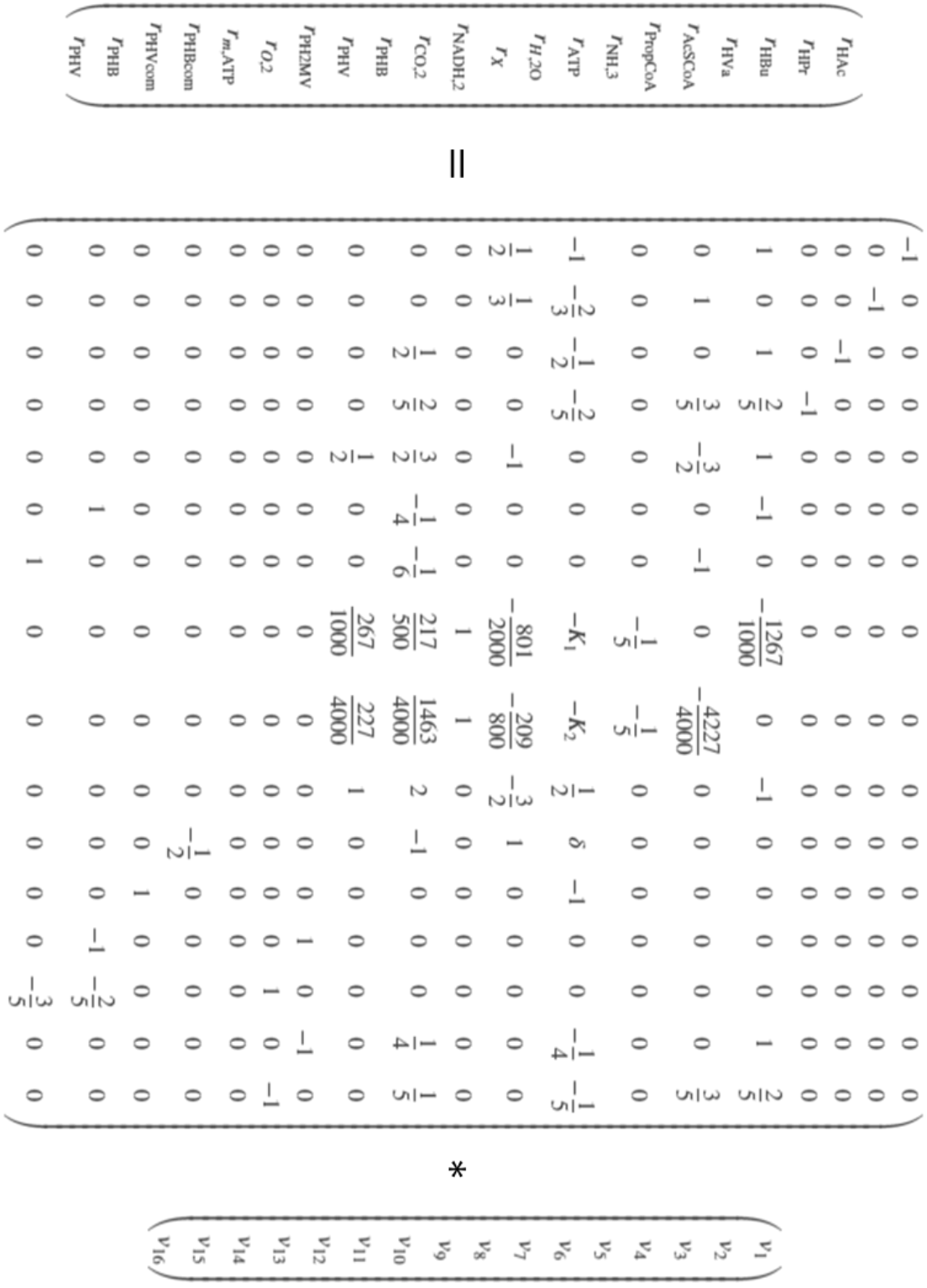

Figure A. 3: Model Stoichiometric Matrix (excludes PH2MV)

Appendix B: Figure Permissions

Nicholas M. Guho
University of Idaho
Moscow, ID 83843

December 5, 2019

Re: Copyright permission

To whom it may concern:

I hereby grant permission to any graduate student at the University of Idaho to whom Dr. Eric R. Coats is an advisor to reprint any figure from my master's thesis "Polyhydroxyalkanoate Production Coupled with Waste Treatment Using a Three-Stage Sequencing Batch Reactor System Fed Dairy Manure" to which I hold the copyright in their own master's thesis or doctoral dissertation.

Sincerely,

Nicholas M. Guho

University of Idaho

Figure B. 1: Figure permissions for Figure 2.4 and Figure 2.6

Cody Sprague <CSprague@mountainwtr.com>
Thu 12/5/2019 1:09 PM
Crozes, Alexandre (croz3219@vandals.uidaho.edu)

Hey Alex,

[redacted]

Yes, you can reproduce those figures, [redacted]

Thanks,

Cody Sprague, E.I.T. | Mountain Waterworks, Inc.

Figure B. 2: Figure permissions for Figure 2.1 and Figure 2.3

ELSEVIER LICENSE
TERMS AND CONDITIONS

Dec 05, 2019

This Agreement between University of Idaho -- Alexandre Crozes ("You") and Elsevier ("Elsevier") consists of your license details and the terms and conditions provided by Elsevier and Copyright Clearance Center.

License Number	4722651503311
License date	Dec 05, 2019
Licensed Content Publisher	Elsevier
Licensed Content Publication	Journal of Biotechnology
Licensed Content Title	Polyhydroxyalkanoates, biopolyesters from renewable resources: Physiological and engineering aspects
Licensed Content Author	Gerhart Braunegg,Gilles Lefebvre,Klaus F Genser
Licensed Content Date	Oct 27, 1998
Licensed Content Volume	65

Licensed Content Issue	2-3
Licensed Content Pages	35
Start Page	127
End Page	161
Type of Use	reuse in a thesis/dissertation
Portion	figures/tables/illustrations
Number of figures/tables/illustrations	1
Format	both print and electronic
Are you the author of this Elsevier article?	No
Will you be translating?	No
Title	A Predictive Metabolic Model for Polyhydroxyalkanoate Production by a Mixed Microbial Consortium cultured under Aerobic Dynamic Feeding Conditions and fed Dairy Manure Fermenter Liquor
Institution name	University of Idaho

Expected presentation date	Dec 2019
Order reference number	13197
Portions	Fig. 2. Pathways of PHA synthesis in R.eutropha, except for Pathway VII. Page 137.
Requestor Location	University of Idaho 402 South Lilly Street MOSCOW, ID 83843 United States Attn: University of Idaho
Publisher Tax ID	98-0397604
Total	0.00 USD

Figure B. 3: Figure permissions for Figure 2.5

Figure B. 4: Figure permissions for Figure 2.2